

**POLITECNICO DI MILANO**

Facoltà di Ingegneria Industriale

Corso di Laurea in  
Ingegneria Meccanica



*Novel technique for DIC speckle pattern  
optimization and generation*

Relator: Prof. Emanuele ZAPPA

Co-relator: Ing. Paolo Mazzoleni

Tesi di Laurea di:

Simone GUALTIERI    Matricola 765841

Anno Accademico 2011- 2012



## **Index**

<b>List of figures.....</b>	<b>5</b>
<b>List of tables .....</b>	<b>8</b>
<b>Abstract .....</b>	<b>9</b>
<b>Introduction.....</b>	<b>11</b>
<b>1.1 Brief work description .....</b>	<b>13</b>
<b>DIC technique .....</b>	<b>15</b>
<b>2.1 DIC overview .....</b>	<b>15</b>
2.1.1 Fundamentals of DIC .....	15
2.1.2 Algorithm description.....	17
<b>2.2 Speckle Pattern.....</b>	<b>18</b>
2.2.1 Black vs. White .....	19
2.1.2 Techniques.....	19
<b>2.2 Mean Intensity Gradient Coefficient.....</b>	<b>23</b>
<b>Speckle pattern realization: an innovative technique .....</b>	<b>25</b>
<b>3.1 Purpose.....</b>	<b>25</b>
<b>3.2 How to make it.....</b>	<b>26</b>
3.2.1 Choice of paper type.....	27
3.2.2 Application time .....	27
3.2.3 Pattern shape and size.....	28
3.2.4 Printing phase .....	29
3.2.5 Application on the piece .....	29
3.2.6 Contrast.....	30
<b>3.3 Pattern improvement .....</b>	<b>32</b>
3.3.1 Vector graphics.....	34
3.3.2 Step Optimization .....	35
<b>3.4 Ironing and Printing analysis .....</b>	<b>37</b>
3.4.1 Blob analysis .....	37
3.4.2 Scanner calibration .....	38
3.4.3 Data acquisition .....	40
<b>3.5 Conclusion.....</b>	<b>52</b>
<b>Evaluation of speckle pattern optimization.....</b>	<b>54</b>
<b>4.1 Preliminary procedure.....</b>	<b>54</b>
4.1.1 Realization of MIG graph.....	55
<b>4.2 Scanner test.....</b>	<b>60</b>

<b>4.3 Micrometric screw test .....</b>	<b>62</b>
<b>4.4 Results .....</b>	<b>67</b>
4.4.1 Normal images.....	67
4.4.2 Images with noise .....	70
<b>4.5 Final observations .....</b>	<b>75</b>
<b>Experimental Test (Procedure) .....</b>	<b>79</b>
<b>5.1 Characteristic of the samples .....</b>	<b>79</b>
5.1.1 Electron Beam Welding .....	79
5.1.2 Samples Material .....	79
<b>5.2 Pattern application .....</b>	<b>81</b>
<b>5.3 Settlement procedure .....</b>	<b>83</b>
5.3.1 Positioning lights .....	83
5.3.2 Positioning and synchronization of cameras .....	84
5.3.3 Calibration of cameras.....	85
5.3.4 Aperture and exposure time.....	88
5.3.5 Positioning specimens (and clip gauge) .....	89
<b>5.4 Data Elaboration .....</b>	<b>89</b>
5.4.1 Consideration before of the elaboration .....	89
5.4.2 Brief VIC 3D introduction.....	90
5.4.3 Option choice during the elaboration .....	90
<b>5.5 Final considerations .....</b>	<b>92</b>
<b>Experimental Tests (Results) .....</b>	<b>94</b>
<b>6.1 Considerations of procedure .....</b>	<b>94</b>
<b>6.2 How to find the welding line.....</b>	<b>96</b>
<b>6.3 Results and graphs .....</b>	<b>99</b>
6.3.1 1 <sup>st</sup> sample: Q&P B1-2.....	99
6.3.2 2 <sup>nd</sup> sample: Q&P B2-2.....	108
6.3.3 3 <sup>rd</sup> sample: TWIP 11T .....	112
6.3.4 4 <sup>th</sup> sample: TWIP 8T .....	116
<b>6.4 Young's modulus comparison (Q&amp;P samples).....</b>	<b>117</b>
<b>6.5 Final considerations .....</b>	<b>120</b>
<b>Conclusion .....</b>	<b>122</b>
<b>7.1 Possible future implications .....</b>	<b>123</b>
<b>List of symbols.....</b>	<b>124</b>
<b>References.....</b>	<b>125</b>

## List of figures

Figure 1.1 Example of artificial pattern nowadays used in digital image correlation .....	12
Figure 2.1 Scheme of reference subset and the subset after deformation .....	16
Figure 2.2 Example of patterns with proprieties to be avoided .....	19
Figure 2.3 Example of painted speckle pattern .....	20
Figure 2.4 Example of lithography pattern .....	20
Figure 2.5 Electron-lithographic technique.....	23
Figure 3.1 Ordered and slight random pattern .....	25
Figure 3.2 Summary of procedure .....	26
Figure 3.3 Series of pattern(diameters from 0.05mm to 1mm with step of 0.05) .....	28
Figure 3.4 Proves at different intensity toner.....	29
Figure 3.5 Aluminium painted sample.....	30
Figure 3.6 Sample too reflective after grinding .....	31
Figure 3.7 Colorations at different heating temperatures.....	31
Figure 3.8 Sample after sandblast .....	32
Figure 3.9 Lithography printing.....	33
Figure 3.10 Effects after dimensional reduction by Office Word.....	33
Figure 3.11 Example of raster and vector images.....	34
Figure 3.12 Dots linked together.....	35
Figure 3.13 Pattern at different steps .....	36
Figure 3.14 Example of Sobel's filter with 180 of threshold.....	37
Figure 3.15 Cleaning of image.....	38
Figure 3.16 Images for scanner calibration.....	38
Figure 3.17 Types of acquired data.....	40
Figure 3.18 Mean diameter after printing phase .....	41
Figure 3.19 Waddel diameter after printing phase.....	42
Figure 3.20 Matching rectangular width and height in printing phase .....	43
Figure 3.21 Maximum diameter in printing phase.....	44
Figure 3.22 Number of empty zones in printing phase.....	45
Figure 3.23 Circularity in printing phase .....	46
Figure 3.24 Mean diameter after ironing .....	47
Figure 3.25 Maximum diameter after ironing.....	48
Figure 3.26 Circularity after ironing .....	49
Figure 3.27 Number of "white zones" after ironing .....	50
Figure 3.28 Matching ironing and printing diameter .....	51
Figure 3.29 Comparison between the new speckle pattern with a traditional one (airbrush).....	52

Figure 3.30 Pattern created by a stencil more times .....	53
Figure 4.1 Randomization of the pattern.....	55
Figure 4.2 Blurring in the boundary in case of small and big blob.....	56
Figure 4.3 Pattern generation with blobs at 4 pixel diameter .....	56
Figure 4.4 MIG graph .....	57
Figure 4.5 Different Pattern types on the paper (zoom 400%) .....	59
Figure 4.6 Analysis by scanner .....	60
Figure 4.7 Example of strain calculated after scanner acquisition.....	61
Figure 4.8 Micrometric head.....	62
Figure 4.9 Supply and evaluation unit .....	63
Figure 4. 10 Laser displacement .....	63
Figure 4.11 System of acquisition.....	65
Figure 4.12 Calibration grid.....	65
Figure 4.13 Test arrangement .....	66
Figure 4.14 X displacement in normal image .....	67
Figure 4.15 Standard deviation X in normal image .....	68
Figure 4.16 Y displacement in normal image .....	68
Figure 4.17 Standard deviation Y in normal image .....	69
Figure 4.18 X Displacement on images with $\Gamma=5\%$ noise.....	71
Figure 4.19 Y Displacement on images with $\Gamma=5\%$ noise.....	72
Figure 4.20 X Displacement on images with $\Gamma=2.5\%$ noise.....	73
Figure 4.21 Y Displacement on images with $\Gamma=2.5\%$ noise.....	74
Figure 4.22 Highlighting of Random image pattern ( $\Gamma=0\%$ ).....	76
Figure 4.23 Highlighting of Random image pattern ( $\Gamma=2,5\%$ ).....	76
Figure 4.24 Highlighting of Random image pattern ( $\Gamma =5\%$ ).....	76
Figure 4.25 Highlight of $\varnothing 3$ p4.3 in MIG graph.....	77
Figure 5.1 Missing dots deposition due to accentuated welding bump .....	81
Figure 5.2 Final result after application of the pattern on the piece .....	82
Figure 5.3 Led torch .....	83
Figure 5.4 Instruments settlement .....	85
Figure 5.5 Calibrator image (2 mm step ) .....	86
Figure 5.6 Example of calibration score .....	87
Figure 5.7 Defined AOI with a grid of ROI.....	90
Figure 5.8 Sequences of images acquired by camera during a tensile test .....	93
Figure 6.1 Schema of dog bones .....	94
Figure 6.2 Schema of dog bones .....	95
Figure 6.3 Sample after breaking .....	96
Figure 6.4 Fracture on welding zone through microscope.....	97
Figure 6.5 Points coordinates on the surface .....	98
Figure 6.6 Q&P B1-2 Strain/Stress curves in welding zone (section A-A).....	99
Figure 6.7 Q&P B1-2 Strain/Stress curves in heat affected zone .....	100
Figure 6.8 Q&P B1-2 Strain/Stress curves in base metal zone.....	101

Figure 6.9 Q&P B1-2 Strain/Stress curves between the curves in sections D-D and E-E.....	101
Figure 6.10 Q&P B1-2 Young's modulus.....	102
Figure 6.11 Behaviour of bended sample .....	103
Figure 6.12 Q&P B1-2: Frame No.0 Reference Image.....	104
Figure 6.13 Q&P B1-2: Frame No.4 Sample under loading.....	105
Figure 6.14 Q&P B1-2: Frame No.10 Sample under loading.....	106
Figure 6.15 Q&P B1-2 $\epsilon_{xx}$ before the breaking .....	107
Figure 6.16 Q&P B1-2 $\epsilon_{yy}$ before the breaking .....	107
Figure 6.17 Q&P B2-2 Strain/Stress curves in welding zone (section A-A )...	108
Figure 6.18 Q&P B2-2 Strain/Stress curves in heat affected zone (sections B-B and C-C).....	109
Figure 6.19 Q&P B2-2 Strain/Stress curves base metal zone (sections D-D and E-E) .....	109
Figure 6.20 Q&P B2-2 Young's modulus.....	110
Figure 6.21 Q&P B2-2 $\epsilon_{xx}$ before the breaking .....	111
Figure 6.22 Twip 11T Strain/Stress curves in welding zone (section A-A) .....	112
Figure 6.23 Twip 11T Strain/Stress curves in heat affected zone (sections B-B and C-C).....	112
Figure 6.24 Twip 11T Strain/Stress curves in base metal zone (sections D-D and E-E) .....	113
Figure 6.25 Twip 11T Strain/Stress curves between the curves in sections D-D and E-E.....	113
Figure 6.26 Twip 11T $\epsilon_{xx}$ before the breaking.....	114
Figure 6.27 Twip 11T Young's modulus.....	114
Figure 6.28 Twip 11T : Frame No.0 Reference Image.....	115
Figure 6.29 TWIP 8T Strain/Stress curves in base metal zone (sections D-D and E-E) .....	116
Figure 6.30 Twip 8T Zoom in elastic zone of stress-strain graph in section D-D .....	117
Figure 6.31 $\epsilon_{xx}$ before the breaking TWIP 8T .....	117
Figure 6.32 Durometer Zwick ZHU 0.2.....	118
Figure 6.33 Depth of penetrator during the hardness test.....	119
Figure 6.34 Included samples in phenolic resin.....	120

## List of tables

Table 3.1 Scanner calibration.....	39
Table 4.1 Blobs types .....	58
Table 4.2 Laser sensor specification .....	64
Table 4.3 $\bar{\sigma}$ of displacement along X axis .....	70
Table 4.4 $\bar{\sigma}$ of displacement along X axis adding $\Gamma=5\%$ noise .....	72
Table 4.5 $\bar{\sigma}$ of displacement along X axis adding $\Gamma=2.5\%$ noise .....	74
Table 4.6 Ranking of best pattern .....	77
Table 5.1 Chemical composition of dog bones .....	80
Table 5.2 Areas data.....	80
Table 5.3 Summary of option data during the processing .....	92
Table 6.1 Points coordinate from the welding line .....	98
Table 6.2 Young's modulus Comparison.....	120
Table 6.3 Number of "local" points used for the calculation.....	121

## **Abstract**

The optical method Digital Image Correlation (DIC) has been extensively studied due its capability to measure the entire displacements field over a body surface. This particular propriety makes this method an optimal tool to measure heterogeneous displacements and strains.

The main points of the thesis are the proposal of a novel technique capable to prepare a fully controlled speckle pattern on metal surfaces and the discussion of the speckle pattern parameter which influences the DIC final results.

The technique proposed for speckle pattern generation is very easy and fast to make, economic, reliable, flexible and does not request specific devices. It can be employed also with small specimens where other techniques show the main limits.

Thanks to the possibility to obtain a fully controlled pattern, the technique is used to define which parameters types ( size of the black spots, spacing between them , quality of images etc) are preferable to employ during DIC.

Additionally, the proposed technique was applied to create the pattern on tensile test specimens in order to analyse the strain full field of welded metal samplings with different materials.

**Keywords:** digital image correlation, speckle pattern, optimization, pattern generation, mean intensity gradient, displacement/deformation measurement, tensile test, welded samples.

## **Sommario**

Digital Image Correlation (DIC) è uno strumento di misura ottica non invasiva che permette la misurazione di spostamenti e deformazioni su superfici.

Ampiamente accettata e comunemente utilizzata nell'ambito di prove meccaniche, questa tecnica si basa sui valori di grigio di un'immagine digitale dai quali può determinare la forma e gli spostamenti tridimensionali di un oggetto sottoposto a sollecitazione (termica o meccanica).

Nella tesi viene proposta una nuova tecnica di realizzazione di pattern applicabile su oggetti metallici, molto facile e veloce da utilizzare, economica, affidabile, flessibile, che non richiede particolari accorgimenti per la sua utilizzazione e può essere utilizzata su campioni di piccole dimensioni dove altre tecniche mostrano i loro principali limiti.

La presente tecnica è stata utilizzata durante una prova di trazione per la misurazione di un campo limitato di deformazione, corrispondente ad una zona di saldatura su diversi provini in acciaio (acciai TWIP e Q&P).

Inoltre, grazie all'ottimo controllo dei parametri di realizzazione del pattern (es. dimensioni e passo dei blobs, qualità dell'immagini, ecc), tale procedimento è stato utilizzato per la determinazione dei valori ottimali dei parametri per ottenere misurazioni più accurate possibili.

**Parole chiave:** digital image correlation, speckle pattern, ottimizzazione, generazione di pattern, mean intensity gradient, misurazione di spostamenti/deformazioni, prova di trazione, provini con saldatura.

# Chapter 1

## Introduction

In the last years optical measure systems have a significant technologic development and availability.

They are employed more and more in non-invasive measurements.

Many optical methods have been developed for that purpose, such as optical interferometry, high-resolution moirè and coherent gradient sensing digital speckle correlation method (DSCM)[1], texture correlation [2], computer-aided speckle interferometry (CASI)[3] e electronic speckle photography (ESP)[4].

In 1983, Sutton from the University of South Carolina proposed a technique, called digital image correlation, enables to collect the full field displacement[5].

Digital image correlation (DIC) is a very powerful tool for tracking and image registration techniques for measurements of changes in images.

The idea behind the method is to find the displacement field of the specimen, tracking the deformation of a random speckle pattern applied to the component surface in acquired digital images.

Mathematically, this is accomplished by finding the region in a deformed image that maximizes the normalized cross-correlation score with regard to a small subset of the image taken while no load is applied.

By repeating this process for a large number of subsets, full-field deformation data can be obtained.

Widely employed in many areas of science and engineering, DIC requires that different processing parameters have to be tuned to get the best result; the performances and the uncertainty of the DIC technique strongly depends on some processing parameters, as well as on some experimental conditions.

In particular, this work wants to get into detail of speckle pattern type and parameters( size of the black spots, spacing between them ,etc).

Generally speaking, the speckle pattern on tested object surface can be either artificial or natural (i.e., the texture of the object surface) achieved.

Among the most common methods for pattern application there are self-adhesive, pre-printed patterns, stamps and application of paint speckles with air-brushes, spray cans or brushes.

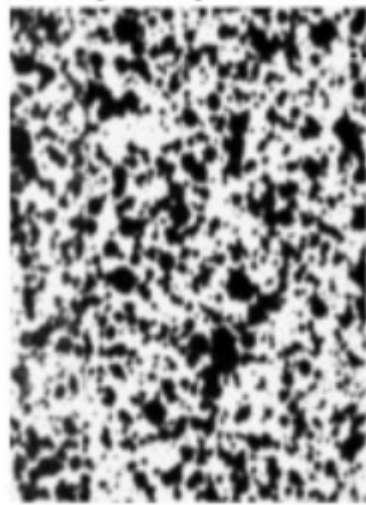


**Figure 1.1 Example of artificial pattern nowadays used in digital image correlation**

The importance of the pattern type and size is due to the fact that, to obtain a reliable and accurate matching, each subset must contain sufficient intensity variations to ensure that it can be uniquely and accurately identified in the deformed image.

So that, the quality of the speckle pattern is closely correlated with the measure errors[6,7,8,9].

Using the DIC technique, the displacements accuracy of different speckle patterns may be change even if taking constant the other parameters.

Today an open question is which is the best pattern in order to obtain the best result.

So that, how to assess the quality of the speckle pattern is undoubtedly an important but confusing problem to the users of DIC.

Various parameters are proposed in order to study the influence of speckle patterns: they are partitioned in local and global parameters.

Local parameters, such as the subset entropy proposed by Sun and Pang [8] and sum of square of subset intensity gradient (SSSIG) proposed by Pan et al. [9], assesses separately the local speckle pattern quality of each subset which is limited to the quality assessment of the local speckle pattern within an individual subset.

On the contrary, global parameters give an overview on a given speckle pattern, taking as hypothesis that the pattern is uniformly distributed on the entire surface.

Recently, a coefficient is used by Lecompte [6] in order to determine the mean speckle size of a speckle pattern. But this parameter presents several poorness points:

First, the concept of speckle size, which was originated from laser speckle technique ,cannot be directly used for some digital images of the specimen surface.

Second, the use of mean speckle size for quality assessment of speckle pattern seems to lack a substantial theoretical foundation.

Third, the computation of mean speckle size using image morphology relies on the practitioner's subjective experience.

So that, another global parameter is taken into consideration to give a quality assessment of the entire speckle pattern :the mean intensity gradient [10].

Different with the mean speckle size, the mean intensity gradient is based on the theoretical model derived for quantifying the accuracy and precision of measured displacements using DIC, and thus has solid theoretical basis.

But another problem is arisen: knowing in theory which is the best obtainable speckle pattern, it is needed to know how to make it.

Actually, a series of techniques exist for making a speckle pattern on surface. But most of all of these techniques can not be perfectly controlled.

The purpose of our work consists of individualising a new kind of technique able to make a controlled speckle pattern.

Then, on a real experimental test the novel kind of pattern will be applied; some final considerations will be taken according the final data.

Due to the controlled pattern, a validation/demonstration of MIG's coefficient will be explained inside this thesis in order to evaluate the pattern quality.

## **1.1 Brief work description**

This work is partitioned in other six chapters:

-the second chapter gives an introduction of digital image correlation technique, focusing on the speckle pattern realization techniques nowadays adopted.

Moreover, a speckle pattern quality coefficient called the mean intensity gradient (MIG) is described in detail and it will be used in sixth chapter.

-the third chapter illustrates the achievement procedure of the new pattern creation technique.

The idea is taken from an homemade printed electronic circuits:

Similar to the technique for transferring the designs on a t-shirt, it is printed (reversed mirror) on transparencies with laser printer or copier and moved with the electric iron.

In order to reach the best result, all the attempts of success and failure are explained.

-the fourth chapter describes the procedure of assessment of MIG's coefficient using our "controlled" technique. In brief, the displacement field of a series of patterns with different prefixed sizes is translated and computed with DIC; a comparison with the final achieved results of each pattern is carried out with the

exact imposed displacement. Knowing that, the random error (standard deviation) of the measured displacements is closely related to the mean intensity gradient and to the used speckle pattern [10], standard deviation will be our parameter for matching different patterns.

We want to evaluate the behaviour close to the welding region. Due to the small welding width, the highest achievable points are the priority. Therefore, the smallest reachable speckle pattern is the goal.

-the fifth chapter consists of tweaking a real experimental test (a tensile test) adopting the novel pattern method with DIC.

The samplings are four dog bones with a welding line in the middle.

The sampling materials are Q&P steel for two of them and TWIP steel for the others.

-the sixth chapter explains the obtained results during the experimental test, focused on the calculation of Young's modulus that changes due to the variation of material composition. Other relevant aspects to be borne in mind are the position of breaking point respect to the welding line and the strains reached along all the pieces.

- the last one will illustrate all the most important observations effort in this thesis.

## **Chapter 2**

### **DIC technique**

In this chapter various fundamental concepts for digital image correlation are presented.

Digital image correlation (DIC) is a very valuable tool for full field displacement measurements. During its utilization, several parameters have to be set in a DIC measurement, namely, speckle size and “density” correlation criteria and algorithm of optimization, subset (or correlation window) size, pitch or subset overlap, gray level interpolation, etc.

The parameter of speckle pattern realization is explained in detail, focused on the most commonly used technique approaches.

In order to determine the quality of different speckle patterns according the order of measures resolution and accuracy, a coefficient is used and explained in detail.

#### **2.1 DIC overview**

Digital image correlation is a kind of technique commonly used for displacements and strains field calculation corresponds to a specific image taking as a reference and the same image subjects to change (displacements, deformations, creations of new compounds...).

DIC applications are so wide in so many fields: in industrial process control, automatic license plate recognition in parking garages, biological growth phenomena, geological mapping, stereo vision, video compression and autonomous robots for space exploration.

As a typical non-interferometric optical metrology with distinct advantages of simple experimental set-up, low-requirement on experimental environment and wide range of applicability, the DIC technique has been widely used for deformation and shape measurement, mechanical parameters characterization as well as numerical, experimental and theoretical cross validations.

##### **2.1.1 Fundamentals of DIC**

The principle of DIC is based on an utilization of grey-scale colour in a distinct area/surface converted in pixel that, after deformation, is subjected to a variation of displacement in all the points. An fundamental assumption is the variation of grey scale during deformation has to be slow.

The procedure consists in recording with cameras some digital images of a specimen undergoing a mechanical transformation and using an image correlation algorithm, the strains are going to be calculated.

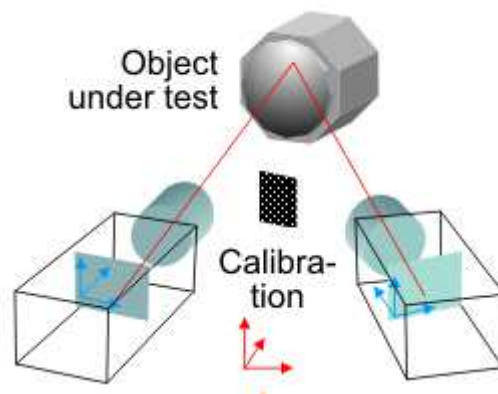


**Figure 2.1 Schematization DIC procedure**

The purpose is the matching of the same points between two images recorded before and after deformation.

The two images are called “reference image” and “deformed image” which , during the measure procedure, are mapped.

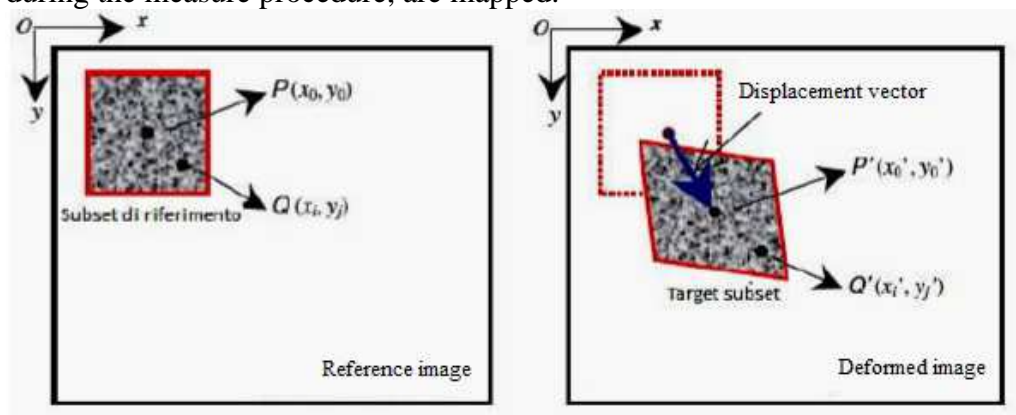


**Figure 2.1 Scheme of reference subset and the subset after deformation**

The method provides a subdivision of reference image into rectangular areas called Region Of Interest (ROI).

It is then provided to search for in the images of the specimen deformed areas that have the greater similarity with each of the ROI of the original image. In fact Generally, it is not possible to find a match for a single pixel of an image in another image; typically the gray value of a single pixel in fact can be found in thousands of other pixels in the second image and there is no univocal correspondence.

### 2.1.2 Algorithm description

In digital image correlation algorithm, to establish correspondences between two images, numerical techniques are used to locate an initially square image subset in a reference image within an image taken under load.

The centre of each subset (Point P in fig 2.2 with coordinates  $x_0$  and  $y_0$ ) is marked in order to provide a reasonable result in terms of displacement for the entire ROI.

To assess the similarity degree between the reference subset and the deformed one, it can be used different correlation coefficients.

The coefficients most commonly used are:

-the sum of the absolute value of the differences (SAD)

-the sum of the squared differences (SSD)

-the cross-correlation (CC).

In the first case the better correspondence is achieved by maximizing the function while in the last two minimizing[11].

Being the marker the geometric centre of the subset, this last provides sufficient information to the tracking algorithm in order to obtain a unique and truthful correlation. The cross-correlation between reference and subsequent subsets of  $(2M + 1) \times (2M + 1)$  pixels is based on the Zero-mean Normalized Sum of Squared Differences (ZNSSD) correlation coefficient:

$$C_{ZNSSD} = \sum_i^M \sum_i^M \left[ \frac{f(x, y) - f_m}{\sqrt{\sum_{i=M}^M \sum_{i=-M}^M (f(x, y) - f_m)^2}} - \frac{g(x', y') - g_m}{\sqrt{\sum_{i=M}^M \sum_{i=-M}^M (g(x', y') - g_m)^2}} \right] \quad (2.1)$$

where  $f(x; y)$  is the gray intensity at coordinates  $(x; y)$  in the reference image (undeformed),  $g(x_0; y_0)$  is the gray intensity at coordinates  $(x_0; y_0)$  in the deformed image and are, respectively, the mean gray values in the reference and deformed subsets. The ZNSSD correlation coefficient is insensitive to the offset and linear scale of illumination intensity offering a robust noise-proof performance[13].

$$f_m = \frac{1}{2M+1} \sum_{i=M}^M \sum_{i=-M}^M f(x, y) \quad , \quad g_m = \frac{1}{2M+1} \sum_{i=M}^M \sum_{i=-M}^M g(x', y') \quad (2.2)$$

In order to allow the deformation of the subset and therefore improving the correlation, different shape functions ( mapping functions) may be used. In the present work, the reference subset is mapped to the target subset by a second-order mapping function:

$$\begin{aligned} x' &= x + \hat{u} = x + u + u_x \Delta x + u_y \Delta y \\ y' &= y + \hat{v} = y + v + v_x \Delta x + v_y \Delta y \end{aligned} \quad (2.3)$$

where  $u$  and  $v$  are respectively the  $x'$  and  $y'$  directional displacement components of the reference subset centre,  $u_x$ ,  $u_y$ ,  $v_x$ ,  $v_y$  are the first-order displacement gradients. The algorithm minimizes the ZNSSD correlation coefficient CZNSSD, solving a set of six non-linear functions, where the minimizing arguments, solution of the minimum problem, correspond to the unknown parameters.

$$p = [u \quad v \quad u_x \quad v_x \quad u_y \quad v_y] \quad (2.4)$$

The set of equations is solved using the iterative Newton-Raphson procedure:

$$p = p_0 - \frac{\nabla C_{ZNSSD}(p_0)}{\nabla \nabla C_{ZNSSD}(p_0)} \quad (2.5)$$

where  $p_0$  is the initial values of the solution  $\nabla C_{ZNSSD}(p_0)$  and  $\nabla \nabla C_{ZNSSD}(p_0)$  are, respectively, the first and second-order derivatives of the correlation coefficient respect to the unknown parameters  $p$ .

This algorithm is highly recommended for practical use due to its higher accuracy, stability and application [18]. More details about this digital image correlation algorithm and shape functions can be found in the works [19] and [10].

## 2.2 Speckle Pattern

The measured displacement results are influenced by the measurement system, the lighting conditions and the speckle pattern.

The utilization of DIC software has needed of a contrasting pattern on the surface of the test specimen.

The object surface exhibits certain proprieties explained below:

-the surface has to be isotropic in order to avoid registration problems.

So that the pattern has to be non-periodic and therefore it has needed of a random texture.

- the surface has not to have a preferred orientation and to exhibit a bias to one orientation
- the surface has to present an high contrast

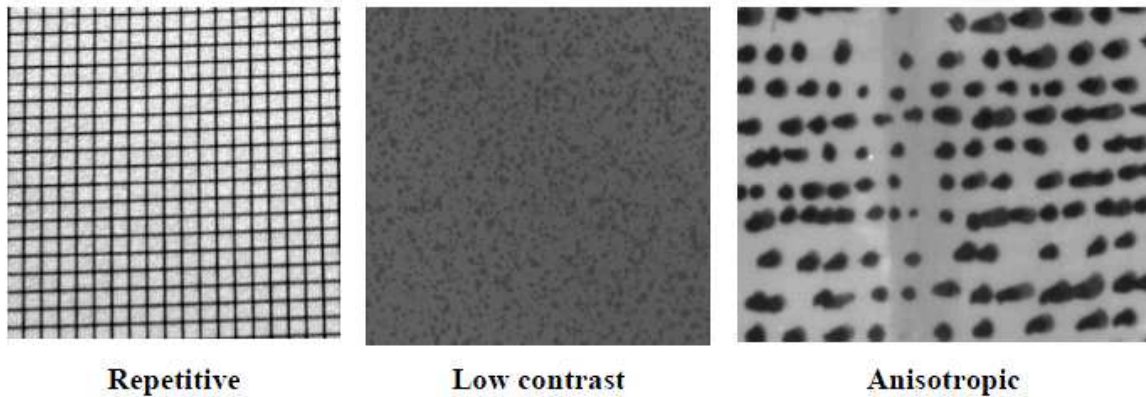


Figure 2.2 Example of patterns with proprieties to be avoided

### 2.2.1 Black vs. White

While we refer to these patterns as speckle patterns, the software only sees a contrasting field; the speckles themselves are not the analysis unit. So, white speckles on black can work as well as black speckles on white, or a high-quality pattern may consist of neither.

### 2.1.2 Techniques

The following paragraph describes some methods of how to make pattern [12].

#### Spray paint

The most common diffused technique for applying a speckle pattern in DIC is with ordinary paint.

Paint can be used with any intermediate-sized specimen that will not be chemically affected by the paint, nor stiffened by it. This is usually exploited for metal, ceramic, and composite specimens from 25mm to 1.25m.

Typically, the surface is coated with white paint in order to achieve the gradient between the background with the paint.

Coating has to be very light on the surface; that is why, heavy coats may lead to drips which, during deformation ,may give wrong strain information on the surface.

The speckle coat with paint should be applied after the base coat becomes at least tacky.

For smaller patterns, simply spraying the paint quickly past the surface in a sweeping motion can give a good speckle size.

For larger fields, larger blobs must be produced. This can be effected by either modifying the nozzle, or throttling the spray. One effective technique is to place the surface horizontally, and spray over it. If the spray nozzle is barely pushed down, large blobs will come out and fall on the surface; the finer mist will spray over the surface, leaving a good, coarse pattern.

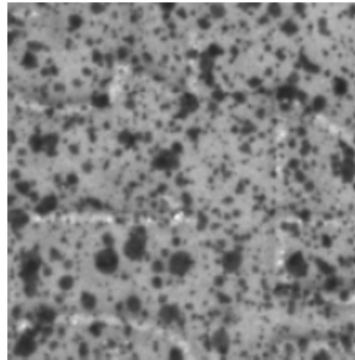


**Figure 2.3 Example of painted speckle pattern**

#### Toner

For very small specimens, a very fine pattern can be applied with toner powder. This method works well for small samples (smaller than 12mm). For this technique, the specimen should be coated white. Then, toner powder can be blown with a small lens blower, or by mouth, onto the surface.

#### Lithography

For extremely small specimens, patterns can be created with lithography or vapour deposition. The pattern below is chrome on glass and the field of view is 500 microns.

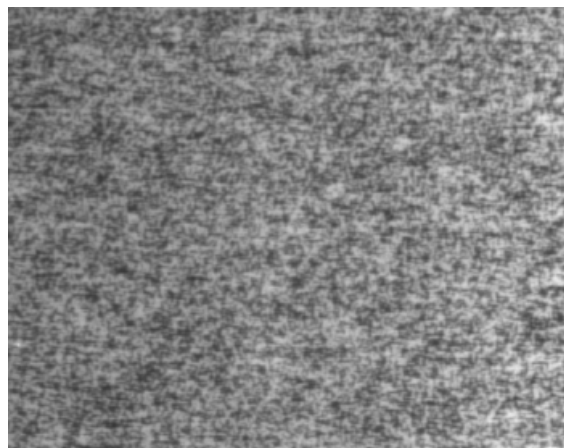


**Figure 2.4 Example of lithography pattern**

### Printing

For medium through large panels, printing of speckle patterns can be very effective. This technique has been used with specimens from (25mm) through (4m).

Raster speckle patterns can be generated and printed on paper or vinyl appliqué. For specimens that will strain, vinyl is recommended. The pattern may be generated in software; printed using a laser printer or commercial roll plotter; and applied to the surface. The pattern below was printed on a full-sheet laser label.

### Stencils

For very large specimens, a stencil can be employed to roll or spray a perfect speckle pattern. Stencils can be made from thin vinyl with water or laser cutting techniques.

### Ink

For some specimens, ink placed with a marker is a good technique. This technique affects the surface minimally, and allows measurement of very high strain. The ink can simply be dotted onto the surface with a marker. This technique can be very time consuming for larger specimens.

The pattern below was placed on a (12mm) wide dog-bone. The specimen is displayed before and after deformation; the correlation was successful at strains up to 400%.

### Grids

While grid patterns are neither necessary nor optimal for DIC, they may be used with caution. Initial guesses must be selected carefully; with a nearly-perfect grid, it is possible for DIC to find a good match that is actually off by 1 or more grid spacing. In addition, the subset size must be large enough that at least one grid intersection is always contained.

### Projecting

For shape measurements, a speckle pattern may be projected onto the surface using a computer and front projector. For this method, room light should be controlled to give high contrast.

Note that because a projected pattern does not stay with a moving surface, this technique is only useful for shape measurement. Displacements may not be accurately calculated.

### Titanium powder

Titanium powder of about 5  $\mu\text{m}$  particle size was mixed with plastic liquid (Collodion, 2% in amyl acetate) and then applied to the specimen surface. When the liquid was dried, a plastic film with random pattern was formed on the specimen surface.

It is very flexible to deform with the specimen and firmly stuck to the surface, even under very large deformations. The density of particle distribution on the surface and the thickness of the plastic film could be controlled by changing the particle density in the liquid.

### Metal film coating [23]

The process is used in nanoscale patterns onto polymeric and metallic materials. Thin films of metallic materials, including gold and silver, are applied on a surface through simplified UV photolithographic method. Then, exposing the piece in nitrogen atmosphere saturated (with a previous sampling heating), a creation of a random pattern occurs.

This technique gives good results in nanoscale deformation.

It can be made only in laboratory; its settling time is quite long and also its cost is expensive.

It is necessary to have specific equipments (photolithographic device) and computing resources to be performed.

### Electron-lithographic technique [13]

The electron-lithographic technique is used for measuring microscale and nanoscale.

Developed by Pinna [14], it consists of an electro-sensitive resin deposition and successively heating at 140  $^{\circ}\text{C}$  for 30 minutes in order to obtain the adhesion of the resin with the sampling.

Then, the resin is irradiated with the electron beam of a scanning electron microscope (SEM), following the pattern. The irradiated line is removed through a specific solvent (Figure 2.6c) and successively the surface is exposed electro-etched using a solution of 40%  $\text{HNO}_3$ . After chemical resin dissolution, the final result is a removal of a thin layer of metal on a sample in order to obtain a pattern.

This technique gives good results and it is controllable.

But it can be made only in laboratory; its settling time is quite long and also its cost is expensive.

It is necessary to have specific equipments and computing resources to be performed.

## Phases of electron-lithographic technique

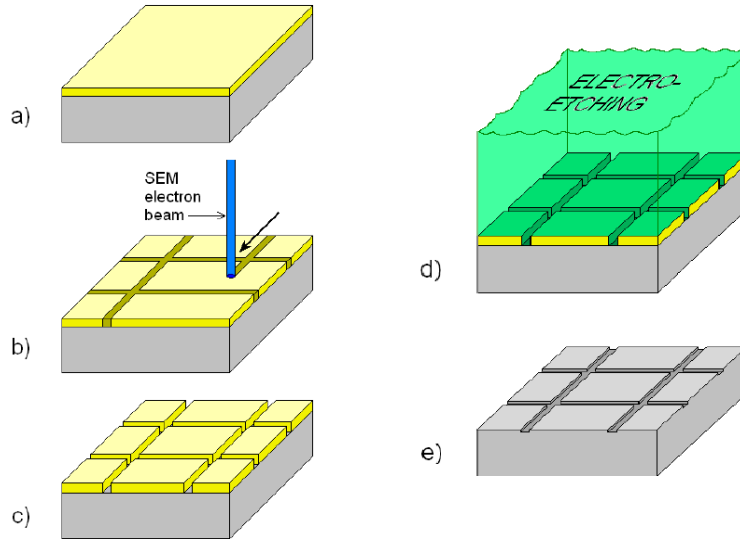


Figure 2.5 Electron-lithographic technique

## 2.2 Mean Intensity Gradient Coefficient

As it has already said in Chapter 1, a global parameter is taken into consideration to give a quality assessment of the entire speckle pattern [10].

Mean Intensity Gradient ( $\delta_f$ ) is defined as :

$$\delta_f = \frac{1}{W \times H} \sum_{i=1}^W \sum_{j=1}^H |\nabla f(x_{ij})| \quad (2.6)$$

Where  $W$  and  $H$  (in unit of pixels) are image width and height of an image,

$|\nabla f(x_{ij})| = \sqrt{f_x(x_{ij})^2 + f_y(x_{ij})^2}$  is the modulus of local intensity gradient vector considering the derivatives at pixel along  $x$  and  $y$  directions ( $f_x(x_{ij}), f_y(x_{ij})$ ).

Knowing that, the mean intensity gradient (MIG) is a global parameter strictly related with the local parameter SSSIG[8], it can be determine an approximate formula as

$$\sqrt{\sum_{i=1}^N \sum_{j=1}^N [f_x(x_{ij})]^2} \cong N \times \delta_f \quad (2.7)$$

With  $N \times N$  the subset dimension.

Taking fixed subset size, it has been seen that MIG varies only in inverse proportion with the bias error and the deviation standard.

Since the mean intensity gradient is a effective global parameter to assess the quality of the whole pattern.

In this work, only filtered images are used and so that the bias effect can be neglected[21]. In order to obtain that [22], propose the use of low pass image filters: such a filter can be applied during the image acquisition defocusing the camera optic or by means of digital filters on the acquired data.

Due to the strong relation between MIG and standard deviation, in our work, this last one will be calculated.

## Chapter 3

# Speckle pattern realization: an innovative technique

### 3.1 Purpose

Based on the modern DIC technology the object surface needs to be prepared in order to obtain a sufficient signal to noise ratio on the surface to be analyzed. The most popular state of the art techniques to produce the pattern include, spraying paint and coating [12].

These techniques are commonly accepted as good methods of pattern creation for DIC technology but, in terms of size position, they create a random patterns quite difficult to be controlled. This can bring some problems in local regions.

Indeed, a non-homogeneous blobs distribution may happen and alarming events, such as big drops formation in specific zones, create a low gradient of gray scale. In such zones the DIC code, has difficulty or, even can not calculate the exact value.

The chapter describes a new methodology of realisation of a pattern technique able to be controlled and easy to make.

The first preliminary considerations are that the process has to be easy, replicable, reliable and the final result should not depend on the human factor (for instance, different users who handle the airbrush may make different pattern results).

Moreover the technique should be flexible in order to change the scale blobs according to the different scale of utilization.

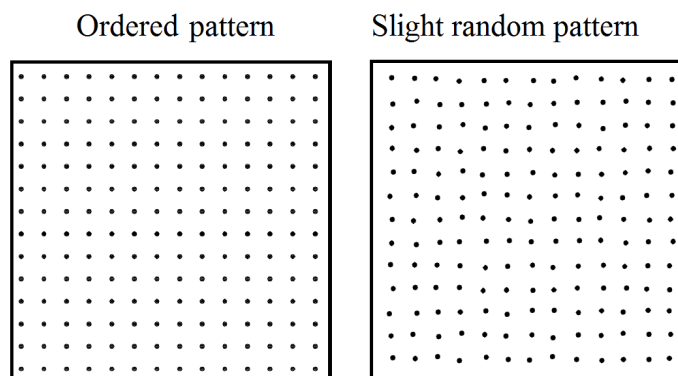


Figure 3.1 Ordered and slight random pattern

An aspect to remember is that we do not want to obtain an ordinate grid, but an controlled grid:

having a regular grid, might induce the ambiguity problem in the DIC computation; therefore, the points will have to be slightly randomized to indentify the uniqueness of each ROI( fig.3.1).

In this thesis a procedure to generate a predefined and controlled pattern is proposed.

### 3.2 How to make it

The used technique is based on a laser printing: briefly, the pattern is applied on all samples ironing on it a paper previously printed by common printer.

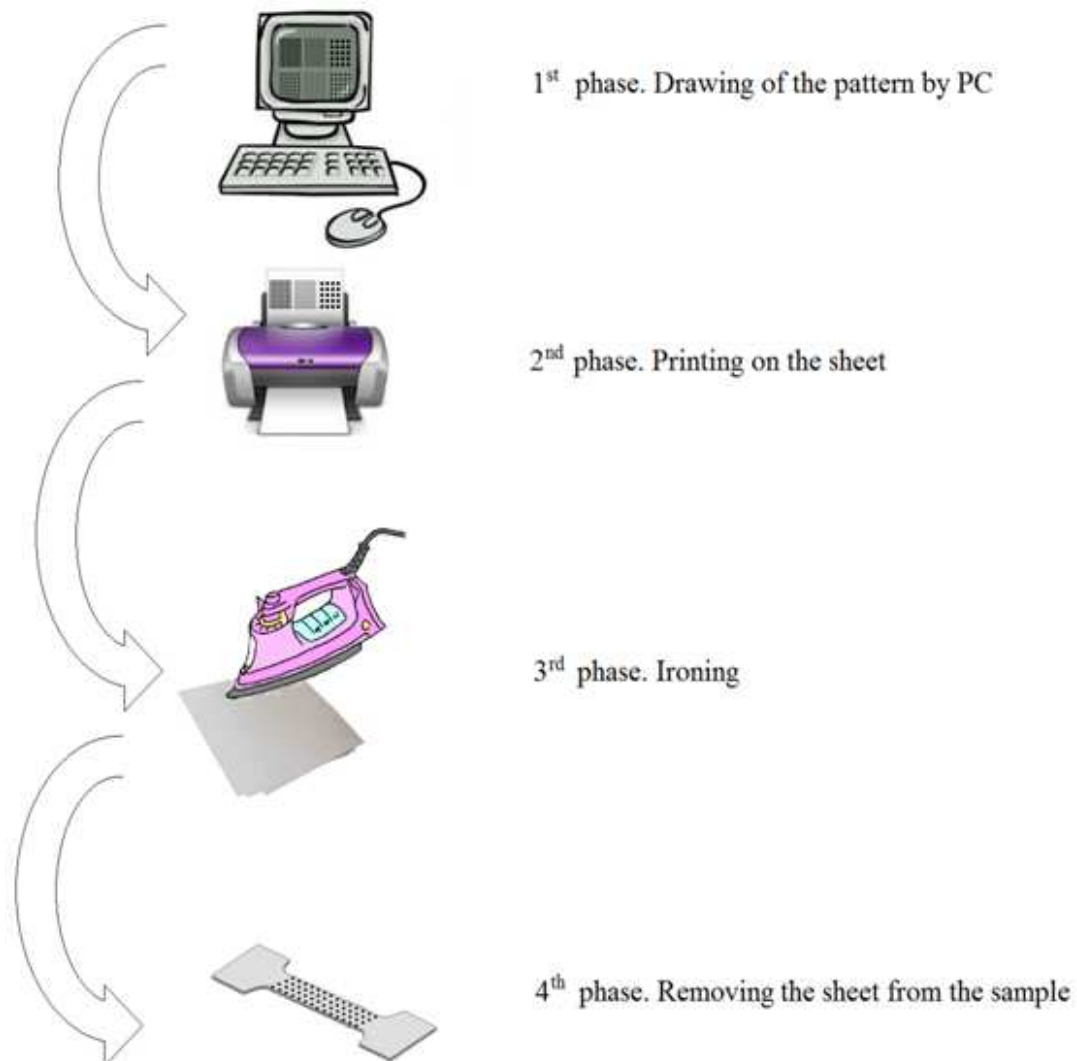


Figure 3.2 Summary of procedure

### **3.2.1 Choice of paper type**

First of all the appropriate kinds of paper for the purpose must be chosen. 3 types of papers are available.

The intrinsic proprieties of paper should be:

-It has to be a very good “ink transportation way” from the printer to the sample; in fact during the printing phase, the ink has to be deposited on the paper and then released on the sample.

- During the printing phase, the ink has to be deposited without being absorbed by paper.

- After printing the ink has a high temperature; thus the sheet must not be deformed or ,even worse, weld inside the printer.

-the sheet has to be smooth in order to have a major contact area with the metal surface where it leans.

The first tested material is the common printing paper.

The problem is that it absorbs a part of ink and then it becomes impossible to the ink to deposit.

The second type is photographic paper; it is a paper sheet covered with plastic on only one side.

In printing phase it is a good material but, unfortunately, the below problem rises up during the ironing phase:

The removing of the paper stuck to the sample after the electric iron can not be done manually; sample needs to be put inside a bowl of water so that the paper becomes softer and the removing becomes easier;

This operation works very good only with pattern having big circles (with diameter  $>0.8$  mm) but with smaller ones it is unpractical.

The last type of paper is a plastic sheet always used in photography.

The printing remains with an appreciate fining and with a good contrast between the spots and the background .

There is not even the problem of removing using water.

### **3.2.2 Application time**

First of all the tests are carried out on aluminium samples.

The time influences very much the final result:

If the piece is subjected for a short lapse of time , the pattern does not result homogeneous and o a part will be deposited on it.

On the contrary, for a too long time, since the high temperature reached from electric iron (about  $120$  °C), the plastic sheet may melt.

Unfortunately, time varies due to the dimensional size: bigger it is, much time it is requested to have an adequate temperature in order to melt the ink; moreover time also depends on the material and its own capacity of thermal diffusion.

By the way, for the used aluminium samples, the estimated time is around 2 minutes and 30 seconds.

### 3.2.3 Pattern shape and size

The best choice of the shape on improving the gradient of contrast for the DIC technique is circular shape: they are easier to be realised by a printer.

Another aspect to be considered is the technique behaviour due to different sizes and steps of dots in the pattern; for this reason a sheet is made with a series of dots with diameter from 0.05 mm to 1mm and with an incremental step of 0.05mm.

Actually the distance from the dots is not considered and so the dots are simply drawn so that they can not touch each other during the ironing.

For the following experimental test (see Chapter 5) the dot size wants to be further on decreased in order to work on small pieces. After that, an optimization of step is performed.

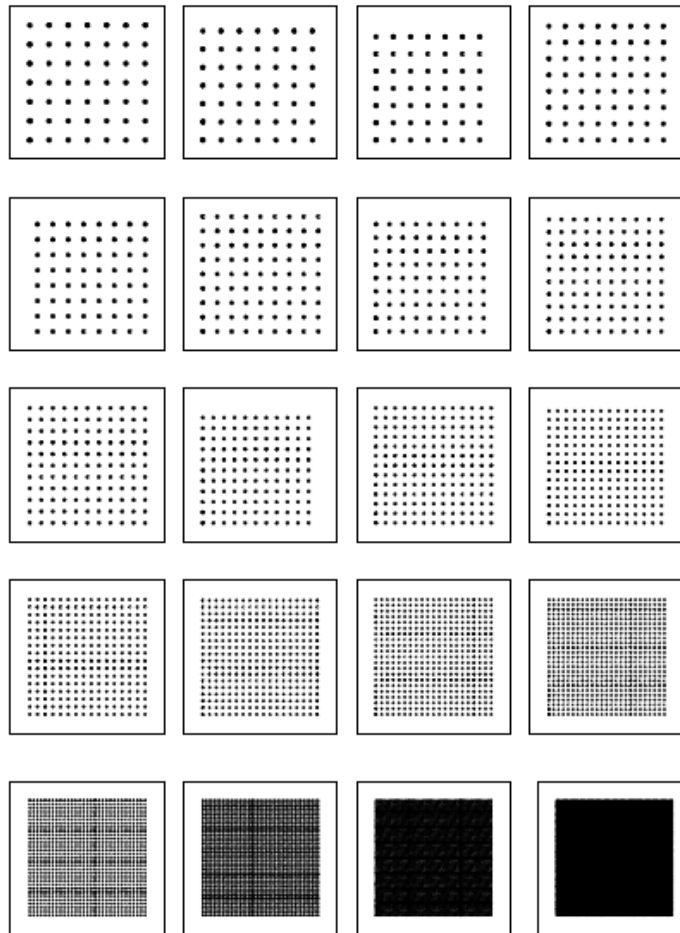


Figure 3.3 Series of pattern(diameters from 0.05mm to 1mm with step of 0.05)

### 3.2.4 Printing phase

The printer is a laser printer named Lexmark T652 dn.

In order to get the best result , some tests are done.

The first tests are done to optimize printer performance. First of all , default options are used:

The result gets better with circles having big dimensions; using a magnifying glass, a worsening with small size is noted.

Thus, “improvement of thin lines” option is chosen, obtaining an improving of the boundary in any dot; but there is not a substantial changing concerning the difficulty of printing small dots.

A further verification is performed changing the toner intensity.

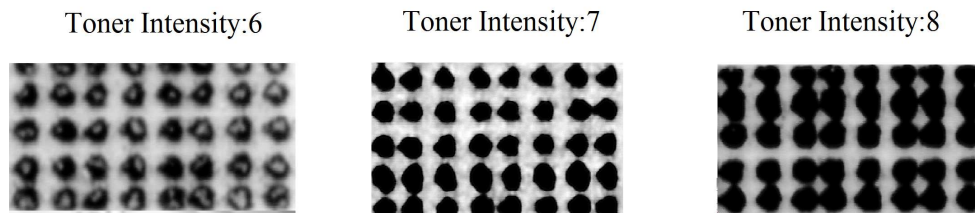


Figure 3.4 Proves at different intensity toner

As it can be seen, the best toner intensity for a pattern with small size is 7.

The last aspect to be observed is that during printing, in case the time that elapses between the tests is long, the toner has to heat every time.

If it is necessary to print only one sheet, it prefers to make two sequentially printings in order to have a better result in the second one.

(the ink is more liquid due to the previous sheet and so it uniformly deposits).

### 3.2.5 Application on the piece

For the ironing a common electric iron at the maximum temperature (around 120°C) is used.

Some notices need to be taken into account: it is preferable that the surface of deposition is straight as much as possible especially with big dimension dots; because they are more far-between and there is a possibility that some circles do not stick.

Another aspect to be kept in mind is to put a cloth between the electric iron and the sheet: the plastic tends to paste and melt on the hot plate making the dots transposition impossible.

Last thing, the surface has to have a low roughness because the plastic sheet can not follow the crest of the piece.

### **3.2.6 Contrast**

To make DIC working in the best way, ROI needs to be got with the contrast as high as possible (DIC works with the gradients); so that the best contrast of colors is obviously white and black. Generally the metallic surfaces have a grey coloration; in addition, as it has been already mentioned above, the surface must be smooth; but this makes it reflective.

For solving the problem, a white layer of enamelled paint is applied on the zone of the aluminium pieces.

This makes the area smooth but not reflective.



**Figure 3.5 Aluminium painted sample**

This solution does not give an efficient result: the pattern does not paste with the zone due to the paint.

Another solution is the utilization of titanium dioxide ( $\text{TiO}_2$ ): it makes the surface white, not reflective, it does not paste to the piece (it is a simply superficial deposit) and it can be removed easily using a cloth.

For the application of titanium dioxide a airbrush is used taking into account that the surface has to have an homogeneous coloration.

But also this technique can not exploit: the surface covered with titanium dioxide is just a light patina that can be removed with the slightest touch; with the ironing no blobs remain on the sample.

Hence other methods have been thought in order to avoid to interpose a foreign substance between the ink and the piece:

-One method consists of grinding the pieces and so making the application of small dots easier; but it makes the area too reflective (fig.3.6).



**Figure 3.6 Sample too reflective after grinding**

-Another method consists in heating the piece at relatively low temperature ( so that the intrinsic proprieties of material do not change); in this way a changing of coloration on the external surface is obtained.

Putting the samples inside an oven (some tests are done changing the temperature and reaching a maximum of 400 °C ( fig 3.7) the exposure time is really short.

The colour tends to yellow and therefore the contrast increases respect to grey.



Heating at 250°C

Heating at 400°C

**Figure 3.7 Colorations at different heating temperatures**

As it can be seen, the surface is still reflective and this solution is discarded.

Another solution is sandblast.

The piece becomes mat and there are not other substances to grasp the ink; the background is clear grey but sufficient for a good contrast with black. Moreover dots stick in any dimension.

Further advantages are a short setting time, a very practical and availability technique.

Therefore sandblast is the best method adopted for the purpose(before the ironing).

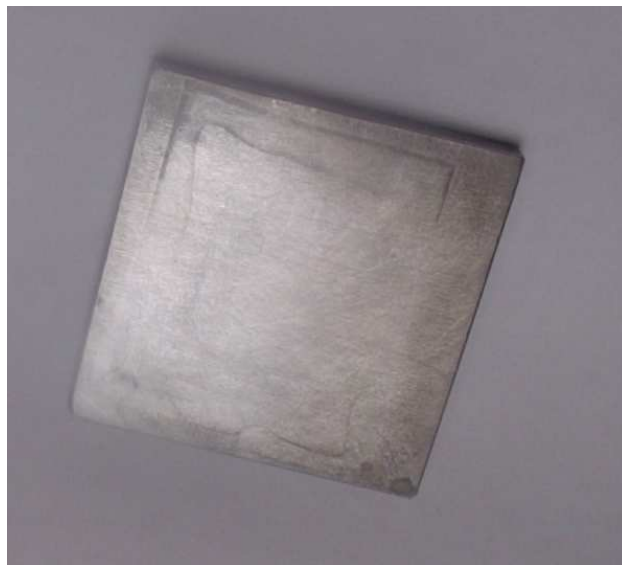


**Figure 3.8 Sample after sandblast**

### **3.3 Pattern improvement**

The minimum pattern diameter reached is  $\varnothing 0.1$  mm.

The application of Controlled Pattern Technique is performed on small pieces.

Therefore we want decrease the dots dimension and step, in order to use the technique in small applications.

The first idea is to employed a plotter instead of a printer in order to have a major resolution.

In fact, plotter can easily reach a 0.01mm resolution.

But the plotter has the inconvenience of using a different kind of ink that it is impossible to melt.

Another idea consists in lithography printing; this solution loses resolution especially with small dots and so also this is discarded.

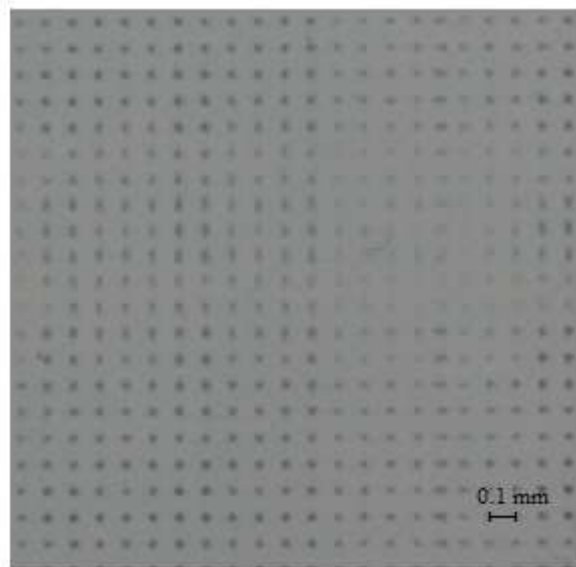


**Figure 3.9 Lithography printing**

After these attempts, an optimization of printing is carried out, most of all focusing on the drawing:

Until now, the pattern is realized by Matlab code and then visualized by Word Office software.

As it can be seen in fig 3.10 ,when the dimensions of circles become smaller, there is already a loss of information in the first step of the procedure (drawing).

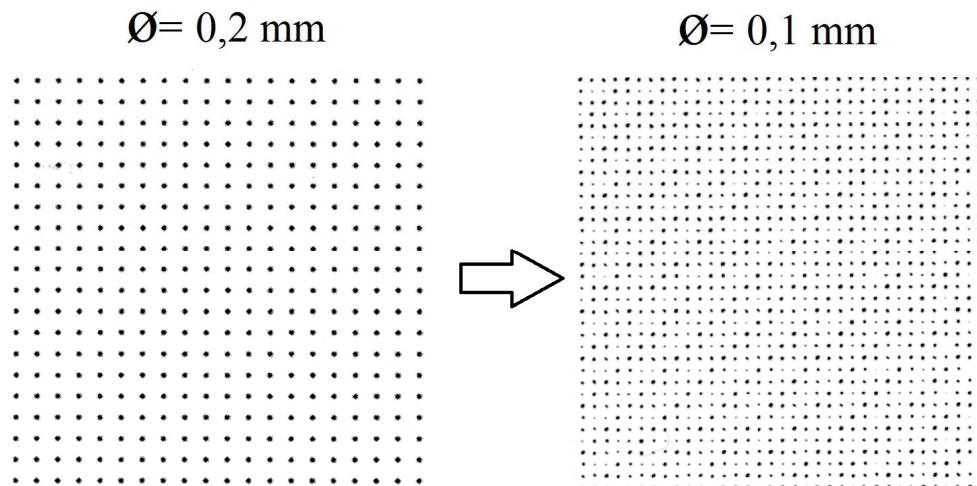


**Figure 3.10 Effects after dimensional reduction by Office Word**

This happens because Office Word is not a vector software.

### 3.3.1 Vector graphics

Vector graphics is a technique used in computer graphics to describe an image. In vector graphics the image is described by a set of geometric primitives that define points, lines, curves and polygons to which colors and even shades can be assigned. It is radically different from raster graphics as raster graphics images are described appropriately as a grid of colored pixels. The main advantages of vector graphics versus raster graphics are the following:

- ability to express the data in a form directly understandable by a human being;
- ability to express the data in a format that takes up less space than the equivalent raster;
- ability to arbitrarily enlarge the image, without leading to a loss of resolution of the image.

On the contrary, the main disadvantage of vector graphics versus raster graphics is that the creation of vector graphics is not an intuitive task as in the case of raster images. The vector programs have many tools to be fully exploited that require different skills.

The vector graphics, as defined by mathematical equations, is resolution-independent, while the raster graphics, if it is enlarged or displayed on a device with a resolution greater than monitor, loses definition. A line which runs transversely in a screen using the raster graphics is stored as a sequence of colored pixels placed to form the line. If we try to enlarge a section of the line we would see the individual pixels that make up the line. If the same line is stored in vector mode the line would be stored as an equation that starts with a point identified with initial coordinates and ends with another point defined with final coordinates.

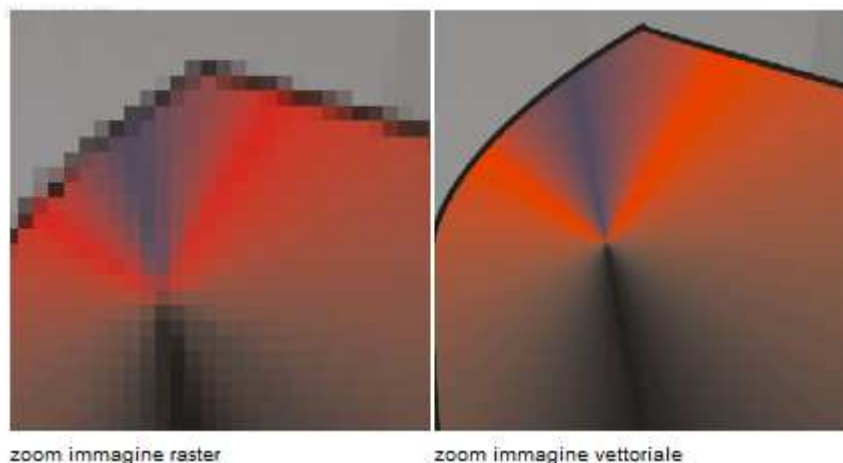


Figure 3.11 Example of raster and vector images

So the final solution is a drawing software (for instance Autocad) that permits not to lose information. Additionally using Autocad's tools a better quality of printing can be got increasing the resolution.

Printing comes out considerably improved and it is possible to have a grid with diameters of 0.05mm.

In reality the grid can reach diameters until 0.03mm but at this point the step becomes a problem.

### **3.3.2 Step Optimization**

The last point is to find, using the printer, the minimum realizable step with the minimum diameter.

In order to get the appropriated step, our hypothesis is that the points have not to link together; so that, the minimum step having this condition (where dots are not linked together) is our starting point.

A series of patterns are made ,changing the step and taking the diameter constant ( $\varnothing= 0.05\text{mm}$ ) .

After printing, an images acquisition is performed using a common scanner (resolution scanner: 4800 dpi) in order to analyze the obtained result.

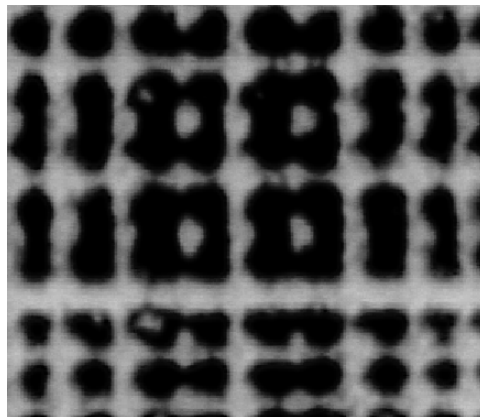


**Figure 3.12 Dots linked together**

The figure 3.12 shows an example of scanning image where dots are linked together.

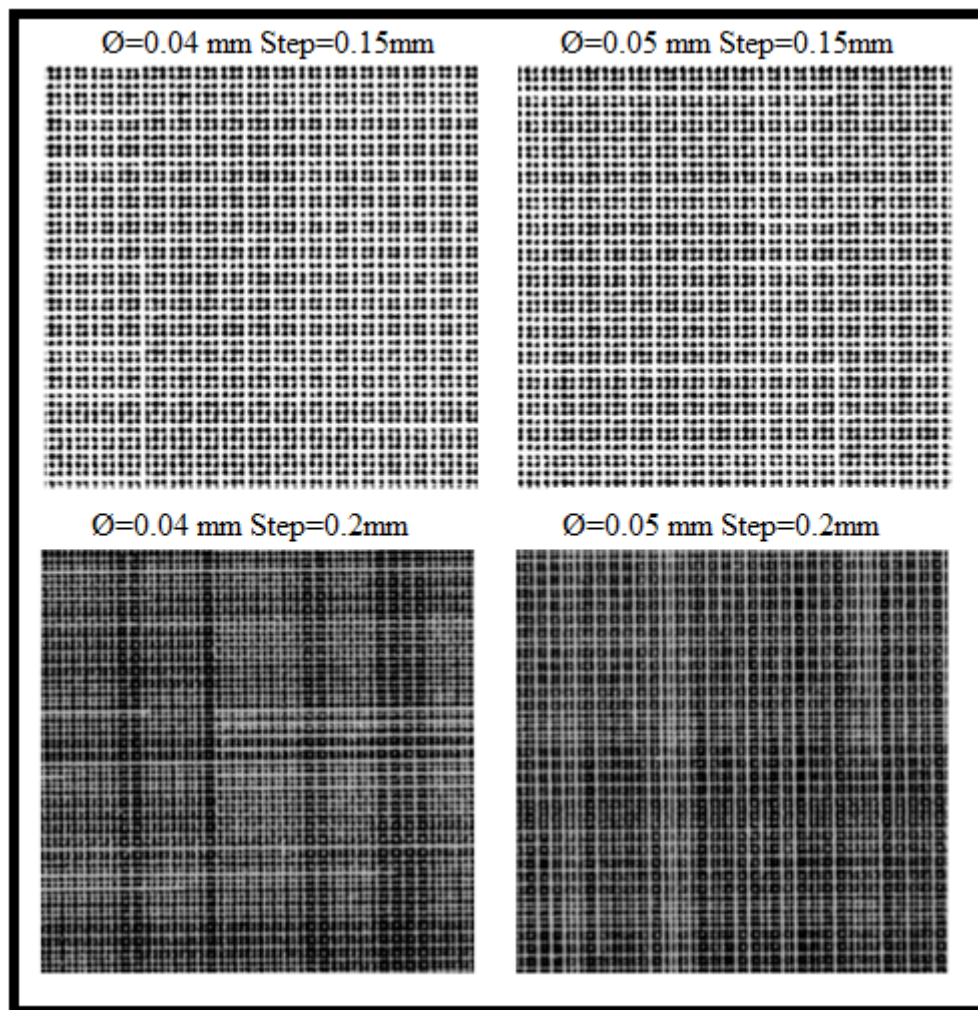


Figure 3.13 Pattern at different steps

As it can be seen in figure 3.13, the circles tend to join also with a big step (0.15mm of step with  $\varnothing$  0.05mm).

This because when the blobs dimensions become smaller and smaller ,the printer does not manage to maintain the order of scale 1:1(during the printing the ink is liquid and tends to spread).

Therefore the final result will not be the expected one.

### 3.4 Ironing and Printing analysis

A dimensional analysis is carried out in order to verify how different real final dimensions are compared to the designed ones.

In order to do that, it is needed to know how many millimetres correspond to one pixel of scanner.

With the aid of Sobel's filter, a blob analysis is performed for obtaining the scanner calibration and the variation of the dots size in printing and ironing phase .

#### 3.4.1 Blob analysis

Blob analysis consists in an evaluation of characteristics of our blobs , such as dimension size, circularity, position etc.

Due to the high contrast between the gray scale of background (approximately white) with the gray scale of the dots (approximately black), it is possible to distinguish each blobs.

Through an images binaryzation, the images are transformed in monochrome images.

A threshold value is needed in order to distinguish the two zones.

The threshold is defined due to have a correct estimation (high threshold level means a reduction of blobs dimensions and low threshold level means an increasing of blobs dimension).

In the program our threshold is 180 in a range from 0 to 255. The same value has been applied for all the analyses in order to obtain comparable results.

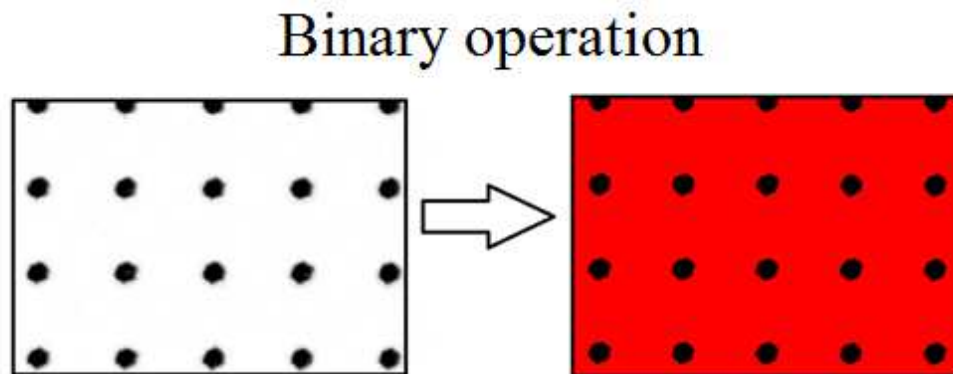


Figure 3.14 Example of Sobel's filter with 180 of threshold

NI VISION ASSISTANT software is employed for Sobel's filter:

In the images there is the presence of noise and dirty and during the analysis both can create some problems.

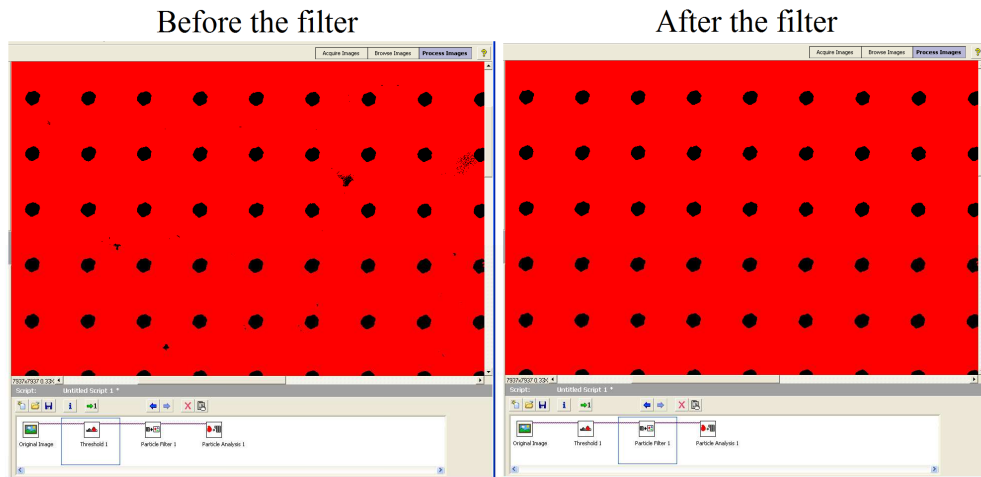


Figure 3.15 Cleaning of image

### 3.4.2 Scanner calibration

As it has already said before, It is necessary to know how many millimetres in the real image correspond one pixel in the same image acquired by scanner. In order to do that, two images ,where the dimensions of circles and their relatively step are known, are printed: one along the X axis and the other along Y axis.

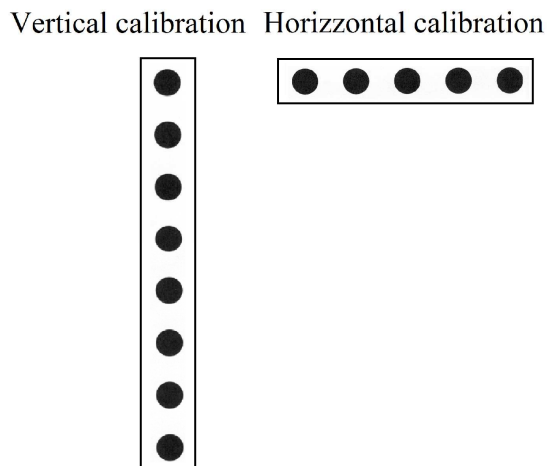


Figure 3.16 Images for scanner calibration

After the Sobel's filtering of images in figure 3.16 , an average of diameters is carried out in both the two directions; this is done to prevent a possible change of calibration values due to the motion optical head of scanner.

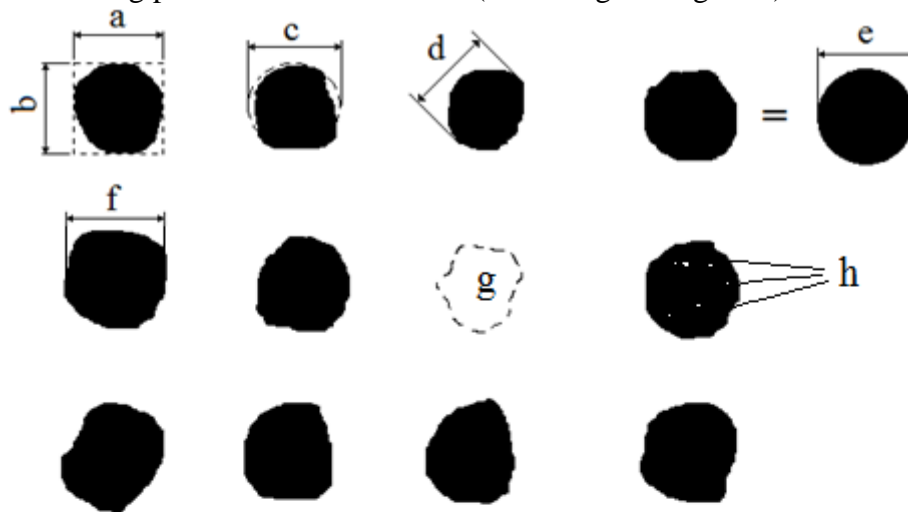
Vertical Image			
Waddel Disk Diameter[pixel]	Dmedio [pixel]	D [mm]	ratio[mm/pixel]
1945	1949,3	10	0,00513
1954,5			
1951,7			
1948,3			
1951,1			
1949,5			
1948,7			
1946			
Horizontal Image			
Waddel Disk Diameter[pixel]	Dmedio [pixel]	D [mm]	ratio[mm/pixel]
1944,9	1940,8	10	0,00515
1944,2			
1943,7			
1935,3			
1935,9			
Coefficient of calibration [mm/pixel]			
<b>0,00514</b>			

**Table 3.1 Scanner calibration**

In the table above, the calibration is equal along the abscissa and ordinate.

### 3.4.3 Data acquisition

After filtering, the data of dots are acquired in printing and ironing phases, considering particular characteristics (according the Fig 3.17).



#### Legend

- a: Bounding rectangular height
- b: Bounding rectangular width
- c: Circularity
- d: Maximum diameter
- e: Waddel disk diameter
- f: Mean diameter
- g: Number of missing dots
- h: Number of holes

Figure 3.17 Types of acquired data

**Waddel diameter's meaning:** it is the diameter of a circle having the same area of the surface taken into account.

The found data are:  
Printing Phase

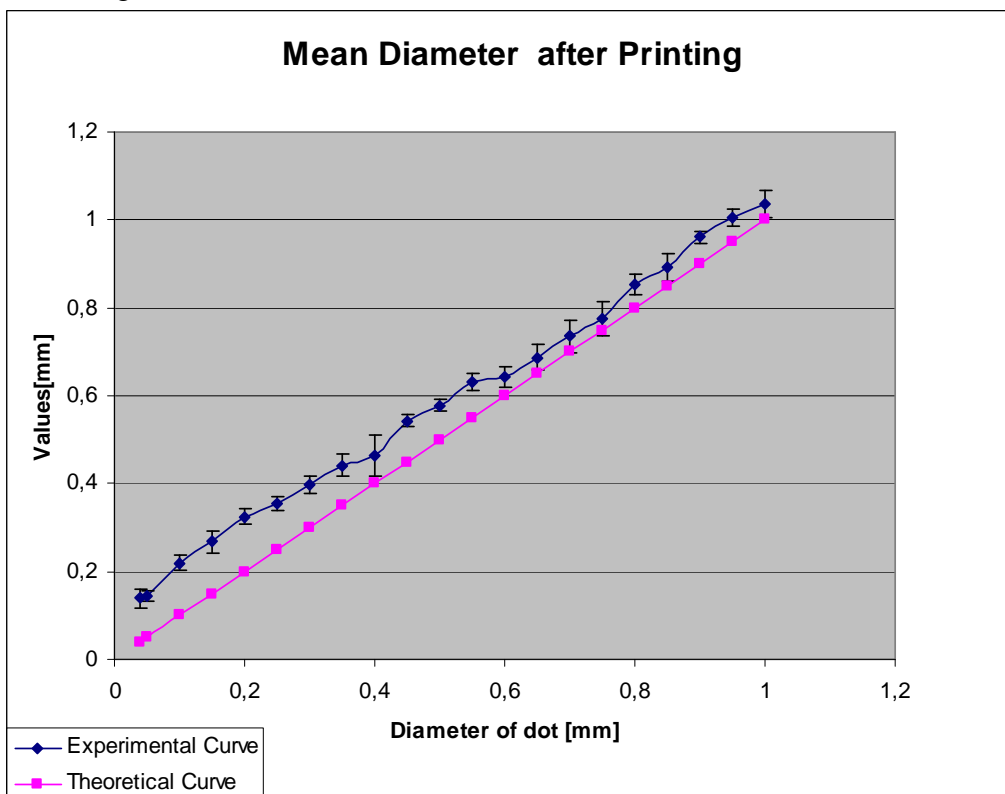


Figure 3.18 Mean diameter after printing phase

The graph above represents the trend of mean diameters after printing with its standard deviation (the blue curve) respect to the designed diameters (the pink curve).

As it can be seen, all the samples the real curve is higher than the theoretical one; in particular, the offset is considerably higher for small dots (especially if it is considered the percentage of error):

For instance, the theoretic diameter of 1mm results now 1,03mm and so there is a variation of 3%.

On the contrary, in the case of 0.05mm, the result is around 0.14mm with a variation of 180% from the drawing.

The conclusion is that the printer with small pattern can not respect the dimensions and this has to be kept in mind for future employment.

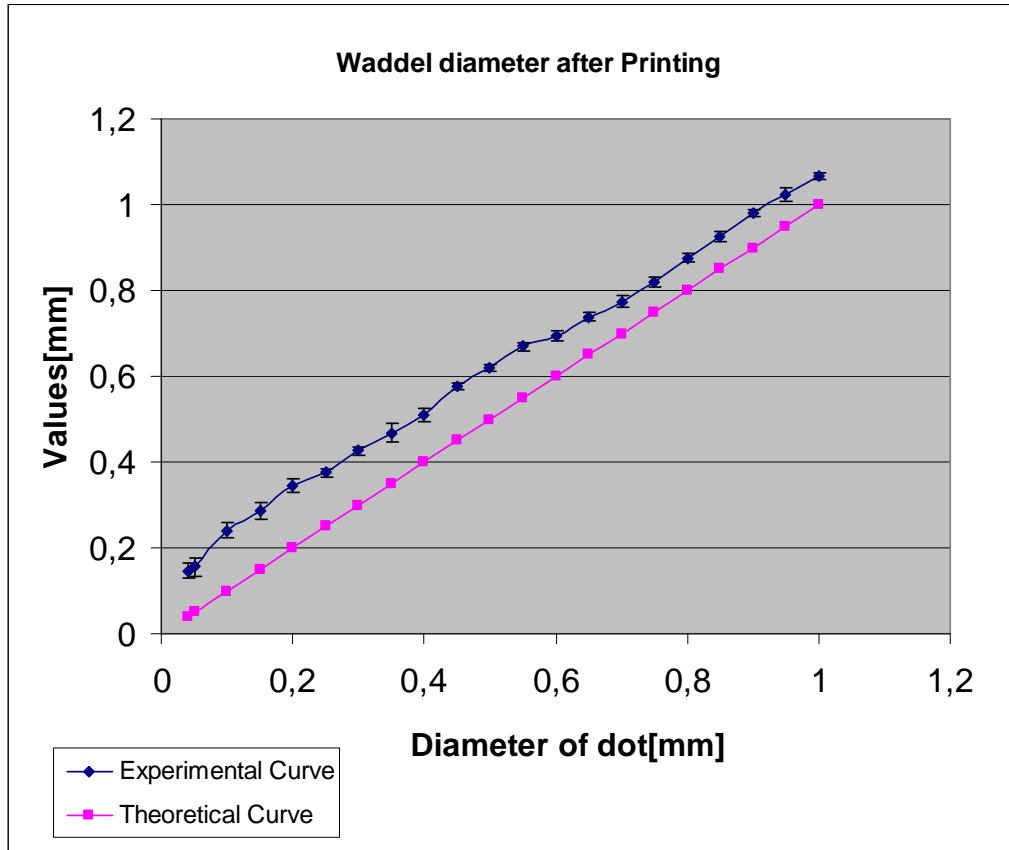


Figure 3.19 Waddel diameter after printing phase

The graph above represents the Waddel diameter; as in figure 3.19 ,the printed dots are bigger than the theoretical diameter. For diameter until 0.6 mm, the absolute difference is considerably higher than the others.

Based on an observation of the laser printer, the dimension could change according to horizontal or vertical direction. So a verify is carried out: on the graph below, the green and blue curves display the trend according to X and Y orientation. The conclusion is there is not a significant difference.

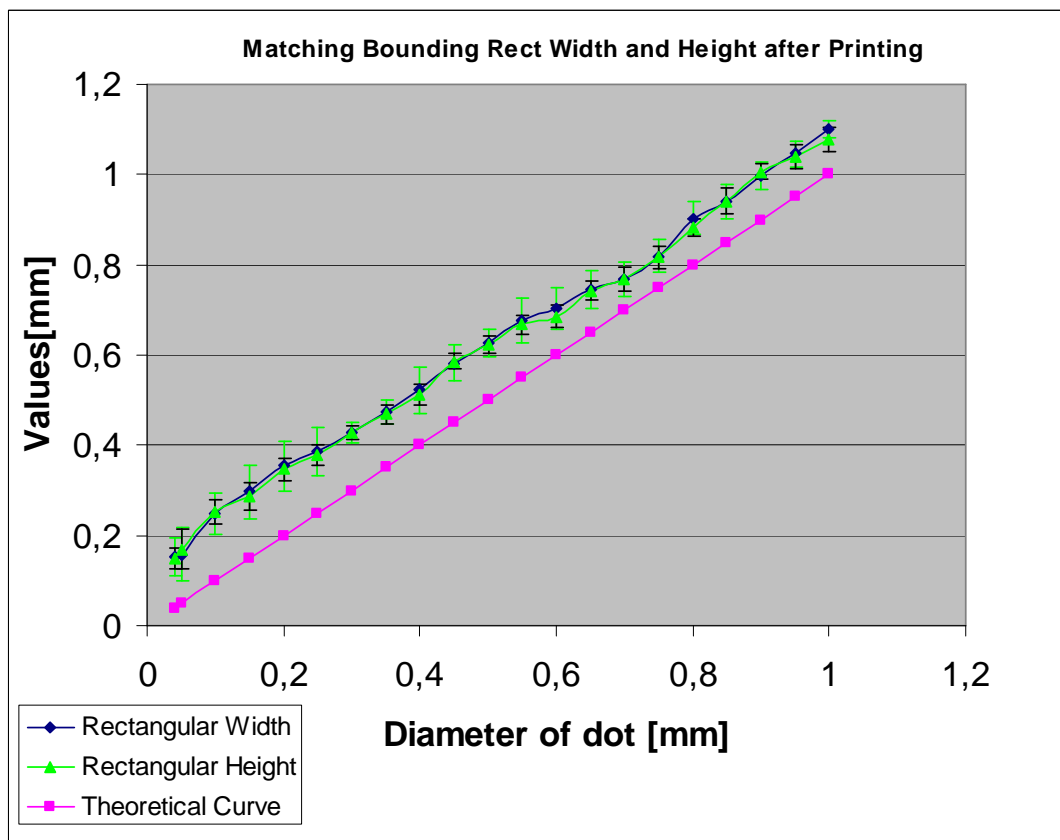
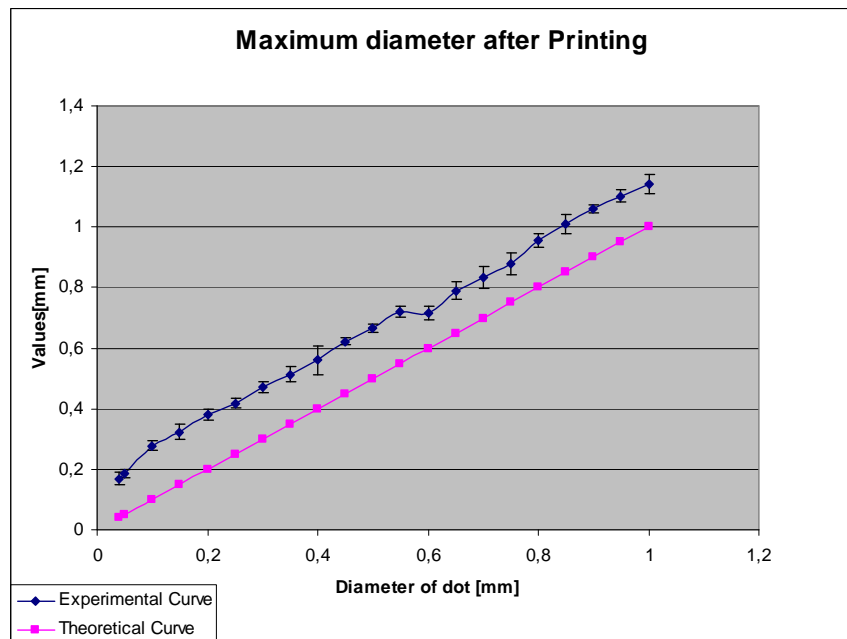


Figure 3.20 Matching rectangular width and height in printing phase



**Figure 3.21 Maximum diameter in printing phase**

The graph above represents the trend of maximum diameters after printing with its standard deviation (the blue curve) respect to the designed diameters (the pink curve).

As the mean diameter graph( fig 3.21) shows, all the samples of the real curve are higher than the theoretical one.

Around to 0.6mm diameter, there is a big variation of offset between the real and theoretical curve.

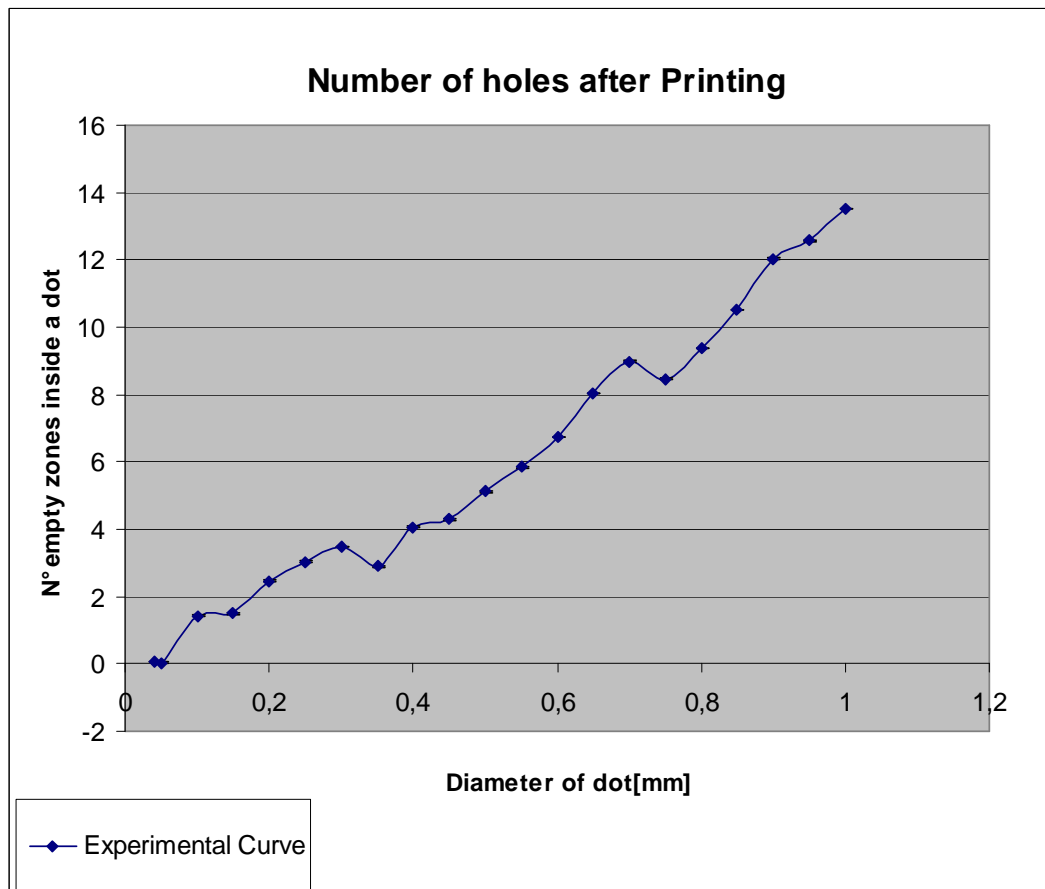


Figure 3.22 Number of empty zones in printing phase

The graph represents the number of “empty/white zones” inside one blobs. As it can be seen, Increasing the dimension of diameter size, the number of “white zones” is higher. That is why, higher area dots means more probability to have empty zones.

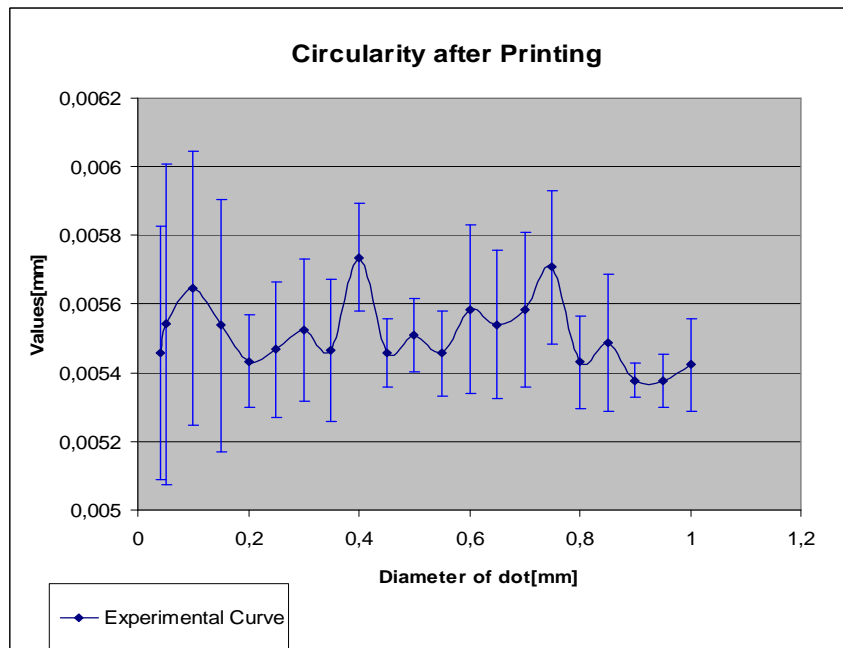


Figure 3.23 Circularity in printing phase

As it can be seen in figure above, the circularity is approximately constant for all the diameters; the circularity goes from 0 to 1 where 0 represents the best situation and 1 the worst one and in our test it is around 0.0055. One aspect to observe is that the standard deviation is higher for small dots.

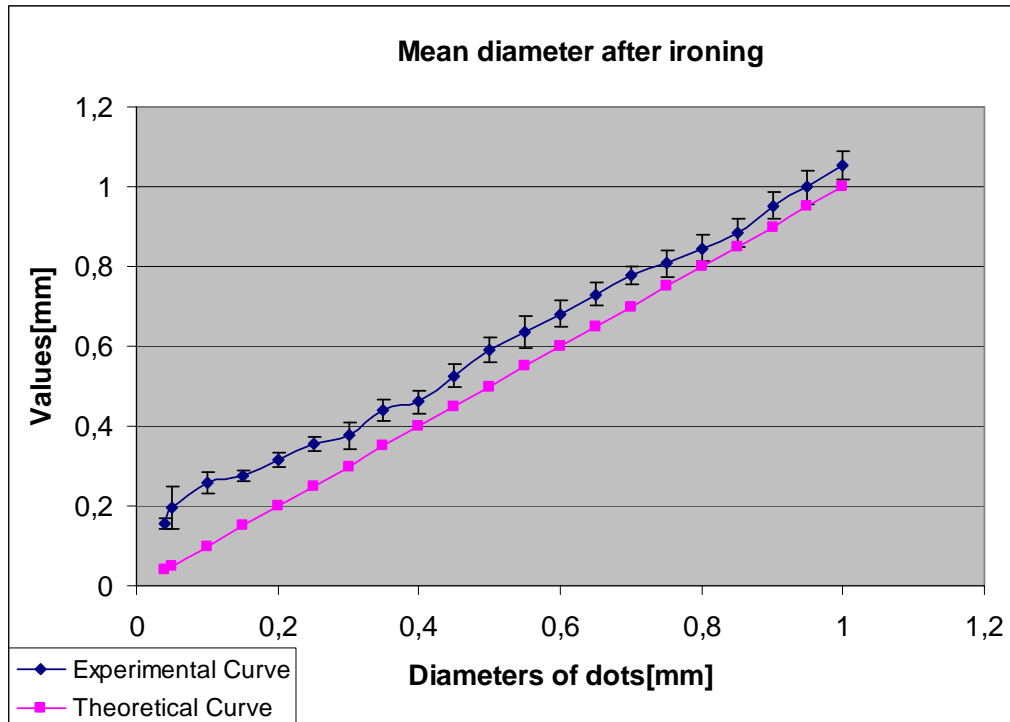
Ironing phase

Figure 3.24 Mean diameter after ironing

After ironing, the mean diameters are acquired; as shown in figure 3.24, the real dimensions are bigger than the drawing ones (the same happens during printing phase).

Comparing to the mean diameter after printing, in this case, there is not a presence of an evident diameter variation at  $\varnothing=0.6\text{mm}$ .

So that, the ink quantity varies correctly according the size blobs, but in printing phase there is a higher ink spread for smaller blobs, probably caused to the printer itself.

The difference increases with the decreasing of size; observing the smallest dots (0.04 mm and 0.05 mm), the final reached result after ironing is completely different from the estimated one (0.13 mm and 0.15 mm).

In conclusion, with the used printer, the smallest reachable dot is 0.13-0.15mm.

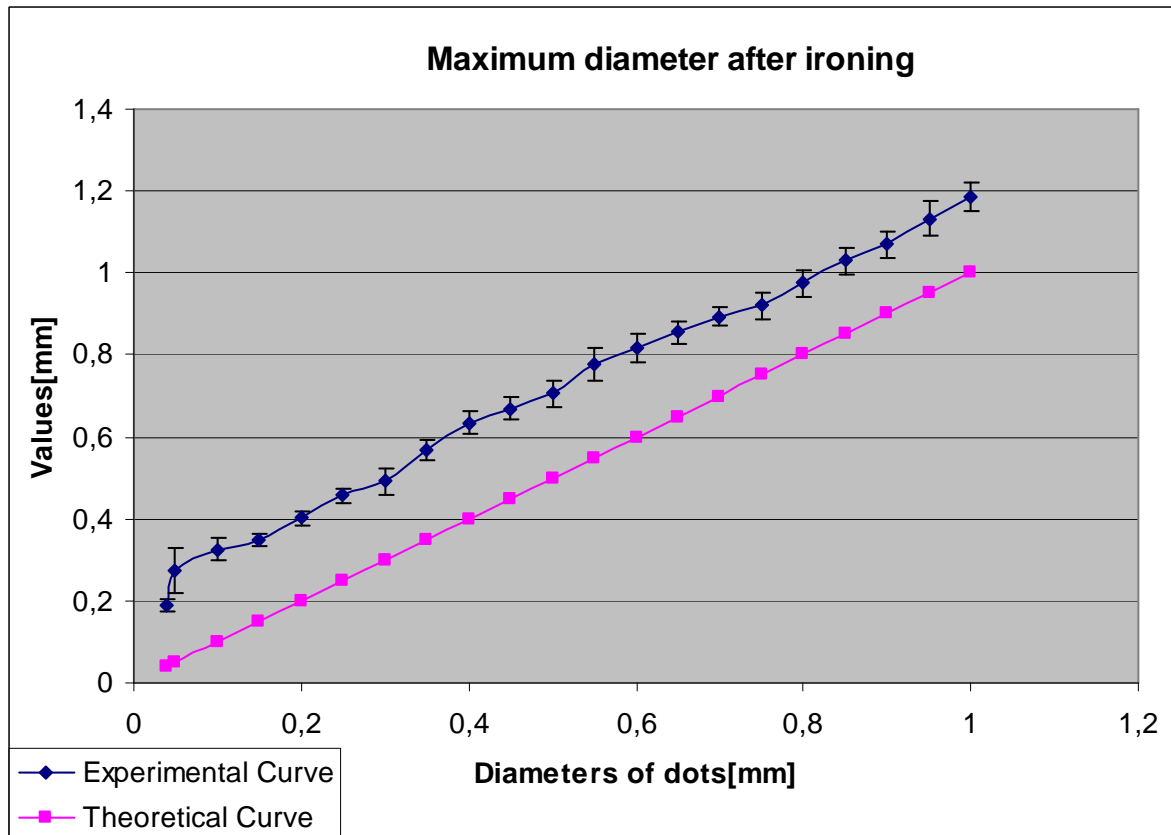


Figure 3.25 Maximum diameter after ironing

The graph above represents the trend of maximum diameters after printing with its standard deviation (the blue curve) respect to the designed diameters (the pink curve).

As the figure 3.25 , matching the maximum diameter after printing with the ironing one, the presence of diameter variation at  $\varnothing=0.6\text{mm}$  is disappeared.

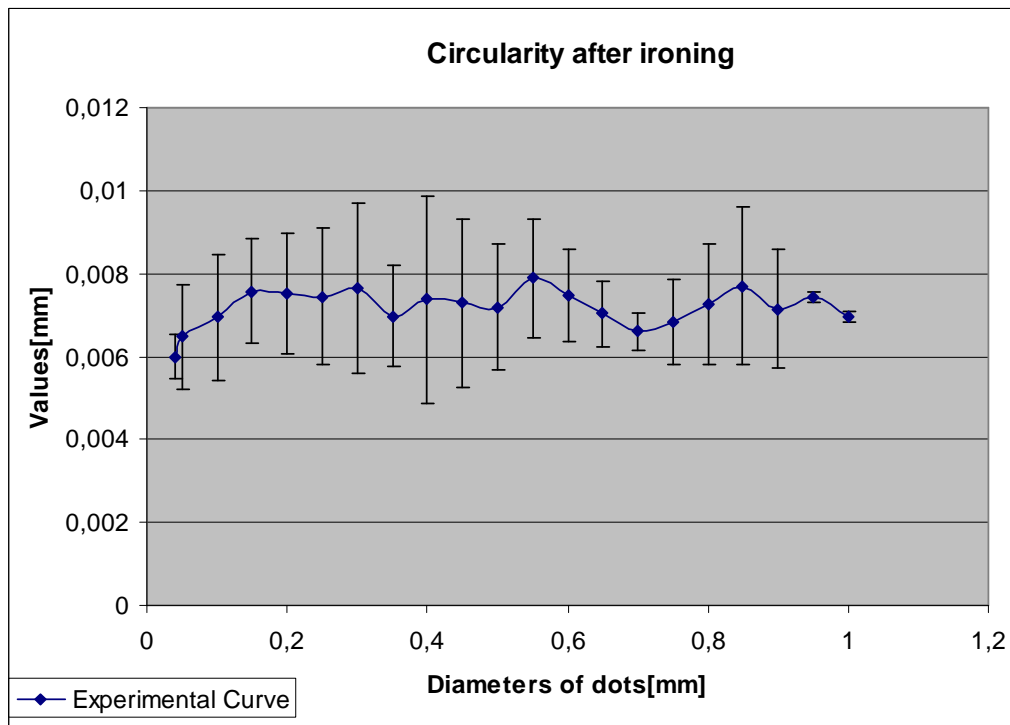


Figure 3.26 Circularity after ironing

The circularity remains more or less constant for all diameters; respect to printing phase, the circularity gets worse (from 0.0055 to 0.007) but, in any case, the value is acceptable.

The number of holes after ironing sensitively decreases:

for instance, in case of 1mm diameter , there are 13.5 “white zones” in printing phase and 0.12 in ironing phase. Therefore, there is an improvement from ink spreading point of view.

Moreover , after 0.6 mm, a stabilization of number of empty zones is denoted.

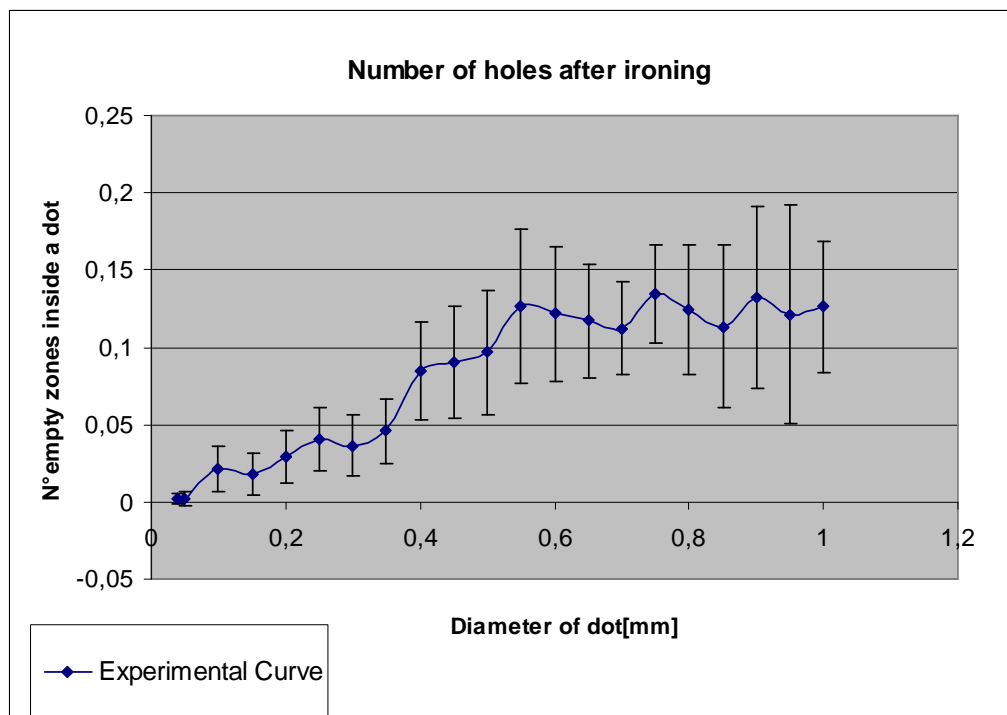


Figure 3.27 Number of “white zones” after ironing

A particular focus:

In printing phase we have not lost any dots in any size; on the contrary, in ironing phase, the number of missing dots is very aleatory (i.e. it depends a lot of printing modality).

A comparison between ironed and printed diameter is carried out. It can be seen that the circles tend to become smaller after ironing for all sizes with the exception of the smallest ones: in this case there is an enlargement of dimension. (when in graph the blue curve passes the pink line)

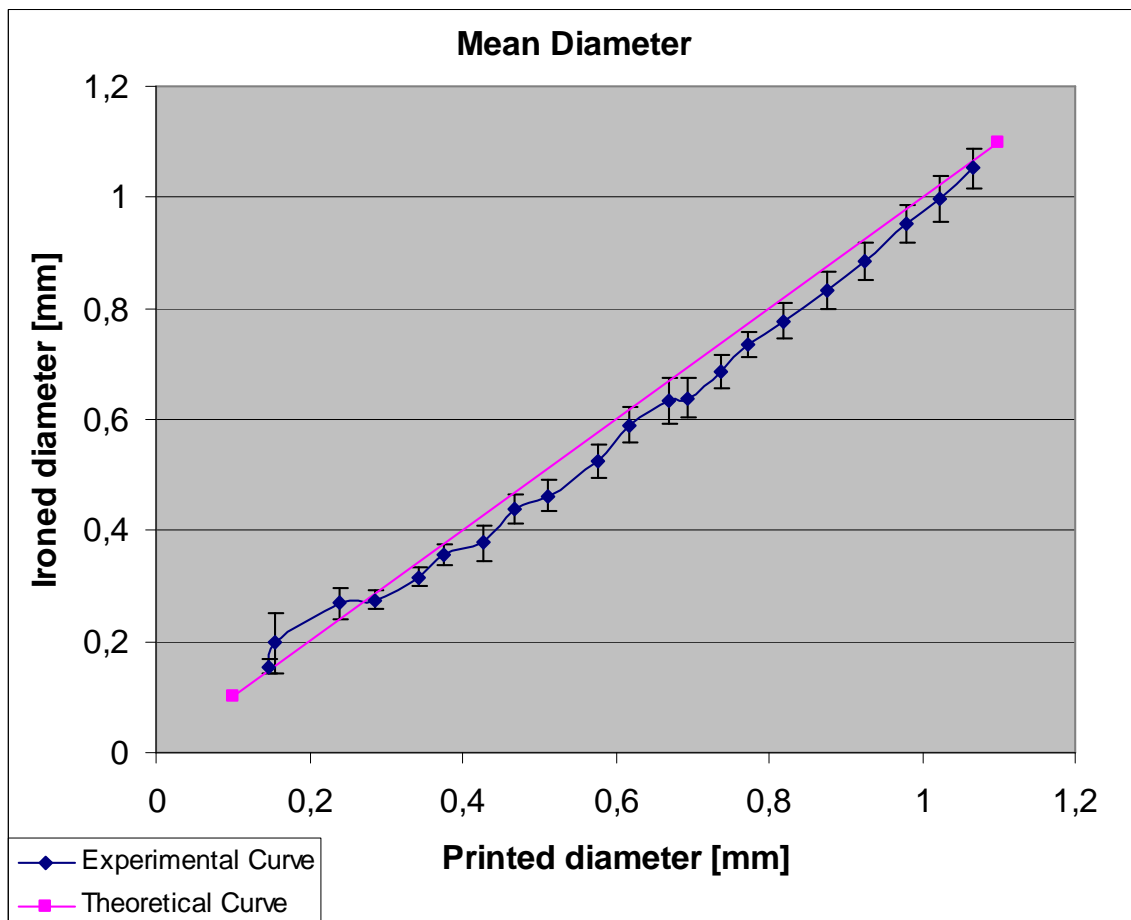


Figure 3.28 Matching ironing and printing diameter

### 3.5 Conclusion

In this chapter an innovative technique to produce a surface pattern for DIC is proposed.

The main issues that need to be considered in the preparation of the speckle pattern are:

- During the creation of small size blobs on the paper, the performances of the printer must be considered in order to avoid problems during ironing.
- To obtain a reduction of size, the unique limitation is the printer.

The advantages of the Controlled Pattern Technique are:

- the excellent uniformity of dots distribution on the considered surface;
- the possibility to choose dots dimensions;
- the easy application modality;
- the availability to reach small “controlled” size;
- no usage of extraneous substance between the ink and the metal surface;

In case of applications that request small blobs size, actually, the possible realizable minimum pattern is 0.05mm of diameter with a step of 0.2 mm (in printing phase), which in ironing phase, becomes 0.13mm of diameter with a step of 0.2mm.

This makes the technique suitable for standard small-medium size specimen (10-500 mm, i.e. commonly tested on a tensile machine).

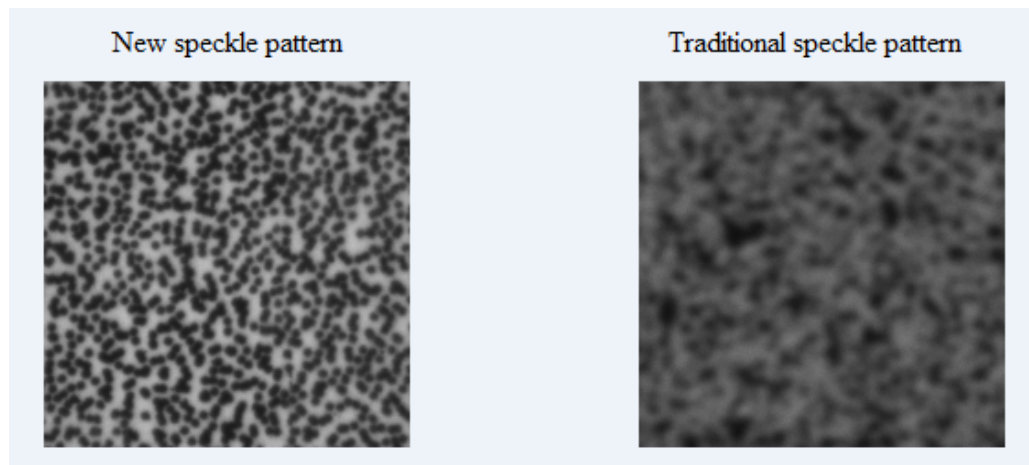


**Figure 3.29** Comparison between the new speckle pattern with a traditional one (airbrush)

Nowadays, in order to obtain such controlled pattern, the unique method is an utilization of a stencil (refer to Chapter 2).

But stencil technique has a series of drawbacks:

- It is expensive due to the stencil cost production and lead time.
- It is not flexible because the holes dimensions are fixed and they cannot change according to the requests.
- It needs time to make it from external manufacturing firm.
- It needs to use more times the stencil if the surface is big; indeed, the pattern appears somewhat regular creating non homogeneity colour distribution (fig.3.20).

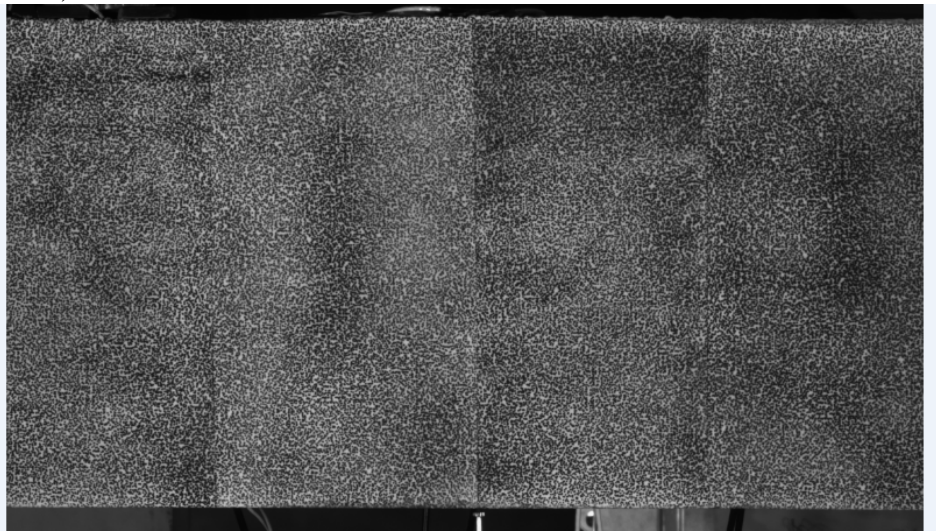


**Figure 3.30 Pattern created by a stencil more times**

-It can not reach smaller dimensions than 0.5 mm (make smaller , the colour tends to join between the holes under the stencil).

For this reasons , on metal pieces , our technique of ironing of a controlled pattern results surely the best.

## **Chapter 4**

### **Evaluation of speckle pattern optimization**

In this chapter it is explained how different types of pattern may give different results in terms of accuracy.

We want to observe that the errors of measured displacements using DIC are related to the quality of the speckle pattern, without considering subset size, overlap, types of DIC criteria , position of initial guess, shape interpolation function.

For doing so, the mean intensity gradient coefficient [10] is used for giving us a parameter of qualification when there is a differentiation of pattern.

With normal techniques of realization of speckle pattern(i.e. airbrush), is impossible to have pre-established blobs size.

Actually, with our possibility of a creation of a “controlled pattern” , it can be verified that an optimal pattern exists in order to obtain the best gradient and indeed the best result.

#### **4.1 Preliminary procedure**

A test is performed, in order to evaluate the changing of final results at different pattern types using DIC software.

A known imposed motion is carried out to a pattern series.

Different patterns are printed on a sheet (fig 4.5).

In order to gain the gradient level as higher as possible, blobs have to remain separated during the pattern creation.

Considering the hypothesis cited before, the calculation by DIC software is performed finding the deviation standard and the average of the imposed motion in each pattern types. Then, we verify if there is a variation of accuracy according the pattern differentiation.

For making so, a parameter called MIG coefficient is employed in this work; MIG coefficient is an operative global parameter for quality assessment of the speckle patterns applied in digital image correlation (refer to Chapter 2).

The choice of pattern sizes is taken referring to the graph in figure 4.4 , where the mean intensity gradient (MIG) changes according the diameter and step.

### 4.1.1 Realization of MIG graph

As it has already mentioned in Chapter 2 , the mean intensity gradient parameter ( $\delta_f$ ) is calculated as:

$$\delta_f = \sum_{i=1}^W \sum_{j=1}^H |\nabla f(x_{ij})| / (WxH) \quad (4.1)$$

Where W and H (in unit of pixels ) are image width and height of an image, and

$$|\nabla f(x_{ij})| = \sqrt{f_x(x_{ij})^2 + f_y(x_{ij})^2} \quad (4.2)$$

is the modulus of local intensity gradient vector considering the derivatives at pixel along x and y directions ( $f_x(x_{ij}), f_y(x_{ij})$ ).

In order to achieve the grey-scale gradient as higher as possible, the blobs inside the pattern have not to join together. Furthermore, each subset in the image has to be identified with uniqueness matching with other subsets. So that, blobs have to be created with a slight randomizing respecting to an ordered blobs grid (fig.4.1).

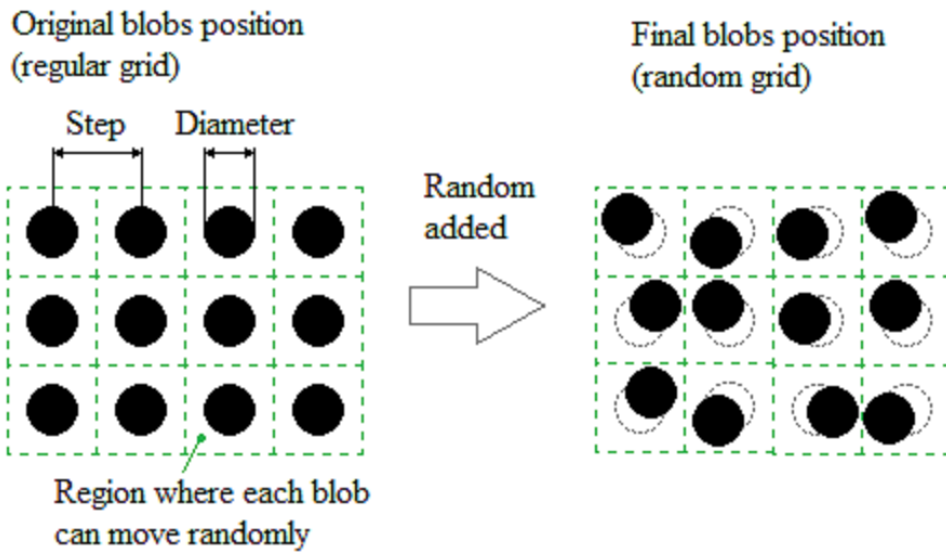


Figure 4.1 Randomization of the pattern

Indeed, each blob is created inside the respective region without crossing the border (the green dashed line).

Hence, the random position value for each blob always has to respect the following formula:

$$Rand.pos. < \left( \frac{Step - Diameter}{2} \right) - 1 \quad [pixel] \quad (4.3)$$

Before the MIG coefficient calculation, a problem rises up during the blob circles realization:

In the real world, blobs are perfectly circular; on the contrary, in digital images they are converted in pixel and so that, there is a blurring of grey-scale on the contour of each blob; this is more evident especially in case of small blobs size where the “boundary ring” is more dominant respect to the entire blob (fig. 4.2).



**Figure 4.2 Blurring in the boundary in case of small and big blob**

For solving this the problem, dots size is increased 10 time respect to the original dimension(i.e. taking a case with dots having 4 pixel diameters becomes 40 pixel); then a filter is employed for avoiding aliasing.

Successively, the dots are downsampled, coming back to the original dimension. Then, knowing from literature that the analysis improves with a filtering of images[15], a Gaussian filter is used ( $\sigma=1$ ) in order to make the blob slight blurred.

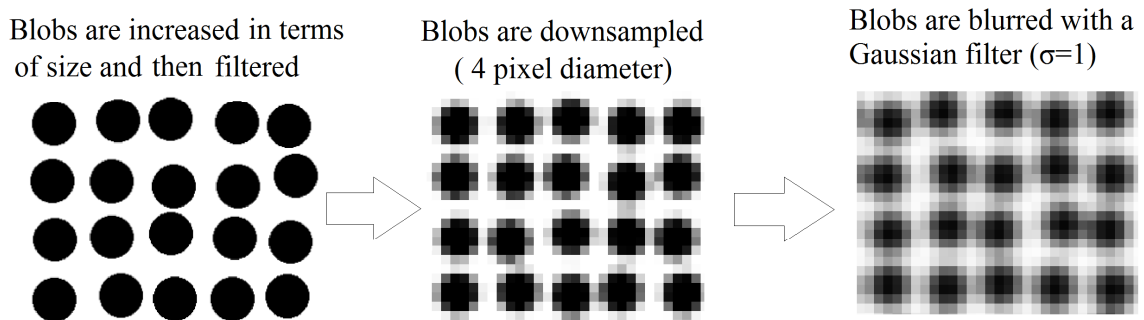


**Figure 4.3 Pattern generation with blobs at 4 pixel diameter**

Patterns generation with different blobs sizes and steps are made and MIG coefficient is calculated.

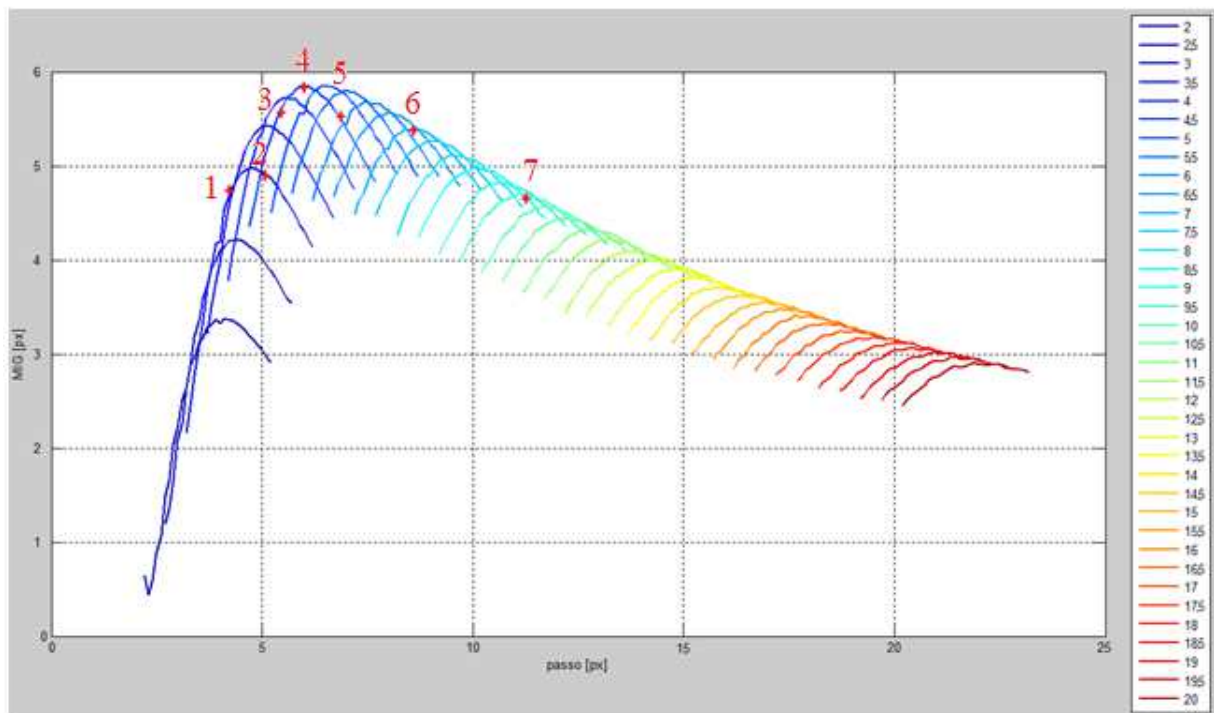


Figure 4.4 MIG graph

The obtained graph represents the variation of MIG coefficient according the blob steps and diameters.

As it can be seen, each “bell graph” is the variation of MIG parameter changing the step, maintaining constant the diameter.

According the whole graph, the best pattern type is 'Ø4.5 p6'; we observe that, for smaller diameters, the gradient decreases sensibly with the reduction of diameters size; on the contrary, for bigger diameter the decreasing is smoothed.

Due to the high number of pattern types, only some points are considered and successively analyzed.

Some samples are picked in “theoretical optimal zone”(the zone closes to the best pattern type) and others in worse zones before and after the “theoretical optimal zone”.

In the graph the chosen points are marked in red.

Remember that, the blobs in each pattern have a slight random position (otherwise during the analysis, we could have problems with the ROI recognition ).

The chosen speckle patterns are:

Pattern types sample	Diameter Ø [px]	Step [px]
No.1	3	4,3
No.2	3	5,1
No.3	4,5	5,3
No.4	4,5	6
No.5	4,5	7
No.6	7	8,6
No.7	9,5	11,1
No.8	Random	Random

**Table 4.1 Blobs types**

The eighth pattern is a kind of pattern used in previously DIC tests which has been created without considering the hypothesis above mentioned. In this work, this pattern kind is called “Random image” and it will be used during a comparison of accuracy with the other patterns.

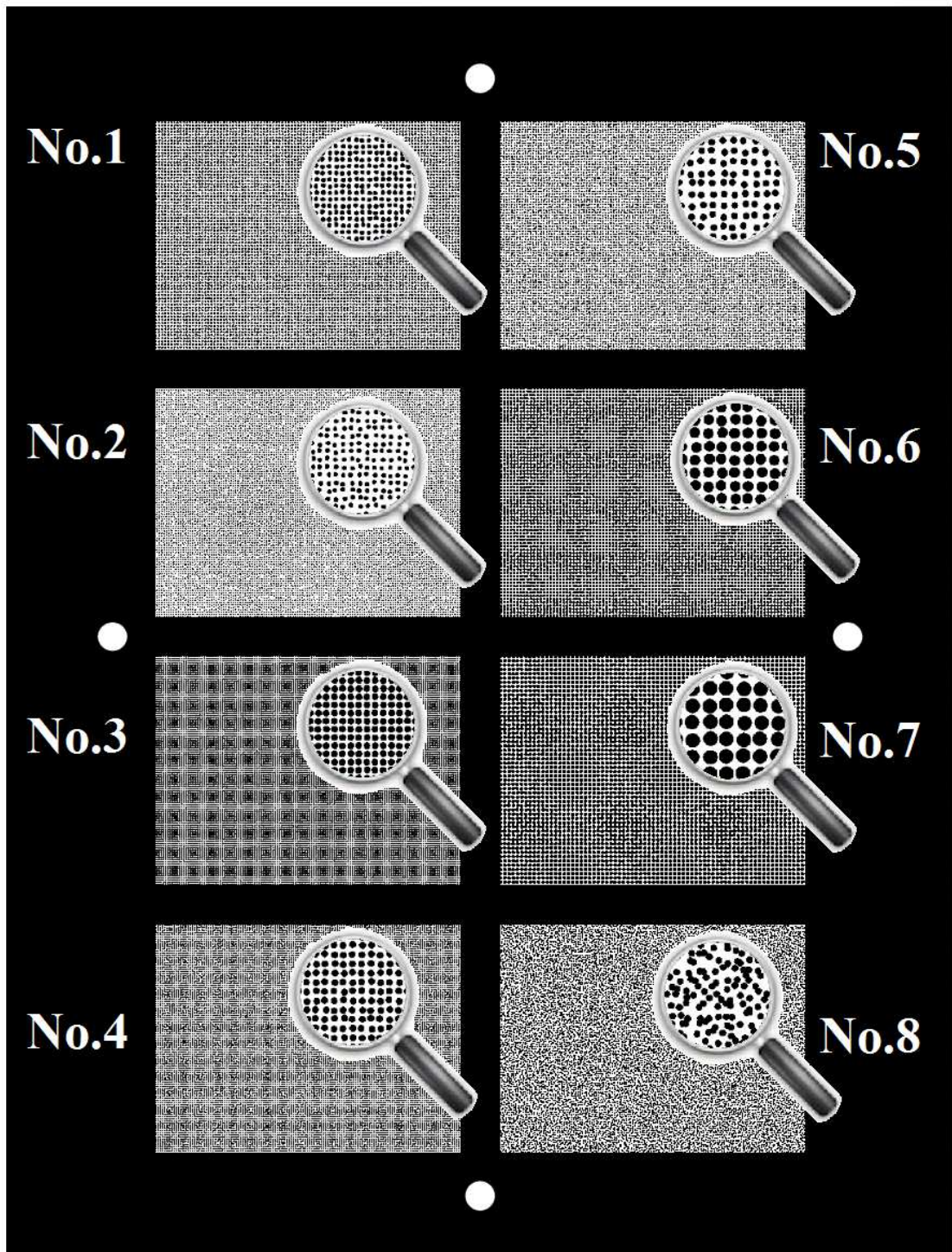


Figure 4.5 Different Pattern types on the paper (zoom 400%)

## 4.2 Scanner test

In order to evaluate the uncertainty of measurement with the variation of speckle pattern, a known imposed motion is carried out ,as comparison with the motion final results found by DIC software.

So that, a test by scanner is performed:

Fixing the pattern sheet inside the scanner, an acquisition of series of images are made; indeed, it means that our imposed motion is a null displacement without deformation.

The advantage is to obtain the result with an easy execution and in a short time. Some images are acquired on the printing sheet and successively analyzed by DIC software.

Imposing  $\epsilon_{xx}=0$  for the entire images sequence, the final result is shown below.

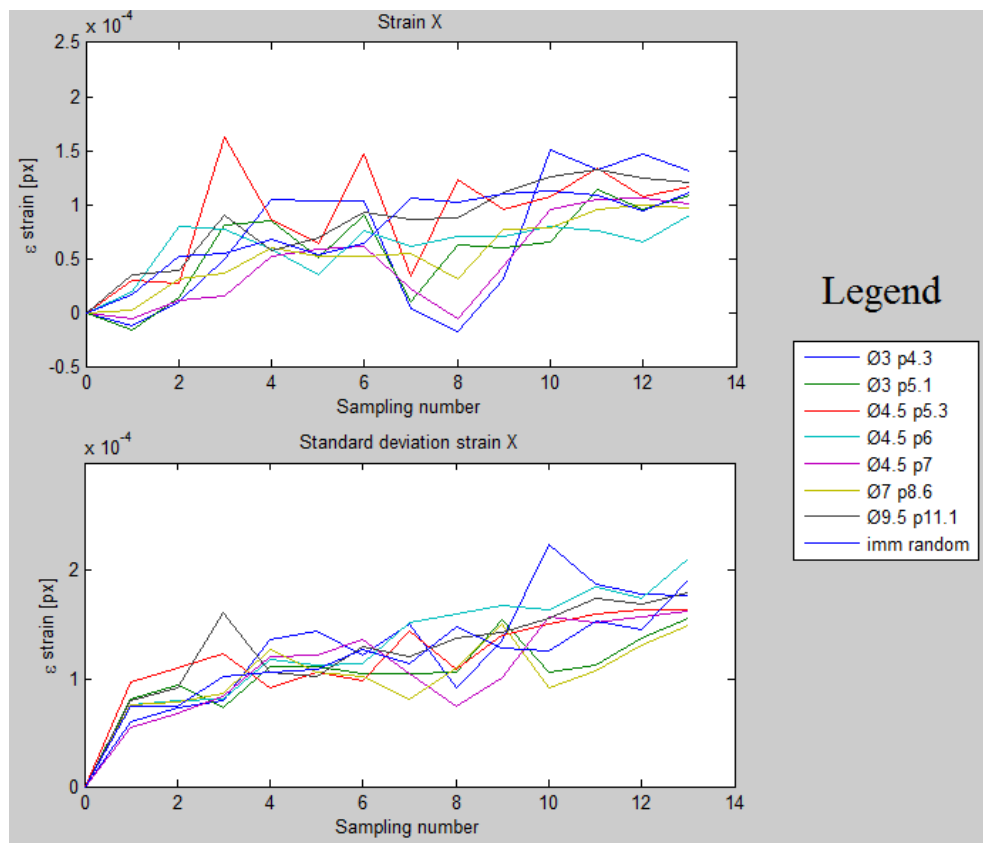


Figure 4.6 Analysis by scanner

The first graph represents the mean  $\epsilon_{xx}$  of 8 different pattern types in 13 images.; instead, the second represents the standard deviation of  $\epsilon_{xx}$  curves.

Unfortunately, during the recording, we recognize the optical head of the scanner has a little displacements respect the glass along y axis.

The strain has to be zero for all types of pattern( because the paper does not moved and we measure only the strain).

On the contrary, the strain measures on the order of  $100\mu\epsilon$ .

Moreover, as it can be seen, there is not a particular speckle pattern better than another.

The reason is on the figure below:

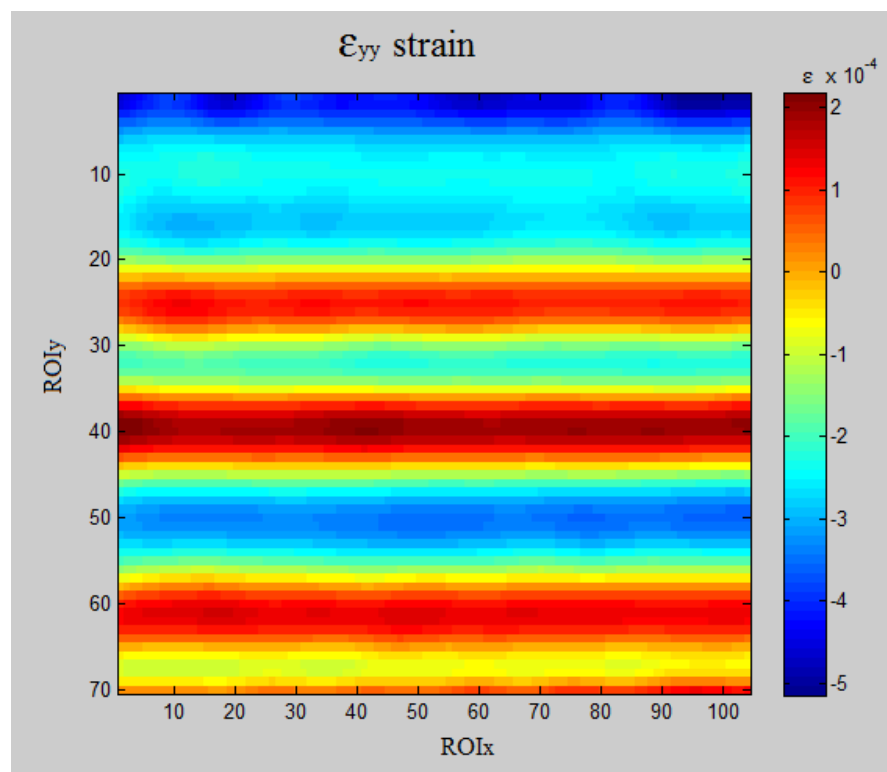


**Figure 4.7 Example of strain calculated after scanner acquisition**

As it can be seen above, DIC software is able to measure the uncertainty of the scanner head motion along Y axis during the relative scansion.

The scanner produces more errors respect that we want to observe.

Hence, the scanner is not a good device for our purpose.

### 4.3 Micrometric screw test

After scanner test failure, another test is tried to be performed.

An imposed translation motion is given, in order to execute small displacements (in a range from 0 to 1 pixel).

An optical CCD camera is mounted above a truck which is regulated by a micrometric screw. Due to the high resolution of our CCD camera, it is possible to record the whole paper (which it contains the different pattern types) into only one photo.

Then, the micrometric head has a resolution of 0.002 mm with an available measurable length of 25mm.



**Figure 4.8 Micrometric head**

For having a major accuracy measurement, a laser is used pointing it on the truck. So the micrometer is used for a “rough” movement and, instead, the laser for the correct measurement.



Figure 4.9 Supply and evaluation unit



Figure 4. 10 Laser displacement

Sensor M7L/		0.5
Casing type		1
Measuring range	[mm]	0.5
Range begin <sup>1</sup>	[mm]	23.75
Linearity $\pm$	[ $\mu$ m]	1
Resolution <sup>2</sup>	[ $\mu$ m]	0.2
Light spot diameter	[mm]	0.1

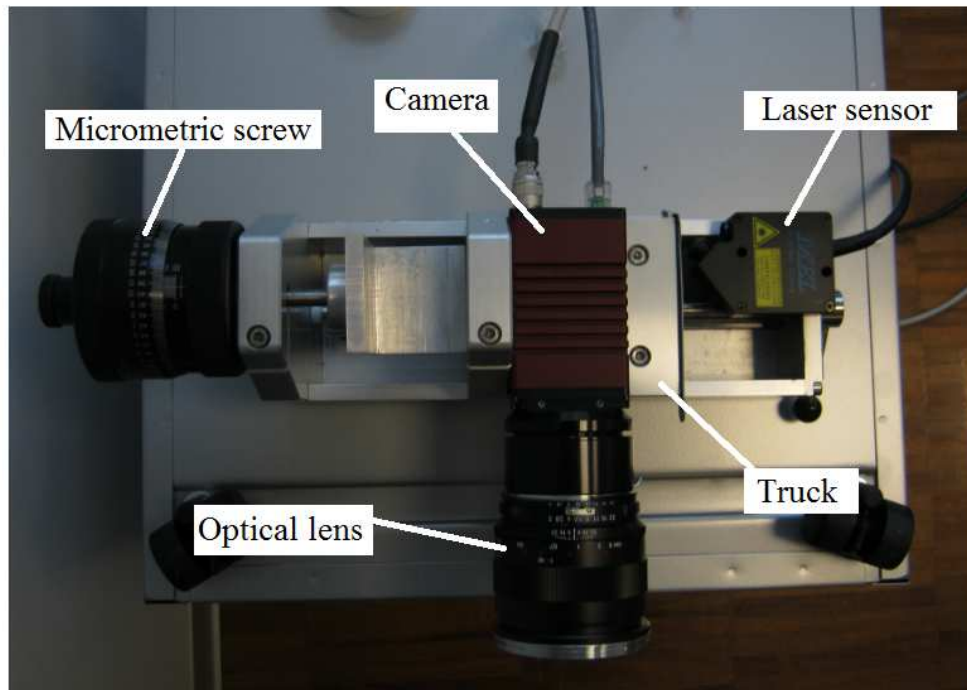
  

Laser protection class	Klasse 2 according to DIN EN 60825-1:2001-11	
Light source	Laser, wave length 670 nm, red visible	
Sampling rate	54 kHz	
Distance output	analog	4-20 mA / $\pm$ 10 V / optional: 0-20 mA, 0-10 V, 0-5 V, $\pm$ 5 V
	digital	RS 232
Impedance	approx. 0 Ohm (10 mA max.)	
Bandwidth	adjustable: 15 Hz ... 10 kHz (-3 db)	
Temperature drift	0.02% of range / K	
Light intensity output	0-10 V	
MIN	+24 V / 10 mA when lower than MIN, LED yellow	
OK	+24 V / 10 mA when higher than MIN and lower than MAX, LED green	
MAX	+24 V / 10 mA when higher than MAX, LED orange	
Error output	+24 V / 10 mA, LED red	
Protection class	sensor head: IP 64, electronic unit: IP 40	
Power supply	+24 VDC / 250 mA (10 ... 30 V)	

**Table 4.2 Laser sensor specification**

Then, a camera with an optical lent is mounted on the truck ;all the system has to be isolated, without being influenced of external disturbances (for example, vibrations of the floor).

So that, at each movement of the micrometric screw and with its relative measure by laser sensor, it is possible to record a sequence of our pattern.



**Figure 4.11 System of acquisition**

A calibration is necessary, in order to estimate the distortion and the focal for the following images acquisition. In our case ,the distortion can be neglected due to the good quality of CCD camera.

The calibration occurs with an acquisition of several images in various positions of a particular grid placed where our pattern paper will be applied; 18 images are taken.

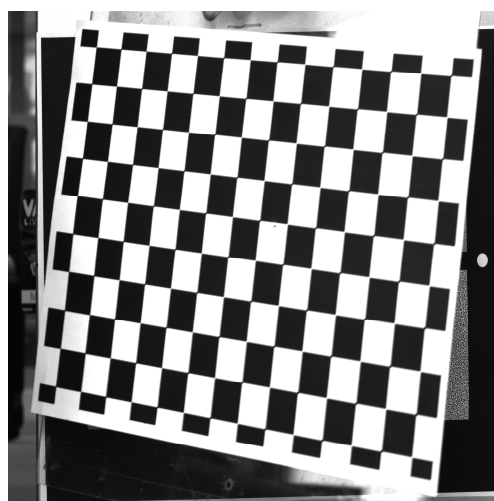


**Figure 4.12 Calibration grid**

The, the pattern sheet is fixed on the wall ,in front of the camera at the distance around of 1 meter.

In order to avoid mistakes in measurement, the camera is regulated by a software for controlling the pitch, roll and yaw; during the setting phase, four white dots around the pattern ( as it can be seen in figure 4.13.) are used for the calibration and they have to remain inside the placement window.



**Figure 4.13 Test arrangement**

Based on a translation rigid motion in a range from 0 to 1 pixel, an subpixel overview is made.

We choose to take fifty images in a length of 2,5 pixels. Hence, it means a movement of  $5 \cdot 10^{-3} \text{ mm}$  in each photo acquisition.

The correct measure position is registered in Volt by laser sensor; the conversion into millimetres is done:

*Measuring range of laser sensor: 0.5 mm*

*Full scale: 0 ÷ 20V*

Therefore the conversion coefficient:  $\frac{0.5}{20} = 0.025$

## 4.4 Results

For evaluating the performances of each pattern, a parameter is performed. Knowing the correlation between MIG coefficient and the standard deviation (refer to Chapter 2), it is enough to calculate this last one.

The mean standard deviation  $\bar{\sigma}$ , is defined as [15]:

$$\bar{\sigma} = \sqrt{\frac{\sum_{i=1}^N \sigma_{meas,i}^2}{N}} \quad (4.1)$$

Where  $\sigma_{meas,i}$  is standard deviation calculated in one single pattern type acquired in one image and N is the number of acquired images.

After the acquisition, an analysis is carried out using VIC software.

The ROI are constituted by 15 pixels with an overlap of 10 pixels.

### 4.4.1 Normal images

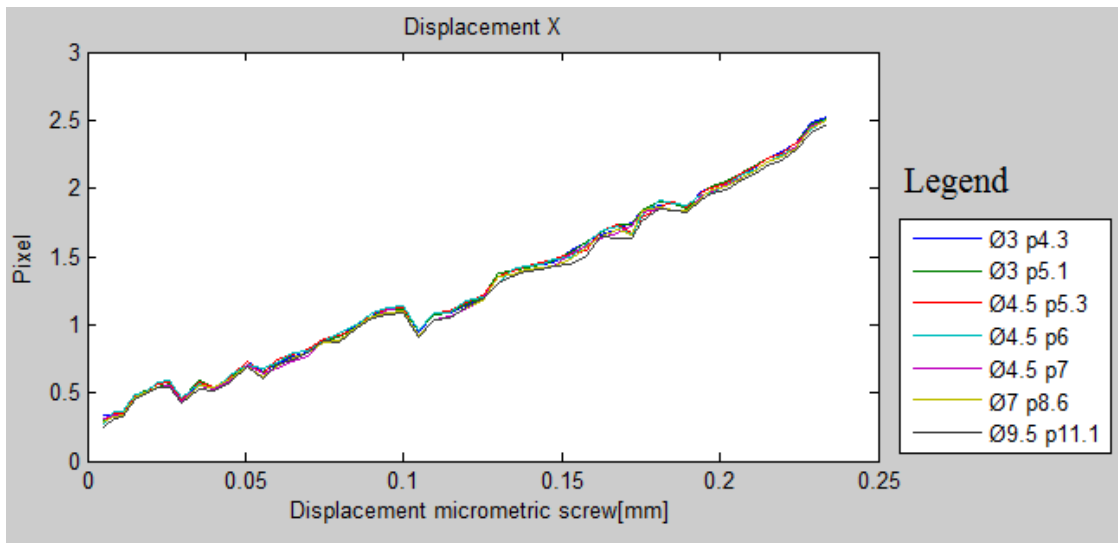


Figure 4.14 X displacement in normal image

In figure 4.14 the abscissa represents the movement in millimetres with the micrometric screw and the ordinate represents the averaged-displacement calculated by VIC software for each type of pattern.

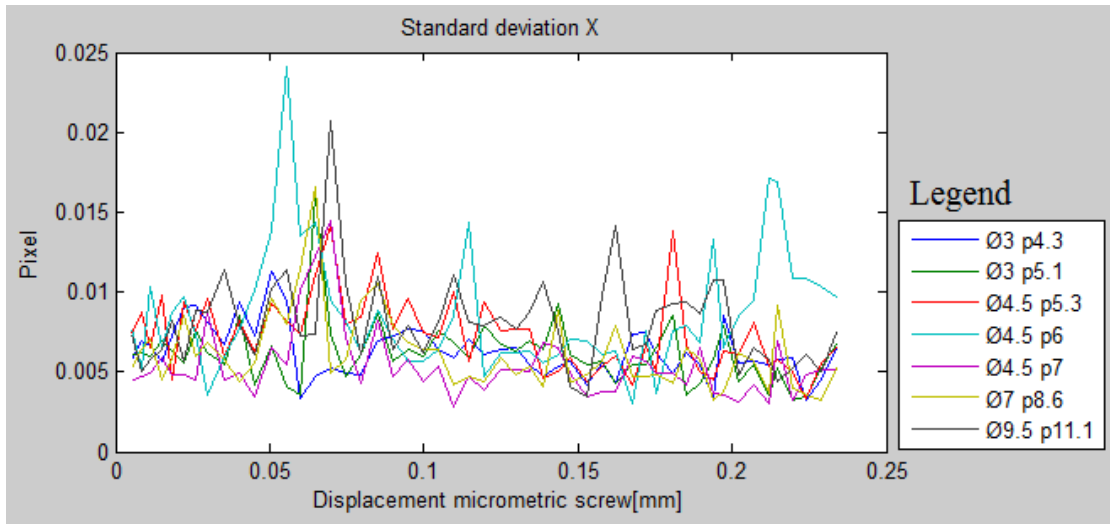


Figure 4.15 Standard deviation X in normal image

The deviation standard should give us an idea of performances for each speckle pattern type.

The abscissa in figure 4.15 represents the movement in millimetres with the micrometric screw and the ordinate represents the standard deviation calculated by VIC software for each type of pattern.

As it can be seen, there is not a significant variation of standard deviation between each other; therefore, it is impossible to note which pattern is better.

(for instance, the best theoretical pattern is 'Ø4.5 p6' (Fig 4.4), but it is not verified through this experiment).

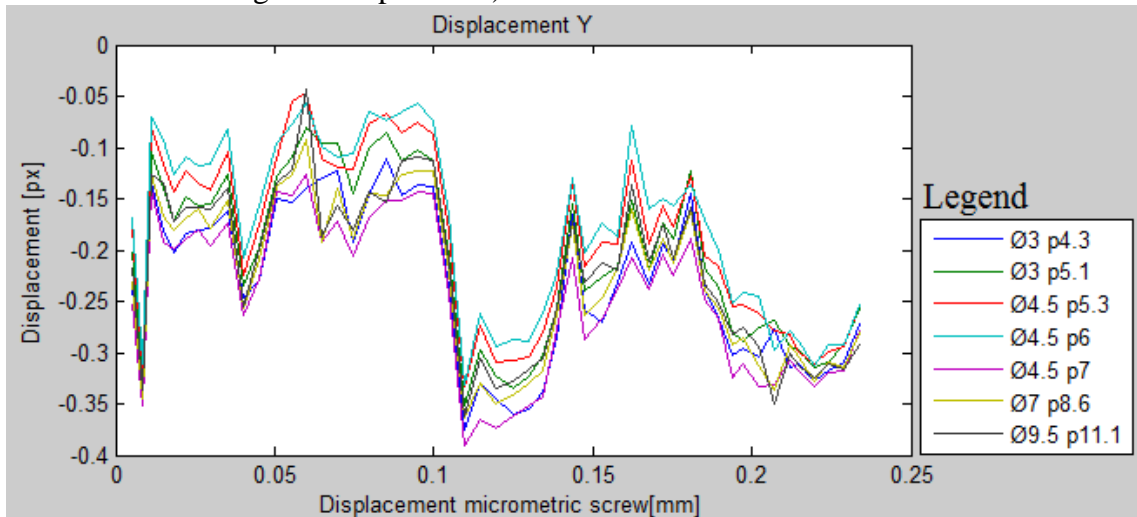


Figure 4.16 Y displacement in normal image

On fig.4.16 during the experiment ,displacement along Y axis occurs, probably for a non-parallelism between truck and sheet.

A discrepancy is evident around 0.1mm due to a sudden movement of camera during the acquisition.

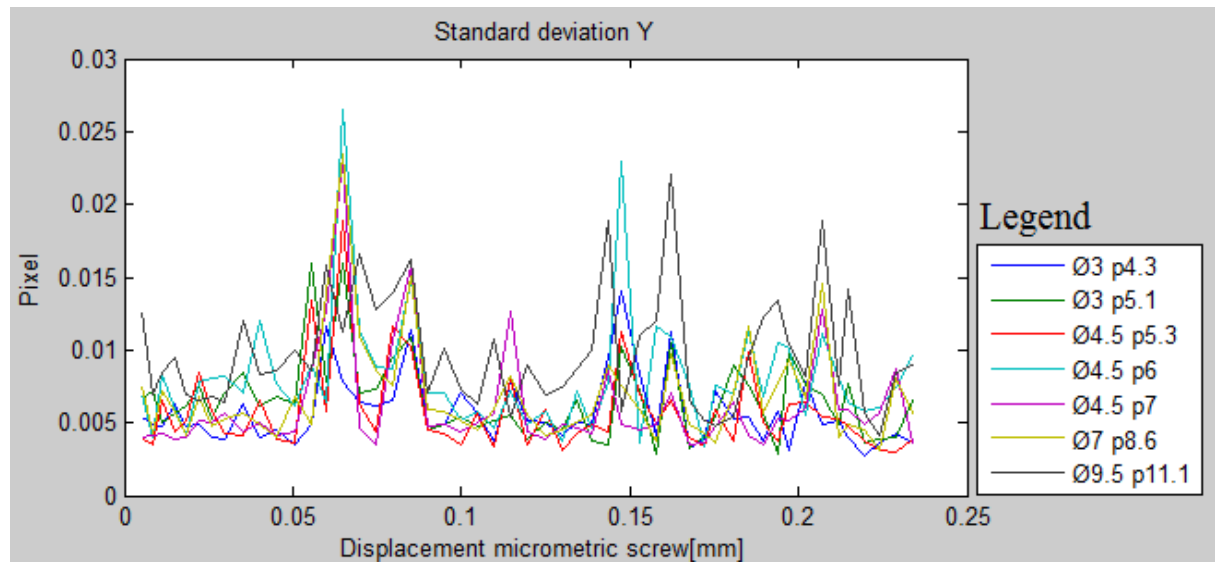


Figure 4.17 Standard deviation Y in normal image

As it has already seen in standard deviation X graph, observing the standard deviation along Y, there is not any differentiation of accuracy among the pattern types. Moreover, as we expected ,the bias effect is not present thanks to the images filtering (see paragraph 4.4).(otherwise it is necessary to consider it together with the standard deviation thought another comparison coefficient).

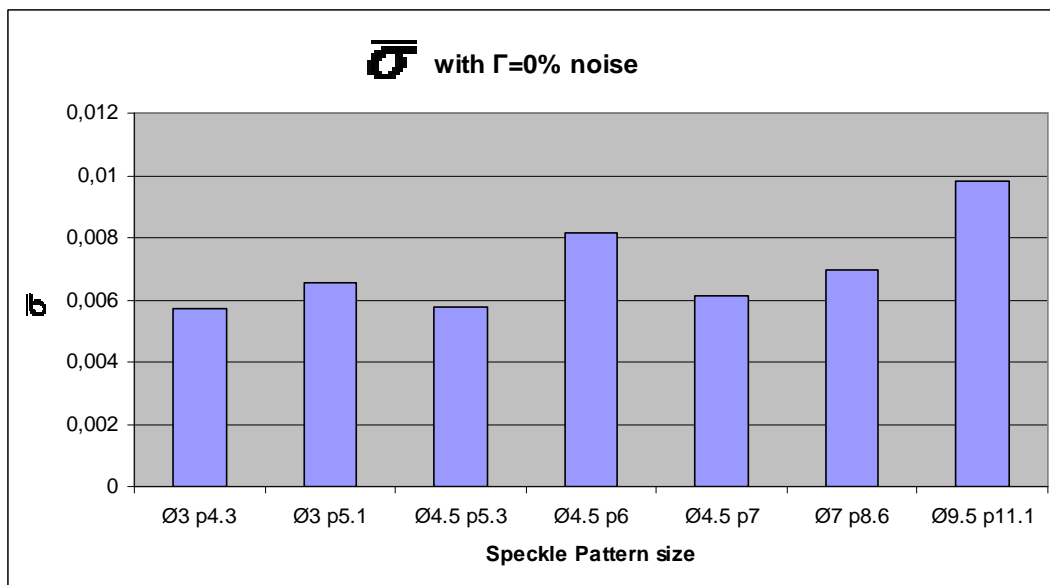


Table 4.3  $\bar{\sigma}$  of displacement along X axis

In the graph above the mean standard deviation is calculated of all pattern types; if  $\bar{\sigma}$  has a low value, means a low uncertainty during the calculation of DIC software.5

According the MIG graph , the best theoretical pattern is 'Ø4.5 p6' but ,as it can be seen, this consideration is not respected.

#### 4.4.2 Images with noise

After these observations, another test is performed in a more critical situation respect to the previous one:

a considerable Gaussian random noise is added into the photos making the images worse.

Percentage of noise is added [20]; to characterize this random contribution the so called percent additive noise is used:

$$\Gamma = \frac{\sigma}{I_{\max} - I_{\min}} * 100 \quad (4.2)$$

Where  $\sigma$  the Gaussian noise,  $I_{\max}$  and  $I_{\min}$  are the intensity limits range of grey scale.

In other words,  $\Gamma$  represents the standard deviation of the additive Gaussian noise expressed as the percentage of the image dynamics  $I_{\max}$  and  $I_{\min}$ .

The simulated noise levels are equal to 0% (no noise), 2.5% and 5.0%

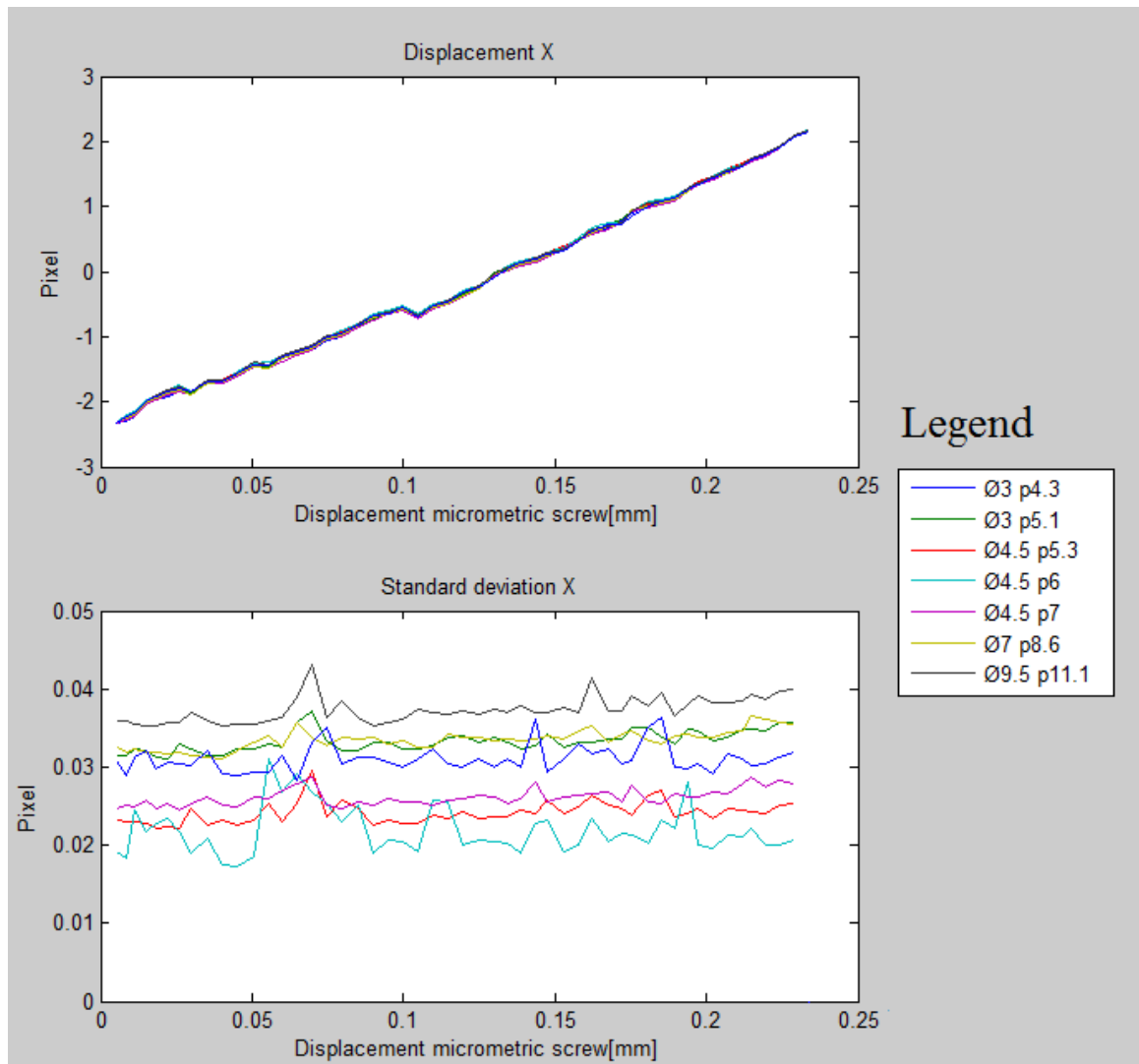


Figure 4.18 X Displacement on images with  $\Gamma=5\%$  noise

On the contrary of the previous test, the types of pattern can be clearly identified due to the standard deviation.

Moreover, the standard deviation (in absolute values terms) is higher than the previous one.

The same happens in Y direction (Figure below).

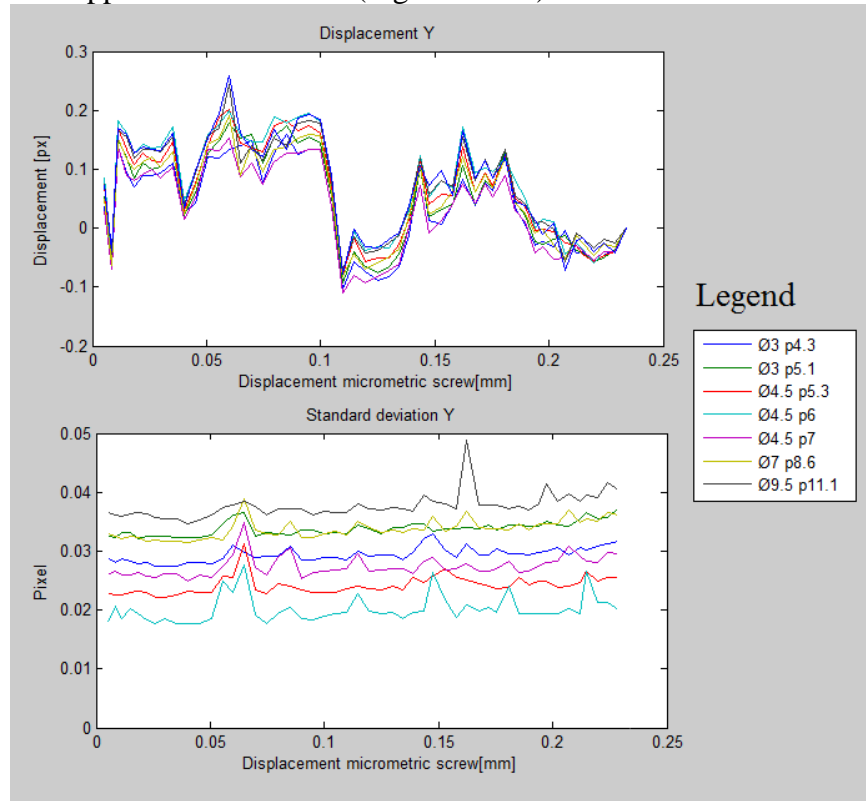


Figure 4.19 Y Displacement on images with  $\Gamma=5\%$  noise

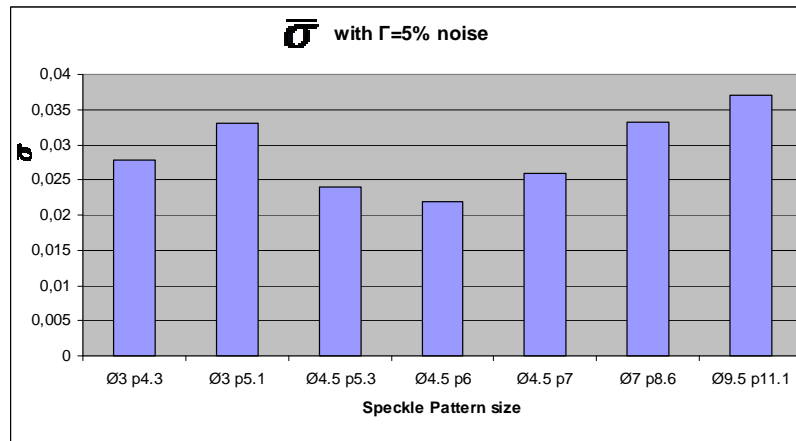
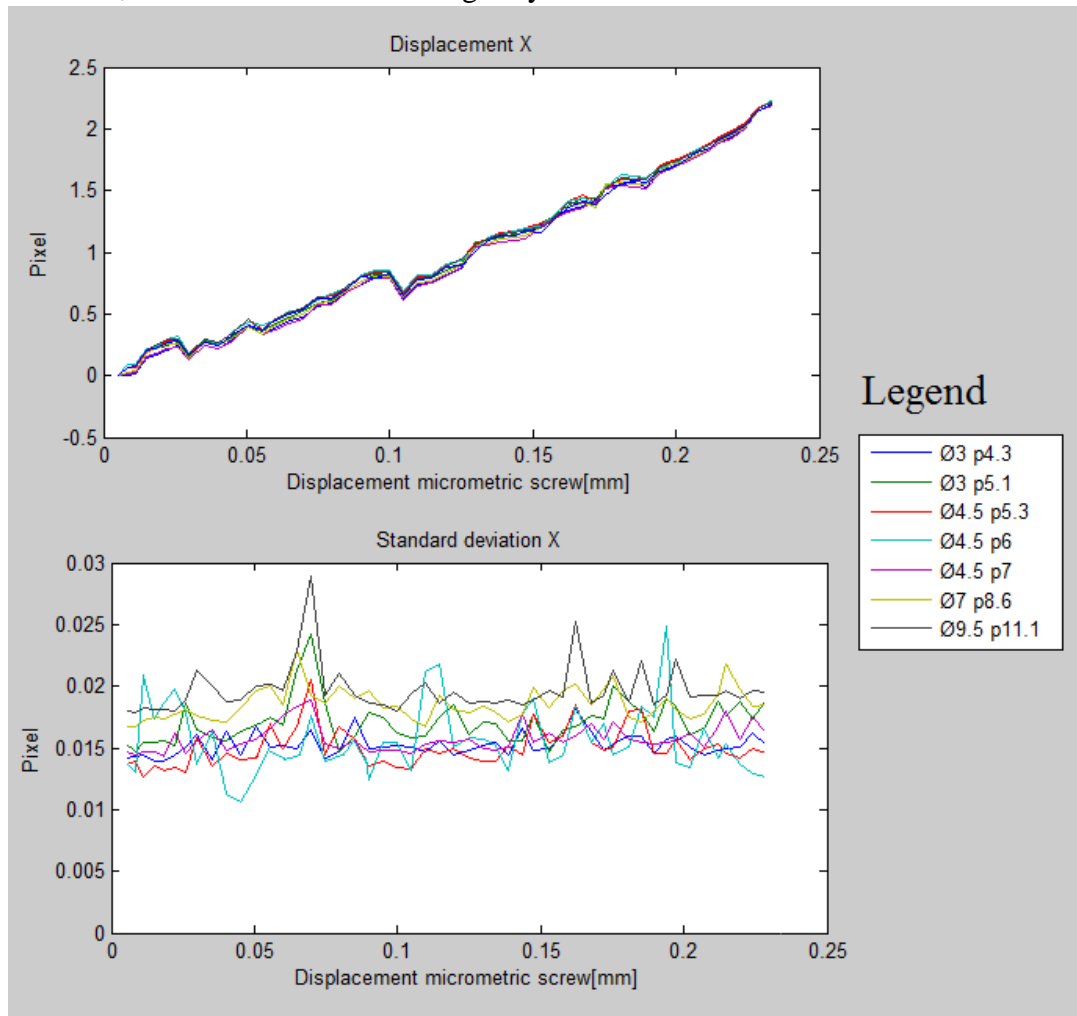


Table 4.4  $\bar{\sigma}$  of displacement along X axis adding  $\Gamma=5\%$  noise

The mean standard deviation is calculated for all pattern types; in this case,  $\bar{\sigma}$  has the lower value in 'Ø4.5 p6' (as expected, according the MIG graph). The matching of the other patterns is made in the table 4.6.

Then, another test is done adding only  $\Gamma=2.5\%$ .



**Figure 4.20 X Displacement on images with  $\Gamma=2.5\%$  noise**

Decreasing the noise respect to the previous test, standard deviation is lower in magnitude value (before it was around  $0.02 \div 0.042$  pixel and now it is  $0.012 \div 0.022$  pixel).

It is possible to observe a small differentiation among each speckle pattern. But the discrepancies are more evident with higher noise.

The same can be seen in Y direction.

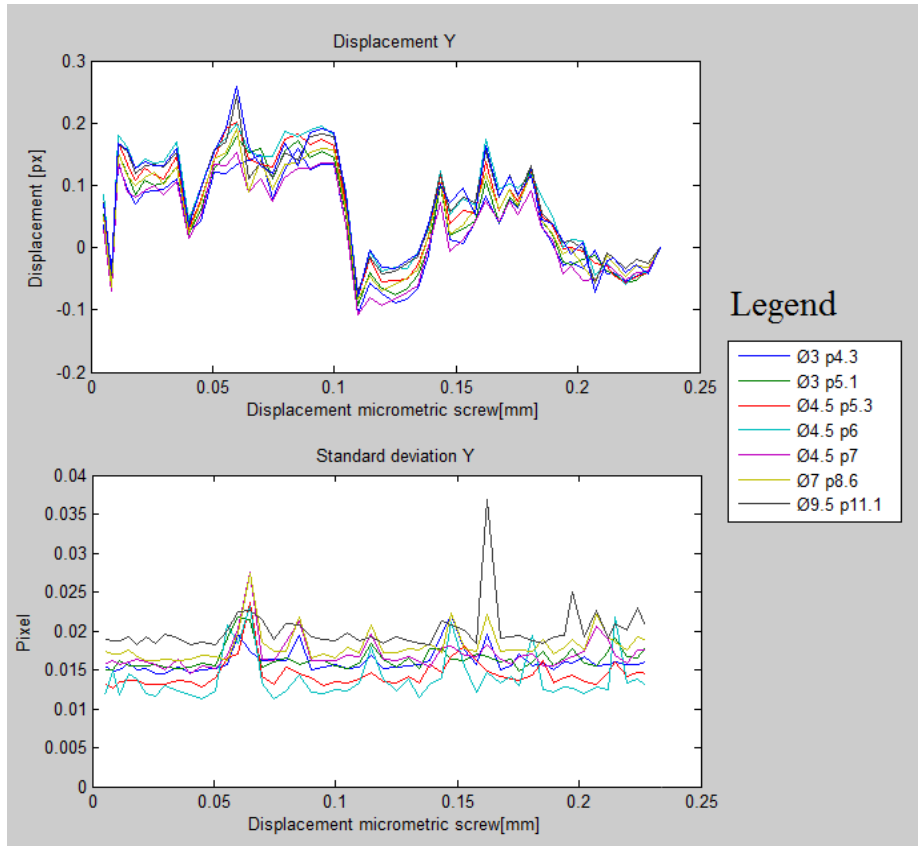


Figure 4.21 Y Displacement on images with  $\Gamma=2.5\%$  noise

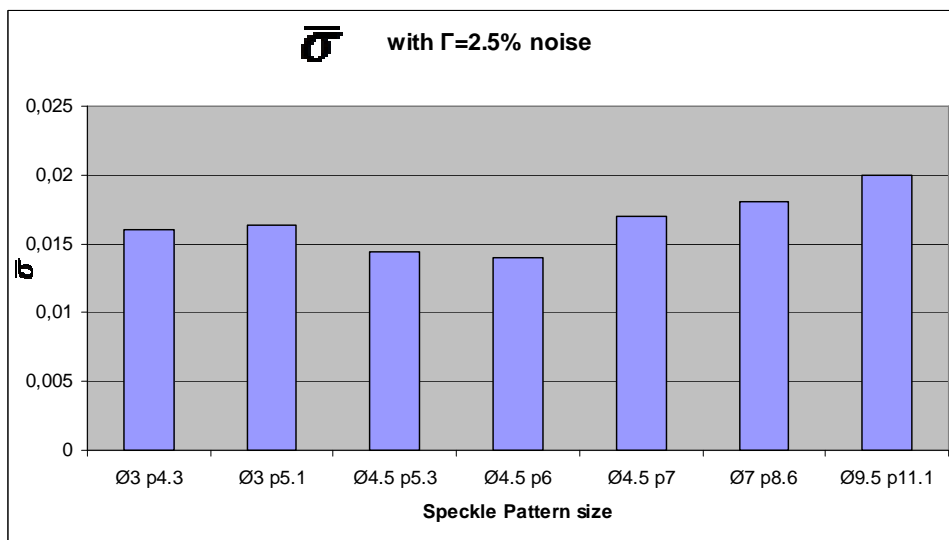


Table 4.5  $\bar{\sigma}$  of displacement along X axis adding  $\Gamma=2.5\%$  noise

The mean standard deviation is calculated for all pattern types; as in case of  $\Gamma=5\%$ ,  $\bar{\sigma}$  has the lower value in 'Ø4.5 p6' (as expected, according the MIG graph). The matching of the other patterns is made in the table 4.6.

#### **4.5 Final observations**

how different types of pattern may give different results in terms of accuracy. We want to observe that the errors of measured displacements using DIC are related to the quality of the speckle pattern, without considering subset size, overlap, types of DIC criteria, position of initial guess, shape interpolation function.

For doing so, the mean intensity gradient coefficient [10] is employed for giving us a parameter of qualification when there is a differentiation of pattern.

With normal techniques of realization of speckle pattern (i.e. airbrush), is impossible to have pre-established blobs size.

Actually, with our possibility of a creation of a "controlled pattern", it can be verified that an optimal pattern exists in order to obtain the best gradient and indeed the best result.

The test is performed, in order to evaluate the changing in terms of accuracy at different pattern types using DIC software (without considering subset size, overlap, types of DIC criteria, position of initial guess, shape interpolation function).

As it has already seen, three series of images are taken into analysis ( $\Gamma=0\%$  noise,  $\Gamma=2.5\%$  noise and  $\Gamma=5\%$  noise).

Based on the final results obtained with the acquired images with  $\Gamma=0\%$ , the errors of measured displacements are not related to the speckle pattern differentiation.

Instead, the analysis of different pattern types in critical situations, such as the high noise presence into images, give us different results in terms of accuracy.

Hence, if a good photo camera is used, the optimal pattern theory can be taken into the background.

From past literature, a kind of pattern (the Random Image cited on page 55) has been employed without considering the optimization pattern theory and it has been compared with the others (see the graphs below).

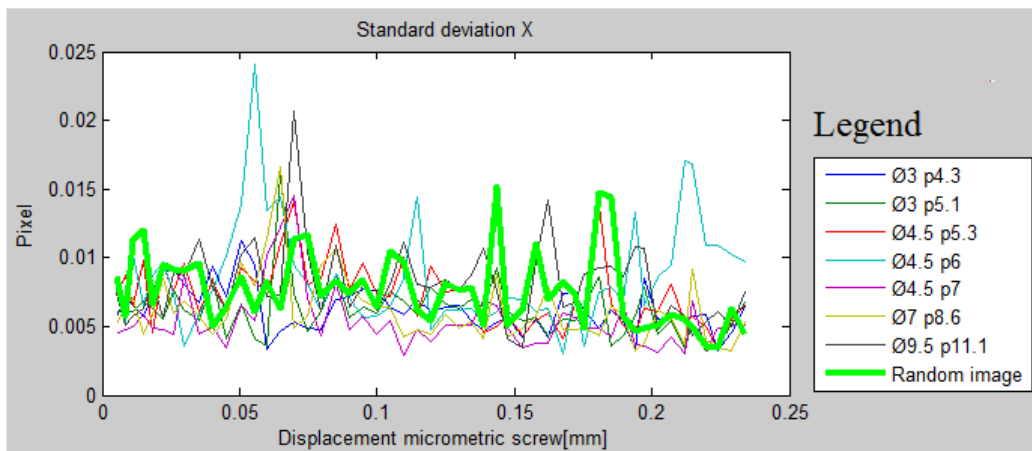


**Figure 4.22 Highlighting of Random image pattern ( $\Gamma=0\%$ )**

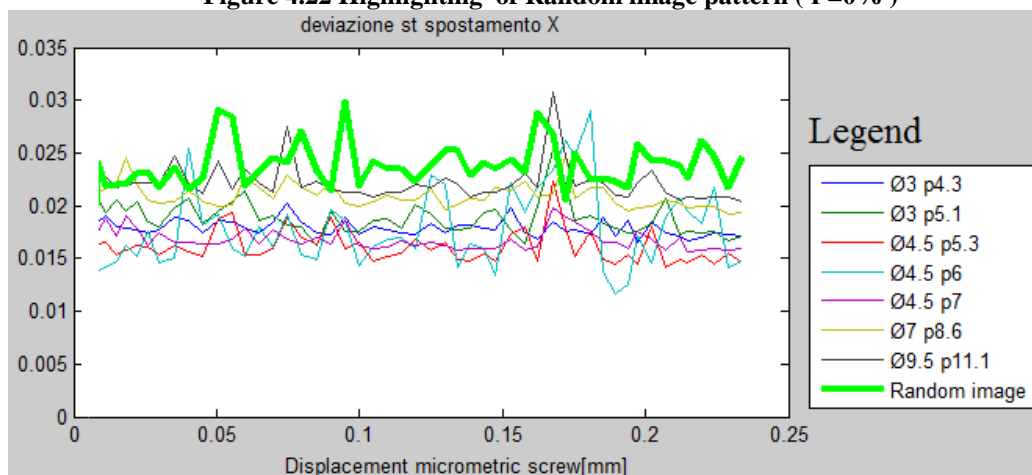


**Figure 4.23 Highlighting of Random image pattern ( $\Gamma=2,5\%$ )**

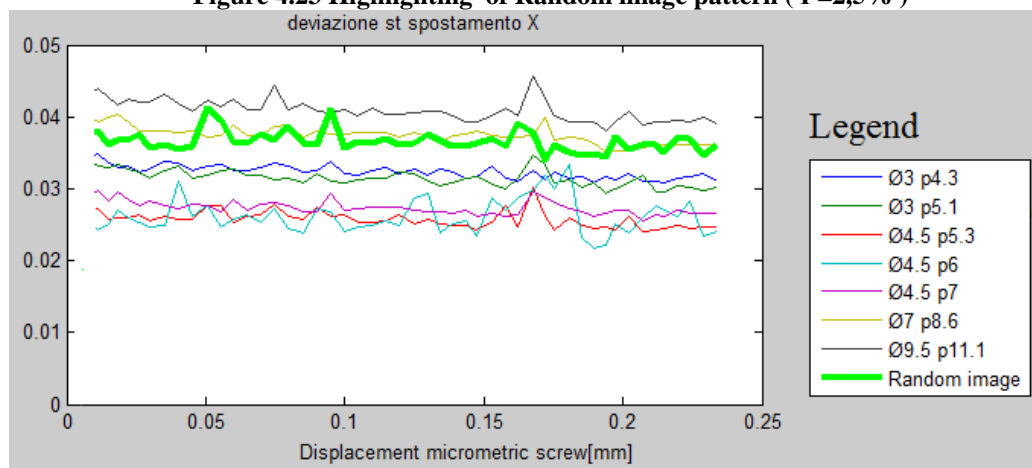


**Figure 4.24 Highlighting of Random image pattern ( $\Gamma=5\%$ )**

In different situations, the Random pattern is not the best choice but its order of accuracy is always comparable with the others (in any case a good gradient).

Therefore, even not to consider the pattern optimization theory, a feasible pattern nowadays used may be applied.

Rank	Pattern from MIG graph	Pattern by VIC software
1st	Ø4.5 p6	Ø4.5 p6
2nd	Ø4.5 p5.3	Ø4.5 p5.3
3rd	Ø4.5 p7	Ø4.5 p7
4th	Ø3 p5.1	Ø3 p4.3
5th	Ø7 p8.6	Ø3 p5.1
6th	Ø3 p4.3	Ø7 p8.6
7th	Ø9.5 p11.1	Ø9.5 p11.1

**Table 4.6 Ranking of best pattern**

As it can be seen, in terms of best accuracy, all the patterns found by VIC software have a correspondence with MIG graph, except for Ø3 p4.3 pattern. This can be justified by the bell curves (fig. 4.25):

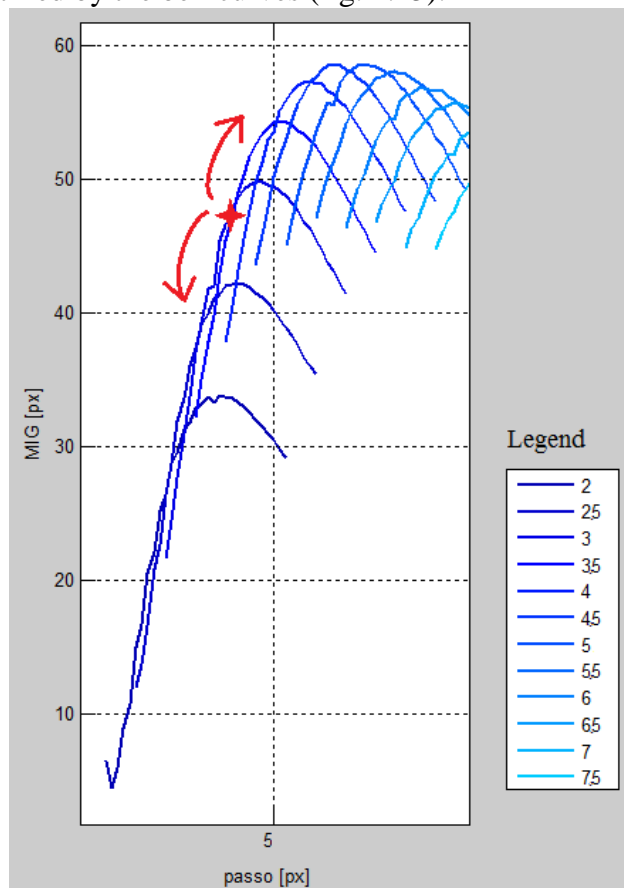


**Figure 4.25 Highlight of Ø3 p4.3 in MIG graph**

Taking a close pattern near to Ø3 p4.3, the coefficient tends to prominently increase (or decrease). So that a small mistake during the procedure (for instance calibration) may create a huge variation in the bell graphs (especially in first part with high gradient).

As It has already mentioned, in presence of a good pattern realization (as our technique is able to make ), the problem of the best pattern choice passes in background.

If in any test the acquisition equipments (camera, lights..) have a good quality and all the possible problems during images processing are taken into account (example. devices position), it is useless to consider some expedients concerning the optimal pattern.

The trouble may rise up in some particular risky cases (i.e. presence of high noise amount) .

An aspect on Controlled Pattern Technique:

From past literature, using other technique of the speckle pattern, for instance the airbrush, a non-homogeneous blob distribution can be created; then, an alarming event is the creation of big blobs or, in worse case, even the drops formation on the surface.

As consequence, the DIC code ,in such zones, has difficulty or, even can not calculate the exact value; if in an unlucky case, where in the interesting zone for the measure (for instance the necking zone before the breaking) there are blobs too big and VIC software does not work very well, the test must be discarded.

During the creation of pattern , an initial hypothesis is that, blobs have to remain separated in order to gain a gradient level as higher as possible.

The situation with random dots, in reality, where they can touch each other, the averaged gradient is not differ so much from controlled pattern created according the hypotheses above mentioned.

On the contrary, a significant difference appears in local level in some ROI where the jointed dots create a low gradient.

## **Chapter 5**

### **Experimental Test (Procedure)**

The new speckle pattern technique described in Chapter 3, can be exploited on any small/intermediate-sized metal specimen (around from 20 mm to 2 m).

In this Chapter, a real utilization of our pattern technique is performed.

In particular, some metal dog-bones 150mm long are analyzed during a tensile test.

The samplings present a welding line about 4mm wide; the requirement is a evaluation of behaviours of each different welded samples during a tensile test, focusing especially in the welding zone.

Therefore, the strains and displacements have to be calculated in a small area and it corresponds of the application field of our pattern technique. Furthermore, the Chapter describes the calculus of Young's modulus trend with the chemical variation in each sample.

The Controlled Pattern Technique is applied on real specimens and the setting procedure test is explained.

Then, through a software, digital image correlation is employed.

A brief description of material sample is mentioned in the following paragraph.

#### **5.1 Characteristic of the samples**

In the middle of each four available dog bones, the welding joint is made by electron beam technique.

##### **5.1.1 Electron Beam Welding**

Electron Beam Welding (EBW): is a technique born in fifties year in Germany and France as a requirement of refractory and reactive welding components.

The welding is created using a concentrated electrons stream at a velocity of 30-70% respect to light velocity.

The main advantage is its deep penetration into the material and its thermal affected region small.

##### **5.1.2 Samples Material**

Two samples are made of TWIP steel (abbreviations 8T and 11T) and the other two are Q&P (abbreviations B1-2 and B2-2).

TWIP(Twin induced Plasticity) steels, invented eight years ago by Professor Georg Frommeyer, are a kind of steel with a high ductility and a good capacity

to absorb energy in the event of a vehicle collision, while maintaining its stability and strength to protect the passenger cabin. Comprising about 20% manganese and small quantities of carbon, aluminium and silicon , TWIP steel can be stretched up to 90% of its length without breaking.

Q&P(Quenching and Partitioning) is a kind of heat treatment of martensite, different to customary quenching and tempering.

On the base of processing, there is a diffusion of carbon from the martensite, in oversaturated phase with carbide precipitation, into residual austenite in order to get it stabilized after treatment[16].

TWIP

%C	%Mn	%Al	%V	%Cr	%Ni	%Si	%S	%P
0.56	18	1.5	0.16	0.46	0.09	0.38	0.018	0.022

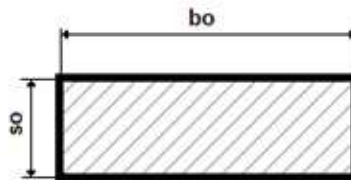
Q&P

	Casting	%C	%Mn	%Si	%P	%S	%Cr	%Ni	%Mo	%Cu	%V	%Al
<b>B1</b>	<b>211</b>	0,217	1,647	1,628	0,0155	0,014	0,03	0,013	0,003	0,011	0,005	0,05
<b>B2</b>	<b>212</b>	0,208	1,824	1,634	0,0161	0,016	0,039	0,017	0,167	0,013	0,006	0,006

Table 5.1 Chemical composition of dog bones

The transversal area dimensions of the samples are shown in the table below:

*Generic Section*



MATERIAL	TWIP 8T	TWIP 11T	Q&P B1-2	Q&P B2-2
bo[mm]	12,56	12,54	9	9,03
[mm]	1,4	1,4	1	1

Table 5.2 Areas data

## 5.2 Pattern application

In order to obtain a major number of points for calculating the local Young's modulus, as small as possible dots are needed. The smallest pattern obtained in Chapter 2 is 0.05 mm diameter with 0.2mm step.

A problem occurs during the ironing:

The samples present in the middle a welding line that is slightly in bump; moreover 3 samples of 4 are not completely plane.

It is very hard to iron especially when welding joint has a small width (because the bump is more accentuated). Especially in regions where an accurate measuring is requested, during pattern dots deposition empty zones are created, making impossible the measurements through DIC software.

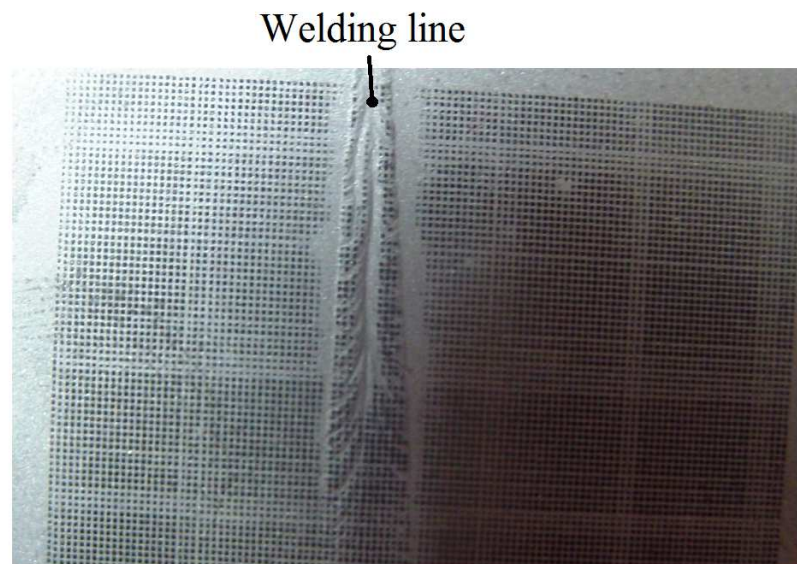


**Figure 5.1 Missing dots deposition due to accentuated welding bump**

The unique solution is to smooth the bump.

Instead, to solve the problem of bending pieces, the solution is to carefully iron following the surface (paying attention especially in the sloping part); then, it is preferred to work on the external surface for an easier execution.

The final result is shown in fig. 5.2.



**Figure 5.2 Final result after application of the pattern on the piece**

### **5.3 Settlement procedure**

Before the tensile test application, the measurement instruments have to be settled in order to use DIC software . The set up is divided mainly in five steps:

#### **5.3.1 Positioning lights**

Led torches are positioned around the tensile machine(fig.5.3).

The prepared specimen is placed on its testing location to set the lights in order to give the attention to the orientation and lightening camera placement.

The sample's face has to be outwards from the test frame.

Generally, the utilization of led-lights is the most adaptive for the purpose: they do not product heating that creates air vortexes due to the variation of temperature; so the cameras can record the airflow instead of the pattern. If heat waves are present in the image, they can easily introduce false strains of several thousand  $\mu\epsilon$ ; so it is critical to avoid them.

If another source light is used, bear in mind that heat waves can be minimized either by repositioning the light source or, if necessary, by setting up a stand fan to blow across the scene. This will generally mix the air well enough to completely eliminate the heat waves.

For our experiment heat waves are avoided because the light-sources are far away from cameras and then they product very low heat.

The lights are used for avoiding the shadings and heterogeneous brightness on the surface.

Leds are 3V with normal white light. For the experiment four led-light are enough.



**Figure 5.3 Led torch**

### 5.3.2 Positioning and synchronization of cameras

The distance between the camera system and the specimen is determined by lenses;

Generally short lenses give better results and give the possibility to easily work but, they have the drawback to focus too close to the specimen and so there is not the possibility of leeway;

The distance is set so that the specimen roughly fills the field of view.

If the specimen is larger than the field of view, we lose data at the edges; if the it is much smaller, our spatial resolution suffers.

In this experimental test, the samples are acquired in 3 dimensions. So that, at least 2 cameras are necessary to make an stereoscopic image.

Hence, the entire area of interest must be visible in both cameras: generally, the specimen should be made just a bit smaller than the field of view, so that pixel-perfect alignment is not necessary.

An aspect concerning the Twip steel is that, due to their high elongation, a major field of view must be considered during the cameras position; otherwise during the traction phase, part of image may be not framed and so that ,a loss of data could be happened.

Using two photo-cameras it is possible to calculate a digital image correlation stereoscopic by a commercial software(VIC 3D).

Each camera has its own optic (ones of 90mm and ones of 180mm) . The model of two cameras is Model Nikon D80 with a resolution of  $3.872 \times 2.592$  (10.2 effective megapixels).

The interesting zone is approximately four centimetres and the conversion parameter from mm to pixel is about 0.01mm.

$$\left( \frac{3872}{4 * 10^3} \right) = 968 * 10^{-5} \left[ \frac{pixel}{mm} \right] \approx 0.01 \left[ \frac{pixel}{mm} \right] \quad (5.1)$$

Where 3872 is the maximum resolution along x axis (in pixel) and 4 are the centimetres taking into consideration on the dog bone.

Two tripods are placed in different positions far from the bone dog (that is why different optics mean different focus); it is possible to mount the cameras on only one tripod but placing them on two different tripods the weight of each camera is better supported.

According to the manual of software[12] the cameras should be positioned somewhat symmetrically about the specimen; this helps the magnification level consistent.

One camera is positioned in front of the bone dog about 320mm; the other one is slanting at an angle of about 30° at a distance of 560mm.

Just for having the possibility to employ 2D DIC software too, one of two cameras is placed in parallel position respect to the flat sample.



**Figure 5.4 Instruments settlement**

The photos acquisition is settled manually: an 100 ISO, images in .JPEG format, exposure time 0.05 seconds. With these characteristics the photos result good and clean for the purpose.

The synchronization of arrangement is made with a single timer with a frequency impulse of 0.5 Hz.

The timer is linked with a single remote control that acts to all two cameras (Fig.5.4).

### **5.3.3 Calibration of cameras**

A calibration operation is carried out at each tensile experiment.

To begin, a grid is selected to approximately fill the field of view.

The calibration means an acquisition of several images in various positions of the grid.

This grid consists of a matrix of white circles with constant step with a black background useful for determining the perspective information(Fig.5.5).

For increasing the accuracy of the future measurement, it is necessary a considerable number of images. More calibration images will give more accurate result.

Moreover there is a possibility to discard some couple of images depending on some errors or a poor accuracy:

- the grid should be visible in both images.

If the grid is too large, it will be difficult to keep it fully in the field of view in both cameras while taking images.

However, calibration images are useful as long as all three hollow marker dots are visible. If any of the three hollow marker dots cannot be seen, then the image cannot be used.

- If the grid is too small, it may be difficult for Vic-3D to automatically extract points;

additionally, more total images will be required to cover the field of view, including the corners.

The choice is fallen in a grid around the size of the samples: circles having a step of 2 mm.

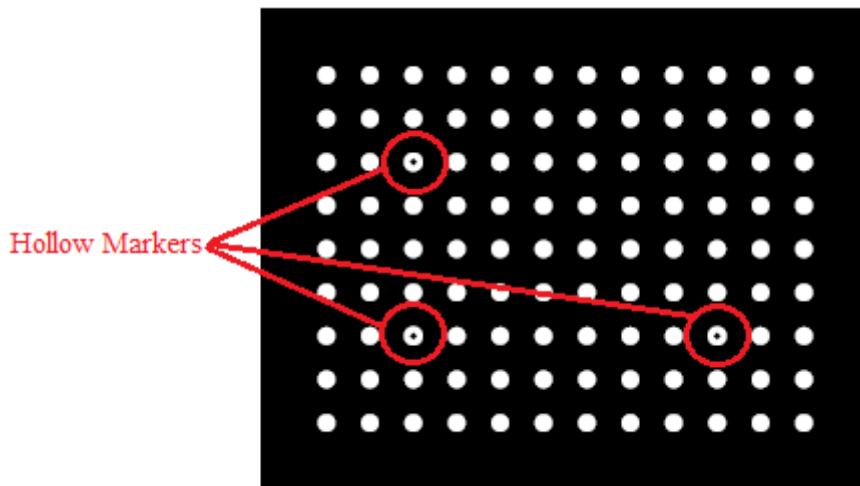


Figure 5.5 Calibrator image (2 mm step )

- Occasionally, lighting configuration can affect grid selection. Some grids may be slightly reflective; under intense or directional light sources, these reflections can wash out the grid image. For these cases, matte grids should be used.

At least four calibration images must be acquired; in addition, the acquisition of redundant images leaves more room to discard poor images (images that contain highlights, defocus, occlusion, or other issues that make them unsuitable for utilization). For a typical setup, 15-20 images should be acquired[12].

To accurately estimate aspect ratio, the grid should be rotated in-plane in some images.

The calibration procedure in DIC software calculates variables about the camera geometry and imaging; it is not specific to a plane or volume in space. Therefore, it is not necessary to position the calibration grid in the exact same location as the intended specimen.

The parameters of calibration are founded from the relationship between the two cameras (called Extrinsic Parameters). These parameters will change if the cameras are moved or tilted.

It is possible to find the parameters of each camera too(Intrinsic Parameters); these parameters change if you move the lens or change the aperture or focus.

Typically, we calibrate extrinsic and intrinsic parameters at the same time, with a stereo calibration. However, in some cases, it is advantageous to calibrate the extrinsic parameters separately or to refine them using a speckle image.

Examples of cases where separate calibration is required:

- Cameras cannot be synchronized;
- Large measurement fields for which a large enough grid is not practical

Examples of cases where stereo calibration may be refined by external calibration:

- The cameras are moved or bumped since calibration. In general, any time you run a correlation and see an higher error than the expected one, you can try to run the external orientation calibration to improve your results.
- Test setup to include nonstandard distortions, such as from a glass pane.

When the calculation is complete, a report of calibration results and error scores will be presented. The errors will be displayed per image, as well as an overall error score:

A calibration score is showed in fig.5.6 .

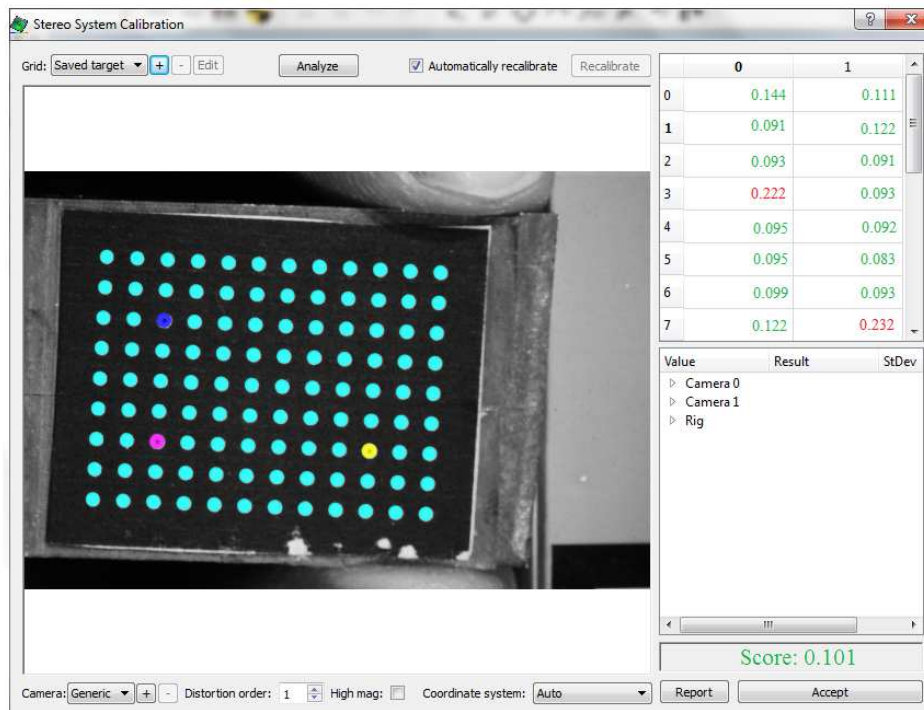


Figure 5.6 Example of calibration score

If we had a good set of calibration images with good tilt and coverage of the image field, the overall error (*Standard deviation of residuals for all views*) should be displayed in green.

If the score is displayed in red, it may need to remove some images or recalibrate. Vic-3D will automatically remove very poor images, but additional images can be removed manually.

If the result is uniformly high, or if you have several high scores, there may be a problem with the setup. These things should be checked for decreasing the standard deviation:

- The grid images are in focus.
- The exposure times are short enough to eliminate motion blur.
- The cameras are secure on the stereo rig.
- The grid is rigid.
- If using a glass grid, confirm that the correct face is towards the camera.
- The cameras are synchronized.

The results after calibration are:

- Angles: three angles between each camera. In general, two angles will be small and one (the stereo angle) will be larger.
- Distances: the distance between camera 1 and camera 2, measured from camera 1.

In our case all calibrations show a quite overall error (tab.5.3 3<sup>rd</sup> row).

#### **5.3.4 Aperture and exposure time**

To make the image sharp through the focus adjustment, it is also necessary to adjust the brightness of the image. There are two controls available for this: the aperture/iris setting on the lens and the exposure time setting of the camera.

The aperture is a hole or an opening through which light travels. Opening the aperture more light can fall on the sensor.

In cameras, the aperture mechanism can be regulated on different apertures, distributed regularly on a scale called f-number.

F-numbers are usually indicated on the lens's aperture ring and typically go from an open setting of F/1.4 or F/2.8 to a closed setting of F/22 or F/32.

Using a bigger aperture (lower f-number) makes the image brighter.

However, the depth of field decreases the range over which the focus is sharp. Even for a flat specimen, some depth of field is necessary because each camera is oblique to the plane of the specimen.

Also, a poor depth of field may make difficult to achieve a wide range of calibration target.

Note that the aperture may not be changed after the system is calibrated.

Exposure time is the amount of time the camera sensor gathers light before reading out a new image. A longer exposure time makes the image brighter but it can also create blur if significant motion happens during the exposure time.

In contrast to aperture, exposure time may be adjusted after the system is calibrated if lighting conditions change or the specimen becomes brighter/darker.

After this point, changing any aspect of the camera system will invalidate the calibration; so all adjustments should be carefully fixed at this point.

### **5.3.5 Positioning specimens (and clip gauge)**

The samples are mounted one by one on the tensile machine taking into account not to move anything else (otherwise the calibration must be repeated again); one extensometer with an opening around 50 mm is employed to the sample for giving us a “rough comparison” between its detected measures with the values found by DIC software

The extensometer gives back only an averaged strain measure between the two points of clip gauge extremity; instead in our case, there is a welding line in the middle which almost certainly has a different strain respect to the metal base. Hence, the extensometer is employed only for an evaluation of strains order and to match with the strains found by DIC software

## **5.4 Data Elaboration**

### **5.4.1 Consideration before of the elaboration**

Before the elaboration, it is needed to know where the welding is positioned respect to the breakage point: with a marking gauge a line is scarred on the pattern where approximately the welding line passes. After that, each sampling is scanned and successively measured by DIC software.

At first view, all the samplings are not broken exactly at centre line: two samplings (Q&P heat treatment) are broken far away from welding joint. On the contrary, considering the two TWIN samplings, the fracture crosses in the welding zone.

A mistake is committed unfortunately during the 1<sup>st</sup> test saving of photos into one camera in double format; so that the frequency of acquisition was not the same to save in time and the synchronization between the cameras was not respected anymore. Therefore, only in this test, 2D VIC is used (the central camera was positioned exactly in front of the sample).

The photos for the triangulation must be renamed creating a series of couples of images composed one by the central camera and the other by the above: the

modality is to rename photos at the end of the file with “\_0” and “\_1” according to the camera.

#### 5.4.2 Brief VIC 3D introduction

The chosen digital image correlation software is VIC3D in order to measure the shape, displacement and strain on surfaces in three dimensions. All the DIC analysis are carried out with an 8-tap optimized interpolation method, selecting a ZNSSD (zero normalized sum of squared differences) criterion, able, in a real application, to automatically compensate scale and offset in the intensity pattern [10,17].

Using it, actual object movement is measured and the Lagrangian strain tensor is available at every point on the specimen's surface.

#### 5.4.3 Option choice during the elaboration

In order to calculate displacements and strains field of the samples, before running the calculation software, an area of interest (AOI) has to be defined. This is the portion of the image that contains the speckle pattern where shape and displacements field are analysed .

Clicking a series of points to define the boundaries of the AOI and using the tools for drawing the shape on the initial reference photo, it is possible to determine the interest area.

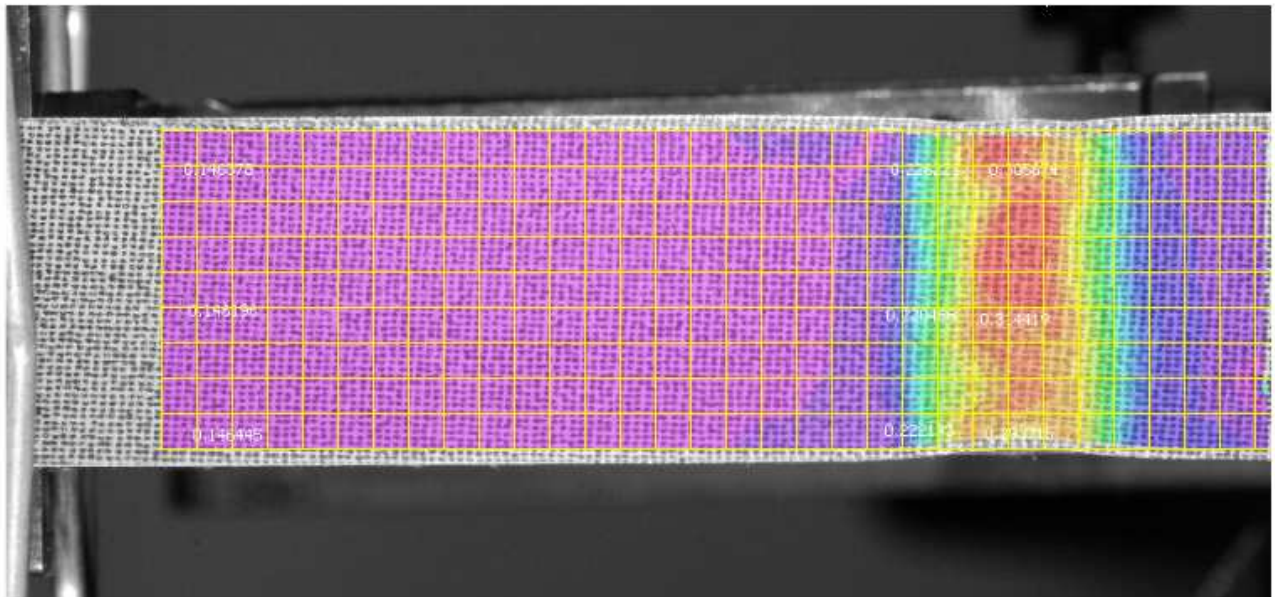


Figure 5.7 Defined AOI with a grid of ROI

### **Placing start points**

Start point is the initial point where DIC software begins the elaboration.

Generally, start point should be positioned in a area of the image with as low as possible motion during the test.

In case of tensile test, the start point is positioned as close as possible to the stationary grip. This helps the automatic correlation.

In Vic 3D , start points are automatically found in the following images.

In some cases, the initial guess point is not found. This is due to some reasons listed below:

- Multiple, large camera angles (rather than a single stereo angle)
- Highly curved surfaces such as cylinders
- Large rotations between successive images
- Very fine or indistinct speckle patterns
- Poor calibration.

It exists a window in the program, where it is possible to place manually start points.

### **Filter size/type**

To calculate curvatures a local filter is used. The *Filter* box allows selection of a smoothing method. The decay filter is a 90% center-weighted Gaussian filter and works best for most situations; the box filter is a simple unweighted averaging filter.

The *Filter size* box controls the size of the smoothing window.

Since the filter size is given in terms of data points rather than pixels, the physical size of the window on the object also depends on the step size used during correlation analysis.

An empirical formula exists to calculate the filter size:

$$\text{Filter-size}=(\text{subset dimension}/\text{overlap})*3$$

In the case the filter number is too small for reaching good results, increasing the size is mandatory [Values on tab 5.3].

#### **-Incremental correlation**

With incremental correlation, each image is compared to the previous one rather than the reference one.

This can be useful in cases of pattern breakdown or extremely high strains (>100%).

This option is only used with 2 samples made of TWIP which have a great deformation.

During processing, the data employed in VIC software are displayed in tab.5.3.

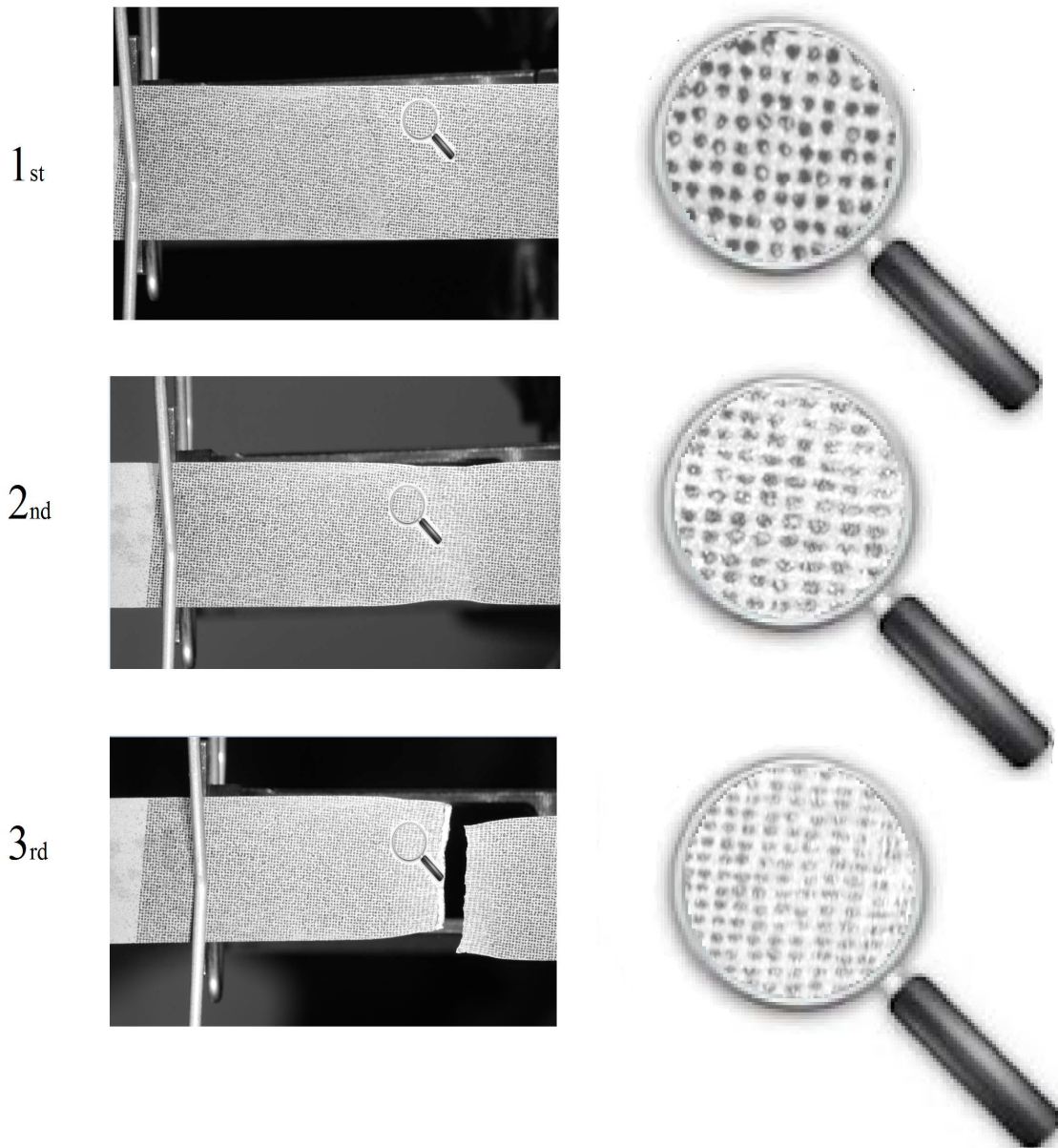
MATERIAL	TWIP 8T	TWIP 11T	Q&P B1-2	Q&P B2-2
DIMENSION				
SUBSET(ROI)[pixel]	23	35	41	41
OVER LAP [pixel]	11	18	20	21
DEVIATION STANDARD $\sigma$				
DURING CALIBRATION	----	0.101	0.293	0.273
CONSISTENCE THRESHOLD	----	0.5	0.4	0.4
MAX MARGIN	0.5	0.6	0.55	0.5
Tensor Type	Lagrange	Lagrange	Lagrange	Lagrange
FILTER SIZE [pixel]	9	9	9	9
POSITION OF WELDING				
MIDDLE CENTRE ON THE				
FIRST IMAGE [pixel]	2128	2287	2538	2375

Table 5.3 Summary of option data during the processing

## 5.5 Final considerations

During the tensile test, the values are taken with an optical measure system in order to obtain local measures along the entire piece that, with a normal setting of tensile machine, are impossible to find.

The result of speckle pattern on a real sample is very good during all the experiments and also in the zone where the deformation is higher(fig. 5.8).



**Figure 5.8 Sequences of images acquired by camera during a tensile test**

A comparison is done with a pattern used commonly in previous test. Our new pattern results more uniformly distributed(fig.5.8) respect to a traditional one.

## Chapter 6

### Experimental Tests (Results)

In this chapter are reported the final results of the tensile experimental tests. The full field of strains are calculated for each sample, focusing especially in the welding zone. Furthermore, the calculation of Young's modulus trend is performed along the entire surface of the samples. In the first part is explained the modality of how the data are taking into account on the samples surface ; then ,the analyses conclusions are described according each sample.

#### 6.1 Considerations of procedure

After VIC 3D processing data of the samples are evaluated.

First of all, we want to represent the strain behavior during the tensile test.

Schematically the main zones on each dog-bone are:

- Base material zone
- Heat affected zone welding (HAZ)
- Welding zone

In order to observe the strain along all the normal sections, points in several regions are picked along an orthogonal line respect to the middle line.

Sections both on the left and on the right respect to the centre line of welding line are taken into consideration to have data that show possible asymmetry.

The below figure shows the schema where the points are picked:

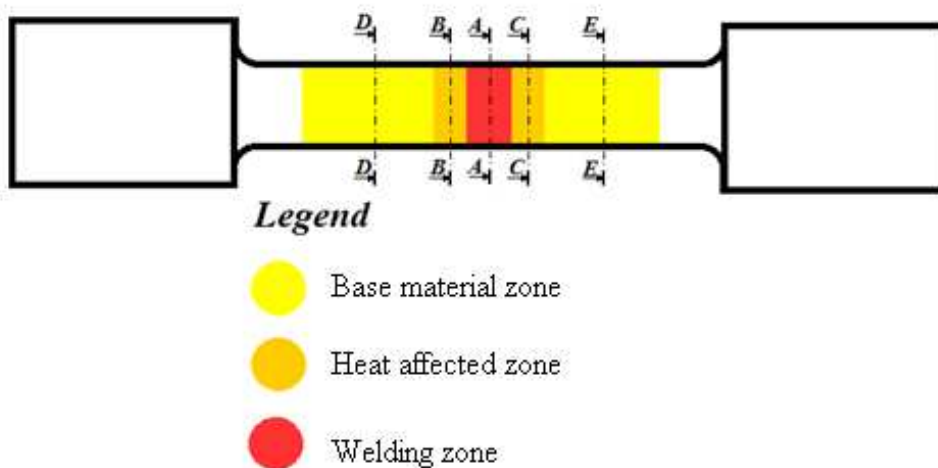
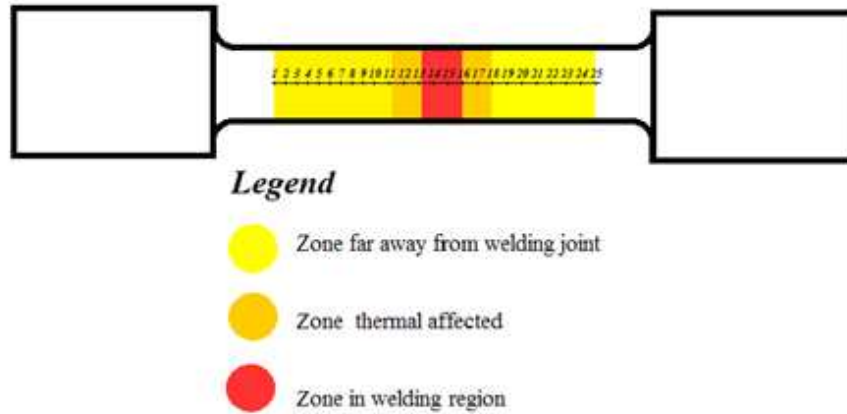


Figure 6.1 Schema of dog bones

In order to evaluate the strain behavior along the X axis, points are picked in a horizontal line respect to the centre line. (fig.6.2) . Beside, the strains on the last image are taken into consideration in order to show the correlation between the measured image with the real broken dog-bone.



**Figure 6.2 Schema of dog bones**

Subsequently, from the initial images, the Young's modulus is calculated: Points are picked on whole the surface; the axial force values are founded by the load cell of the tensile machine. The tensile machine gives us a sequence of force values 10 time faster than our image acquisition time. So that, only one force value each ten are taken. Then, knowing the normal section of the samples (for data area refer to table 5.2) , it is possible to calculate the Young's modulus values

Therefore, the stress can be calculated as:

$$\sigma_n = \frac{F}{A} \quad (6.1)$$

where  $\sigma$  is the stress, F is the force and A is the surface

$$E = \frac{\sigma_n}{\xi} \quad (6.2)$$

where E is Young's modulus and  $\xi$  is the strain in X direction

## 6.2 How to find the welding line

To have a distance reference system on the pieces, the middle line of welding needs to be taken into account as zero point.

Therefore, after the experiment, using a cutter a line is traced where the middle line passes; then the image is acquired by a scanner (an example in Fig 6.3).

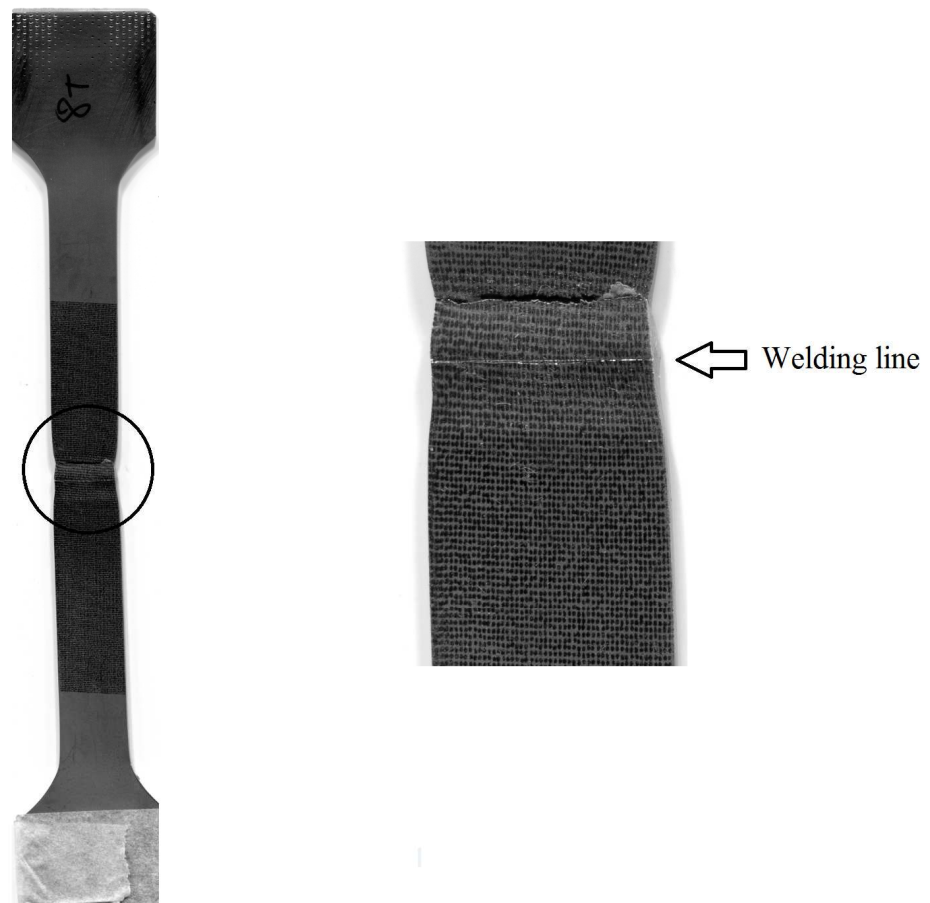


**Figure 6.3 Sample after breaking**

The position of the middle line that passes through the pattern is estimated on the first image of each sample.

Then, being aware of the positions in pixel, they can be simply converted into millimetres using the conversion parameter found during calibration phase.

Successively, taking middle line as reference, zero setting is carried out.

As further aid, the pieces are visualized on the microscope and the distance is approximately measured from the breaking and welding line: knowing the position of the breaking line that can be extracted from the ultimate strain shown in the last image, the welding position is given as a simply difference. This measure is not accurate because the fracture generally is not parallel to the welding line but, in any case, it is useful for having an idea of values order of magnitude.

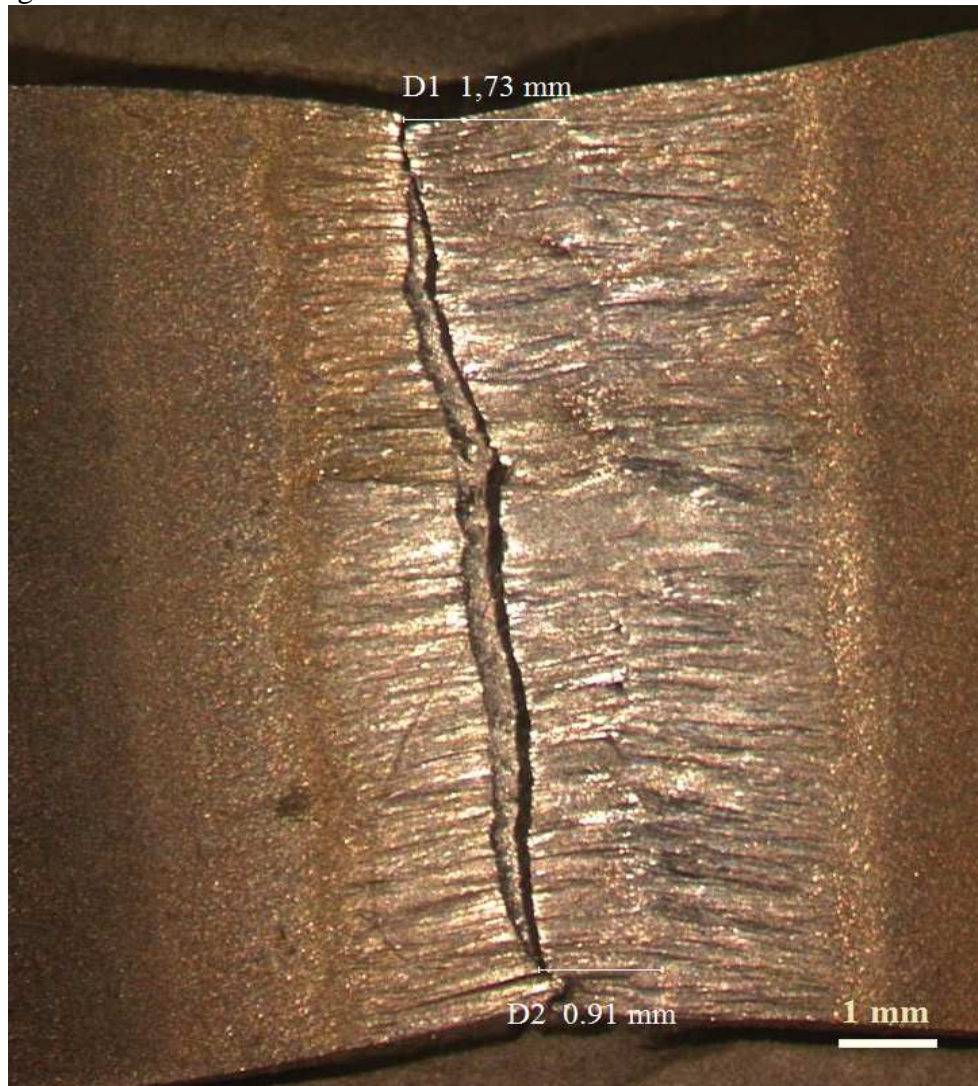


**Figure 6.4 Fracture on welding zone through microscope**

The unique case where it is impossible to immediately convert from pixel to millimetres is for TWIP 8T case: 2D software is exploited and any output is given back in millimetres because calibration does not exist. Therefore, a

coefficient of conversion is found measuring the width of the piece in pixel from an image and then comparing it with the real measure ( $l=12,56\text{mm}$ ).

In each section, along the width five points are picked using the same constant step .

Except for TWIP 8T where sections are not useful (during the test the last images were not acquired), for other samples the points are picked.

The drawing and the table below display the positions of the points in all three samples taking as reference the welding line.

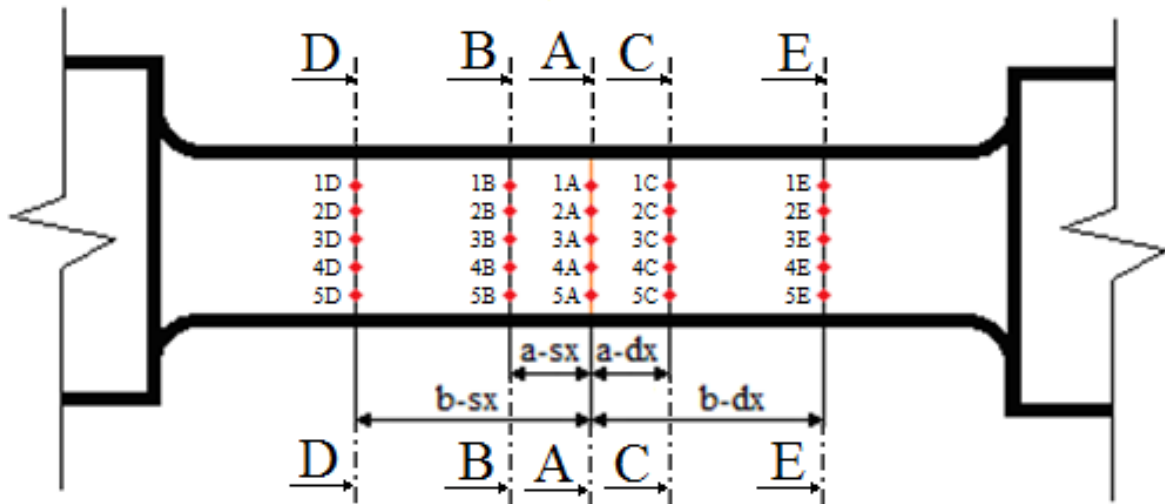


Figure 6.5 Points coordinates on the surface

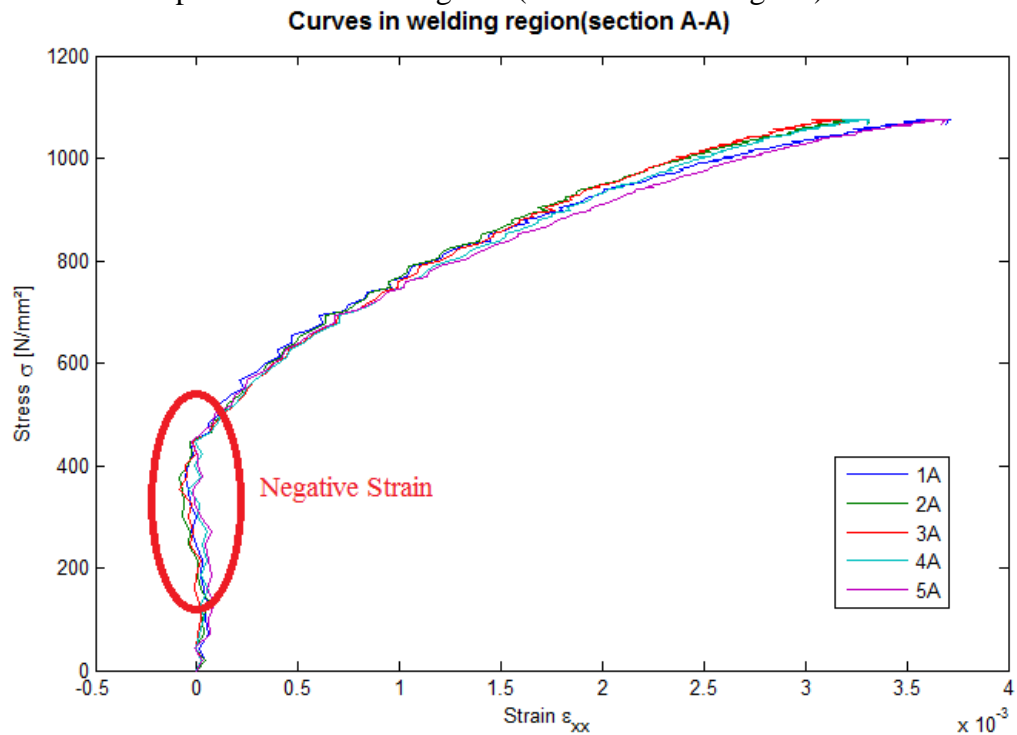
Sample	Distance [mm]			
	a-sx	a-dx	b-sx	b-dx
Q&P B12	-8,4	-2,94	2,94	8,4
Q&P B22	-7,34	-2,09	2,09	7,34
TWIP 11T	-7,63	-2,34	2,34	7,63
TWIP 8T	/	/	/	/

Table 6.1 Points coordinate from the welding line

## 6.3 Results and graphs

### 6.3.1 1<sup>st</sup> sample: Q&P B1-2

The below curves represent the strain behavior ( $\xi_{xx}$ ) in function of the stress in five different points on the welding line (section A-A in Fig.6.6).



**Figure 6.6 Q&P B1-2 Strain/Stress curves in welding zone (section A-A)**

All the curves exhibit small negative strain in the first images that, successively, become positive.

The ultimate strain before the breaking is about 3500  $\mu\epsilon$ .

Small disturbances on the curves profile are present; this is due to the noise during the images acquisition.

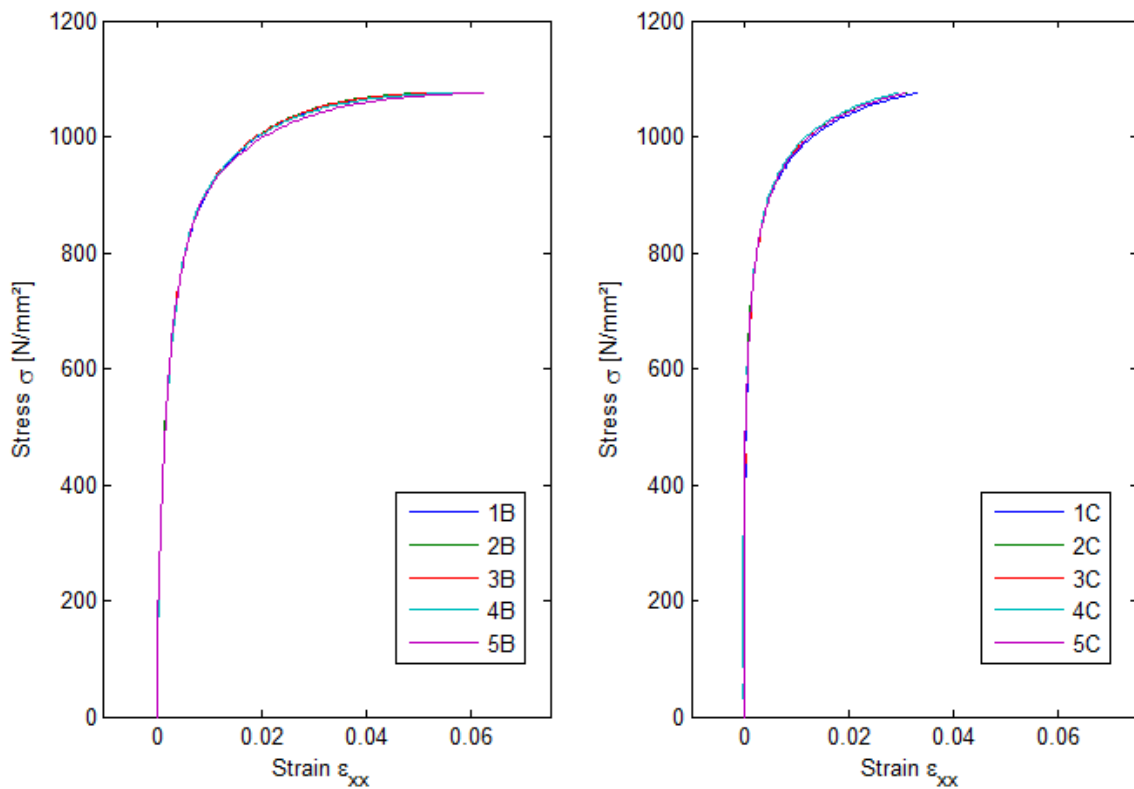


**Figure 6.7 Q&P B1-2 Strain/Stress curves in heat affected zone (section B-B and section C-C)**

Considering the two sections B-B and C-C in heat affected zone taken equidistant from the centre welding line (about 2,5 mm), the variation of  $\epsilon_{xx}$  direction is not significant in each section along Y direction.

On the contrary, matching the two strain-stress curves is noted that the trend is different.

That is why the breaking point is closer to section B-B and indeed, the ultimate strain is higher than section C-C (it results around 7000  $\mu\epsilon$  in sect. B-B vs 3000  $\mu\epsilon$  in sect. C-C ).

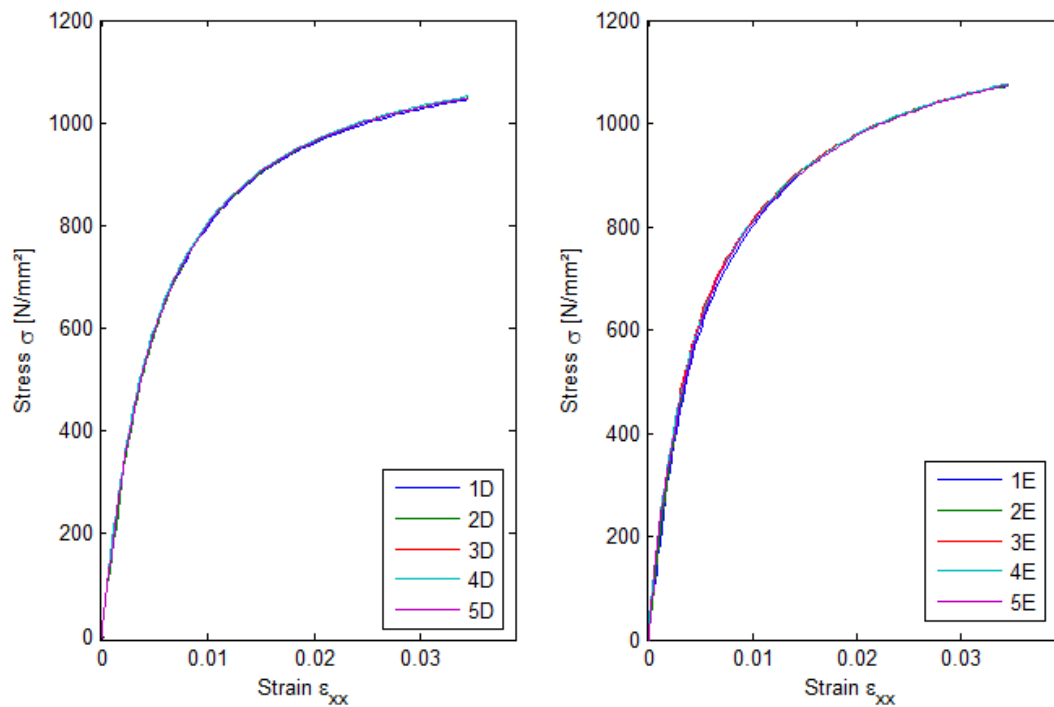


**Figure 6.8 Q&P B1-2 Strain/Stress curves in base metal zone (sections D-D and section E-E)**

In the sections D-D and E-E (fig.6.8) practically identical curves are noted in every points. A verify of the difference between the two sections is made (as shown below).

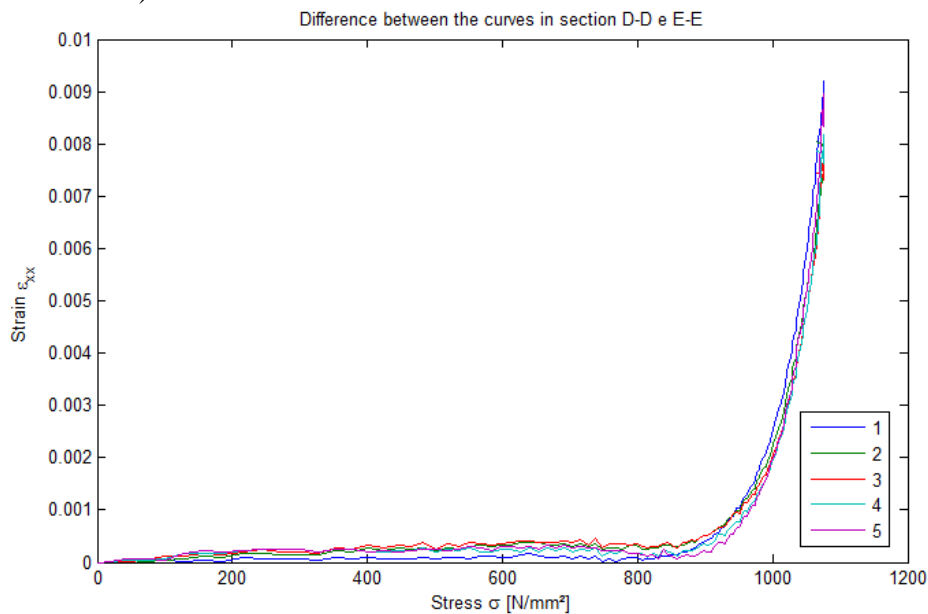


**Figure 6.9 Q&P B1-2 Strain/Stress curves between the curves in sections D-D and E-E**

As it can be seen, the first part  $\Delta\varepsilon$  tends to zero for all the points and then it increases for the last stress points reaching a maximum difference of  $8700 \mu\varepsilon$ . This is why, the yielding zone is influenced of the breaking point which is closer to section B-B (the distance from breaking line and the points on the left side is approximately 5 mm).

The graphs in fig.6.8 are used for calculating Young's modulus in order to evaluate which frames are acquired during the elastic phase.

From the formula (6.2),  $E$  is calculated using a linear regression considering all points in the elastic linear part of the strain-stress curve. The obtained results are shown below:

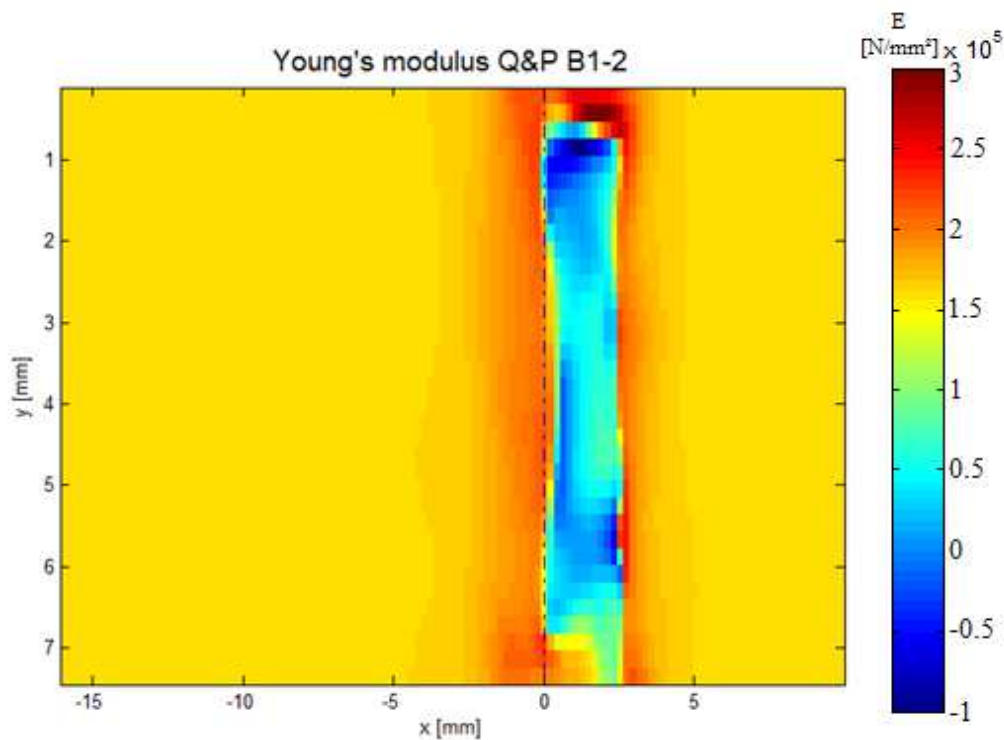


Figure 6.10 Q&P B1-2 Young's modulus

The blue dashed line represents the centre line of the welding.

The yellow zone represents the base metal; an average is made resulting about 175 GPa.

While going closer to the junction, some values are negative (the blue region). That is why, as already seen in fig.6.6, a negative strain occurs and hence, after a regression, the final result is negative.

Furthermore it is noticed that, the blue negative region is on the right side respect to the centre line.

Probably this is due to the fact, the sample is not completely straight.  
During the tensile test, the piece tends to become flat and in the welding zone bending occurs. The welding line behaves like a yielding constrain .

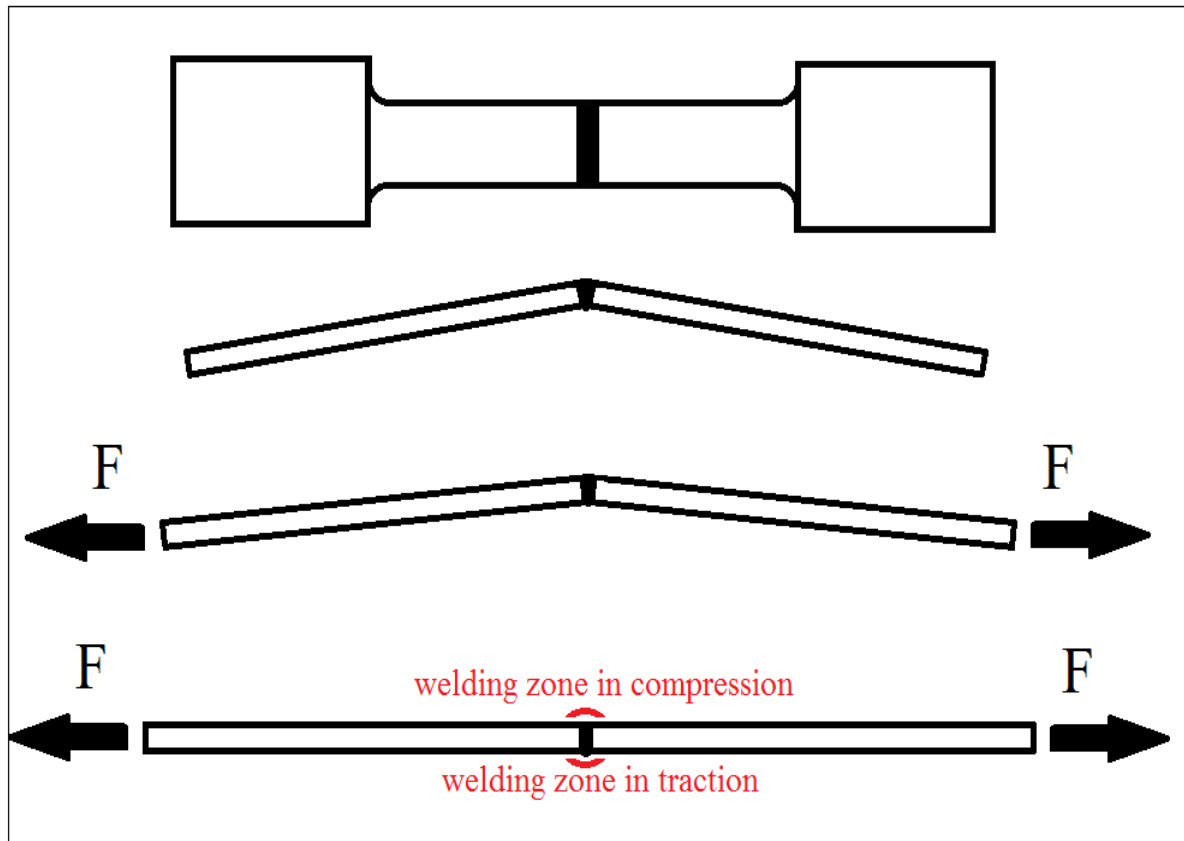


Figure 6.11 Behaviour of banded sample

A furthermore confirm is given thanks to VIC 3D software which gives back the images of sampling during the experiment.

The total number of acquired frames of Q&P B1-2 sample during the tensile is 135; three images are taken in elastic region for explaining the behaviour of the bended sample.

The coloration represents the strain  $\epsilon_{xx}$  on the surface of the sampling during the test.

In fig.6.12, the frame No.0 is the undeformed image taken as the reference image; as it can see, the figure shows a bump exactly in the welding zone and the sample is not perfectly welded straight.

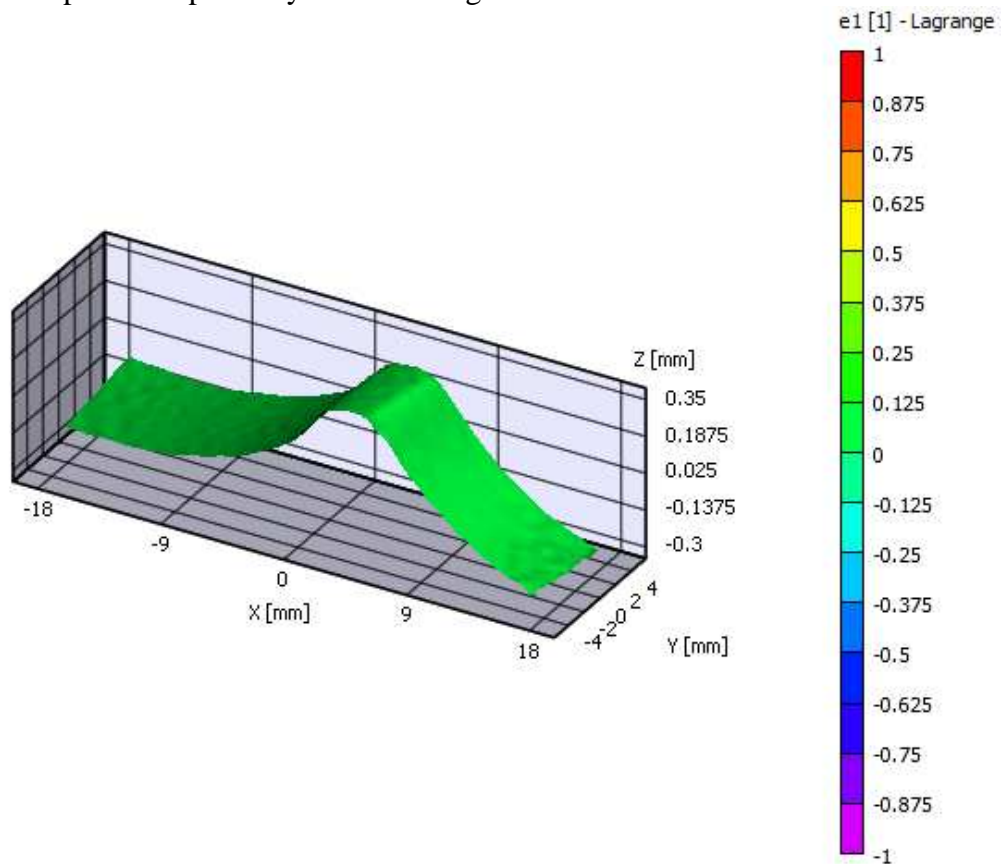
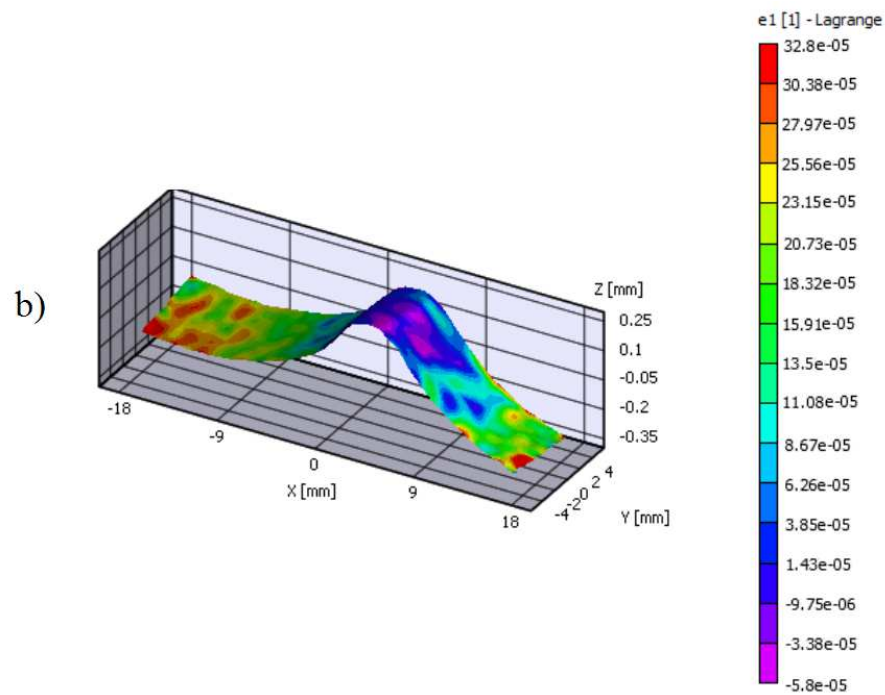


Figure 6.12 Q&P B1-2: Frame No.0 Reference Image



**Figure 6.13 Q&P B1-2: Frame No.4 Sample under loading with negative strain in welding zone**

The figure 6.13 shows the sample under loading.

As it has already said,  $\epsilon_{xx}$  in welding zone (the violet zone) is negative during the traction.

On the contrary, the highest strain is in the base metal zone.

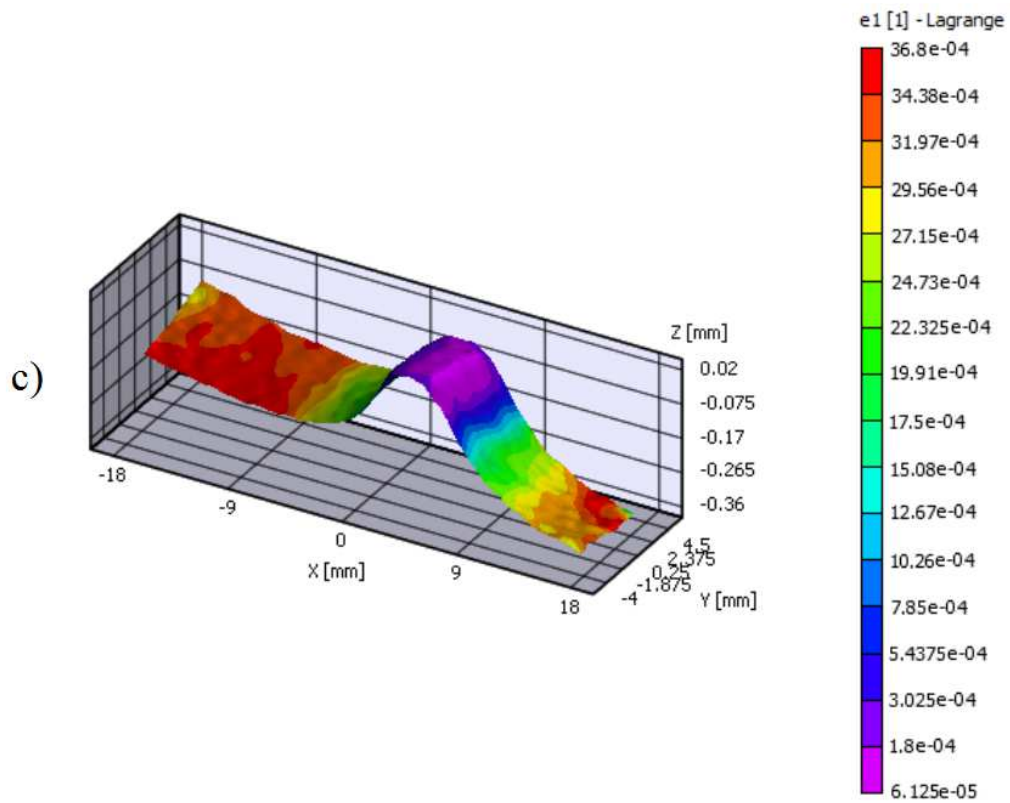


**Figure 6.14 Q&P B1-2: Frame No.10 Sample under loading with positive strain in welding zone**

Carrying on with the test, the strain  $\epsilon_{xx}$  in welding zone becomes positive but, we are in the plastic region now. Hence, it is impossible to calculate Young's modulus correctly in welded region.

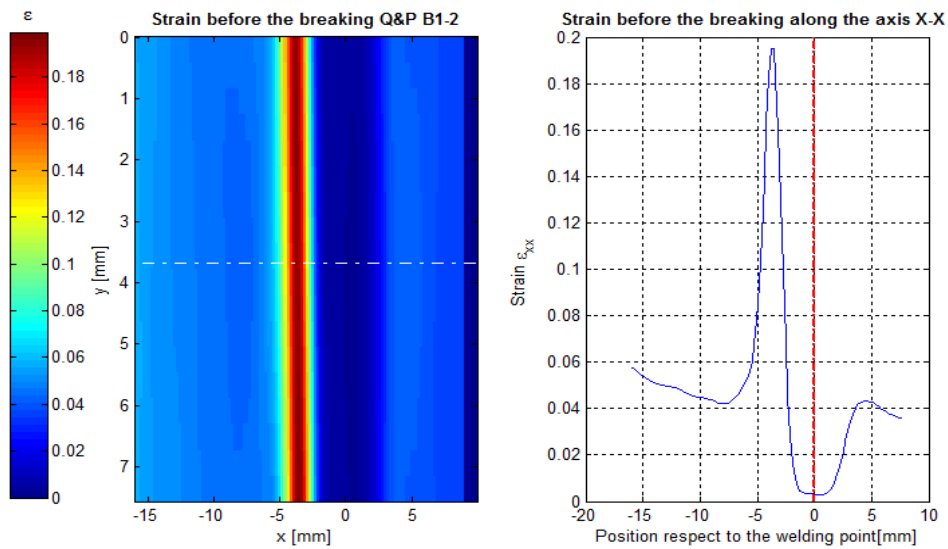


Figure 6.15 Q&P B1-2  $\epsilon_{xx}$  before the breaking

Concerning Q&P B1-2, the figure 6.15 shows the ultimate strain before the breaking.

Tracing a line along x (white dashed line) and projecting on the graph, it is possible to note where the piece breaks after few seconds. The distance respect to the welding line coincides with the measure taken with the microscope (about 4mm). Another aspect to be highlighted is that the strain in correspondence of welding zone is the lowest of all the piece.

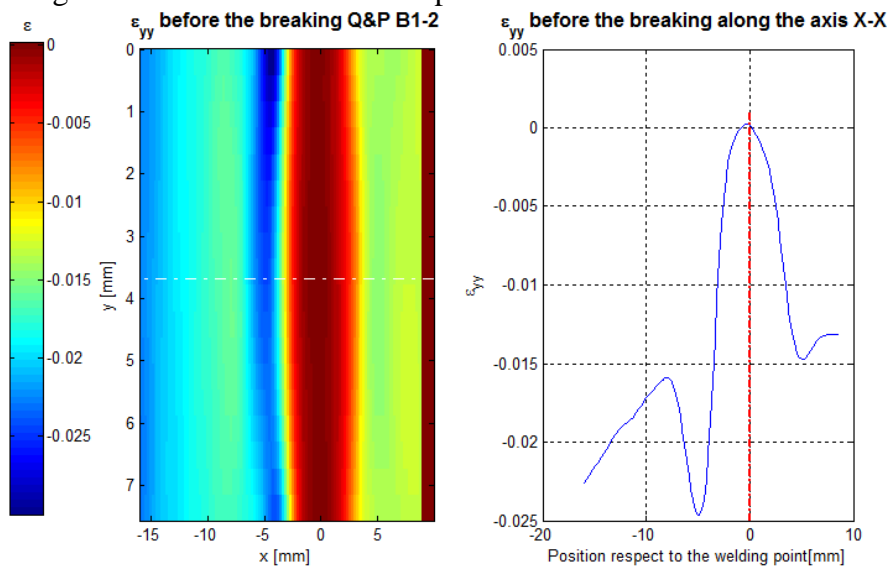


Figure 6.16 Q&P B1-2  $\epsilon_{yy}$  before the breaking

Using VIC 3D software is possible also to analyse the strain  $\epsilon_{yy}$  along X direction that usually with the common measurement instruments is not feasible. In the figure above shows  $\epsilon_{yy}$  in the last image of the experiment; in the welding region there is not deformation (or at least it is really small), on the contrary, in the region of the breaking, the deformation is high ( $-0.025\epsilon$ ) and necking phenomena occurs.

### 6.3.2 2<sup>nd</sup> sample: Q&P B2-2

In fig.6.17, as like for Q&P B2-1 sample, there is a small compression on the initial images.

The reached maximum strain is  $6000 \mu\epsilon$ .

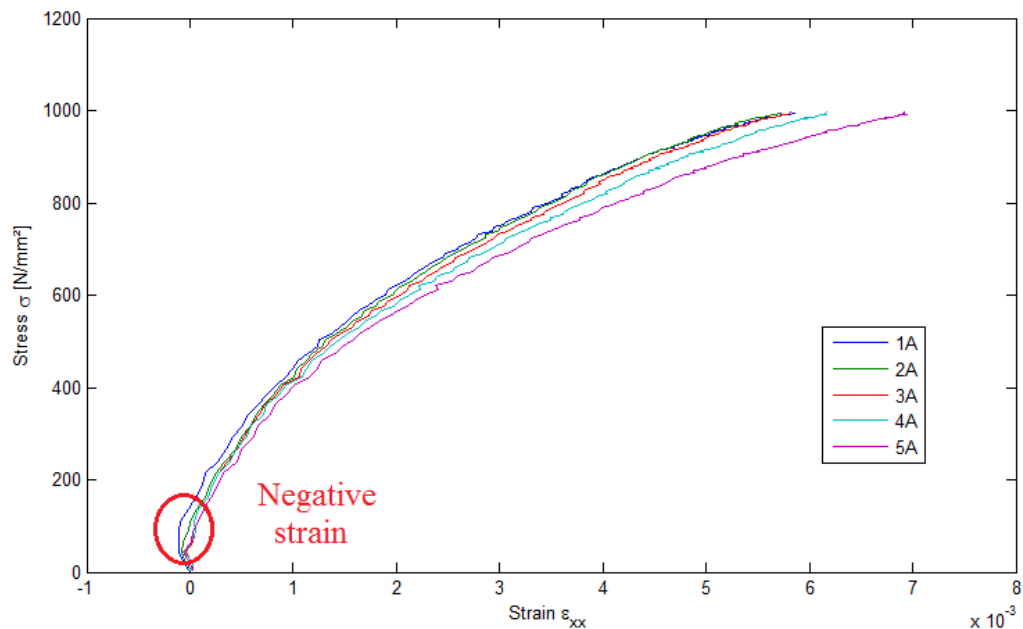
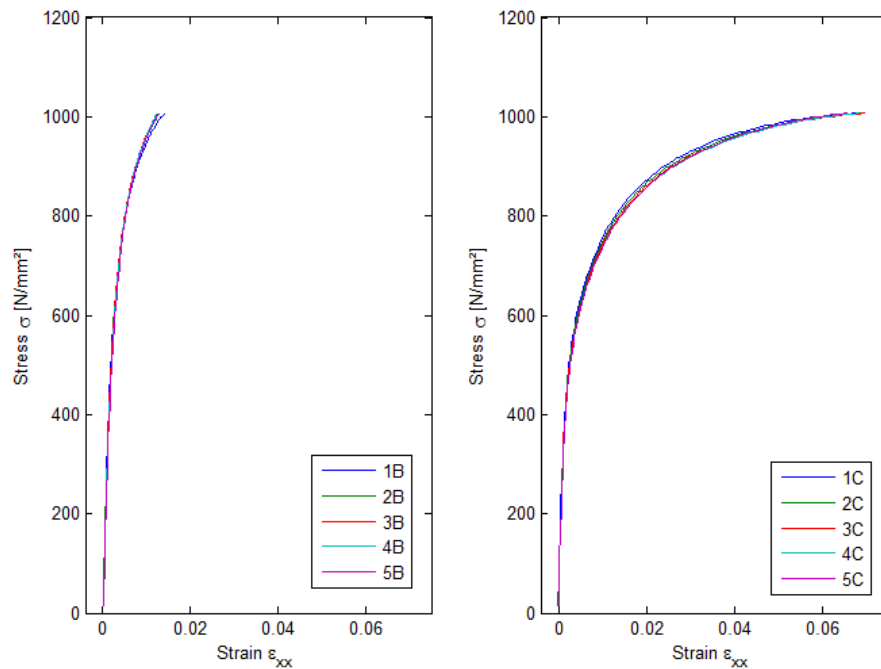


Figure 6.17 Q&P B2-2 Strain/Stress curves in welding zone (section A-A)



**Figure 6.18 Q&P B2-2 Strain/Stress curves in heat affected zone (sections B-B and C-C)**

In sections B-B and C-C ( fig.6.18 ) some points are taken and it is observed that there is not a significant variations of strain along y axis.

There is an asymmetry between the two sections taken equidistant from the centre welding line ( about 3 mm ). That is why breaking point is on the right side close to section C-C; in addition there is a small compression in the section C-C.

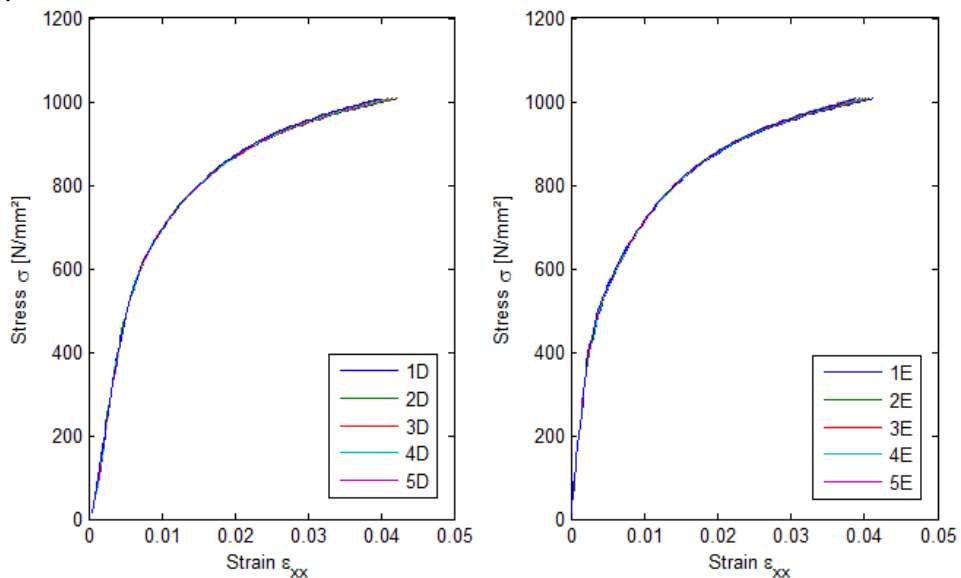


**Figure 6.19 Q&P B2-2 Strain/Stress curves base metal zone (sections D-D and E-E)**

The sections D-D and E-E show graphs practically equal.

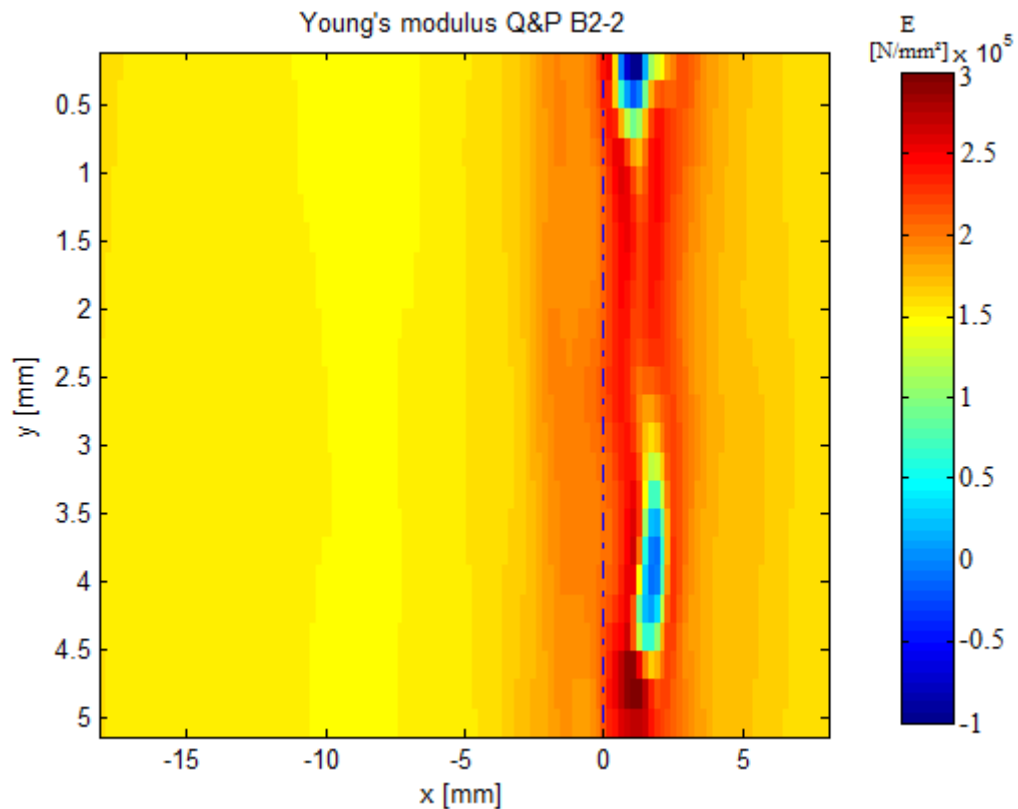
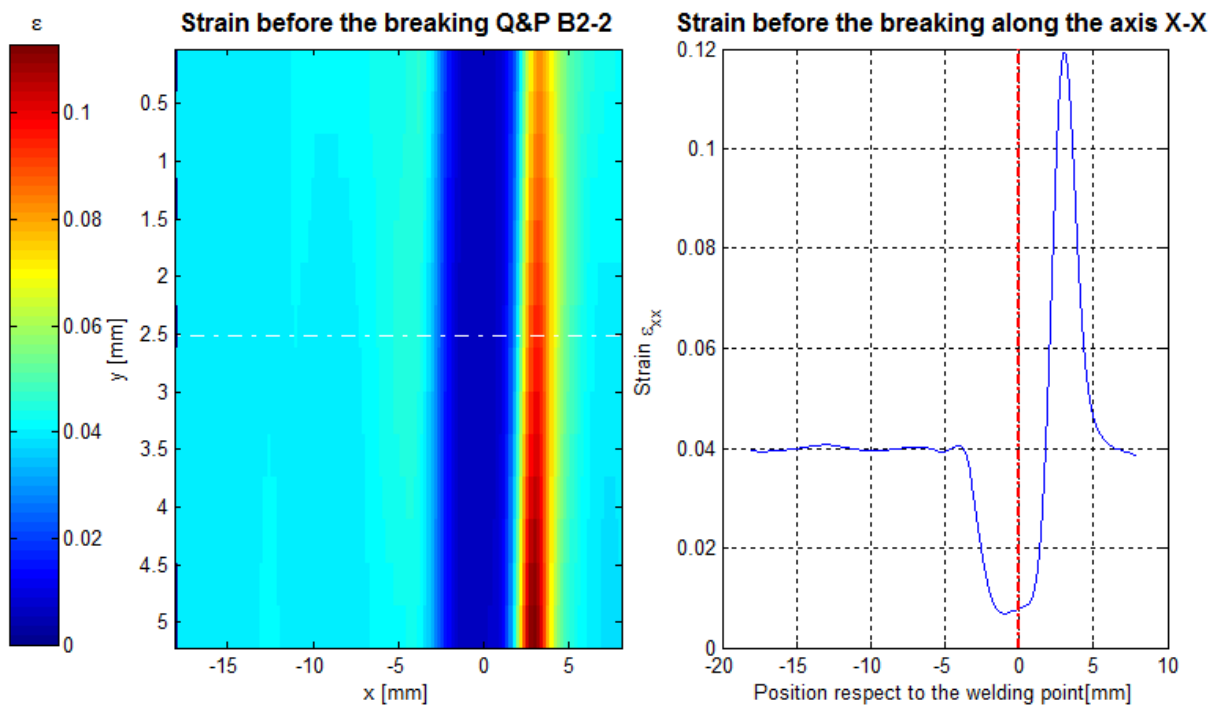


Figure 6.20 Q&P B2-2 Young's modulus

Far away from the blue dashed line the Young's modulus is about 184 GPa. Also for this case, E values can not be taken into consideration in the welding zone: the fig.6.20 indicates compression in some images and so that, after a linear regression, some values are high (the red regions) and others negative (the blue regions).

Another interesting aspect is that the highest values of E are present only in the right part of the welding line.



**Figure 6.21 Q&P B2-2  $\epsilon_{xx}$  before the breaking**

In Fig.6.21 the blue zone refers to the position of the welding whereas the red zone refers to the breaking point.

Tracing a line along x (white dashed line) and projecting on the graph, it is possible to measure the distance respect to the welding line and where the piece breaks after few seconds. The distance respect to the welding line coincides with the measure taken with the microscope (about 3.3mm).

Another aspect to observe is that the strain in correspondence of welding zone is the lowest in all the piece.

### 6.3.3 3<sup>rd</sup> sample: TWIP 11T

As it can be seen in fig.6.22, there is a huge deformation in the welding region (more than 90% and higher than previous one).

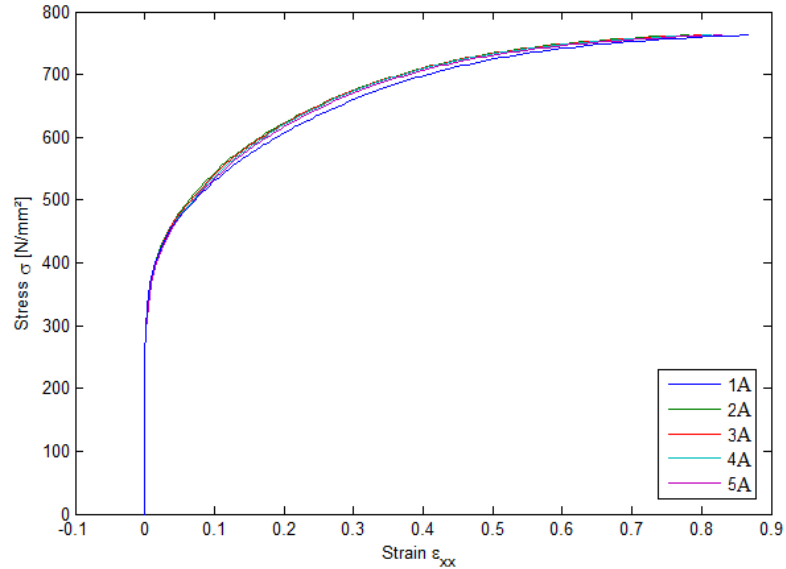


Figure 6.22 Twip 11T Strain/Stress curves in welding zone (section A-A)

In the following figure, the strain-stress curves in heat affected zone result smaller than the maximum strain in welding region(0.25ε vs 0.9ε); that is why the breaking point in this sample is closer to the welding zone.

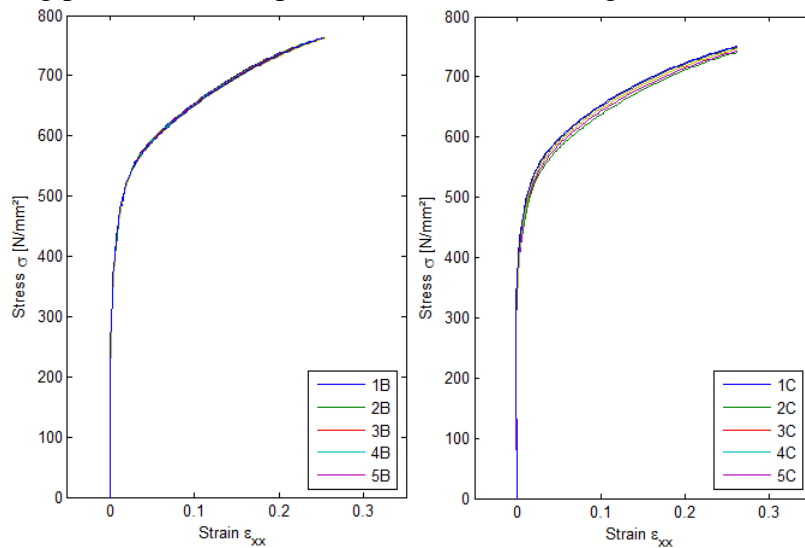


Figure 6.23 Twip 11T Strain/Stress curves in heat affected zone (sections B-B and C-C)

The maximum strain reached in base metal zone is smaller than the strain in the welding region (around  $0.15\epsilon$ ). As it is expected, two curves are equal.

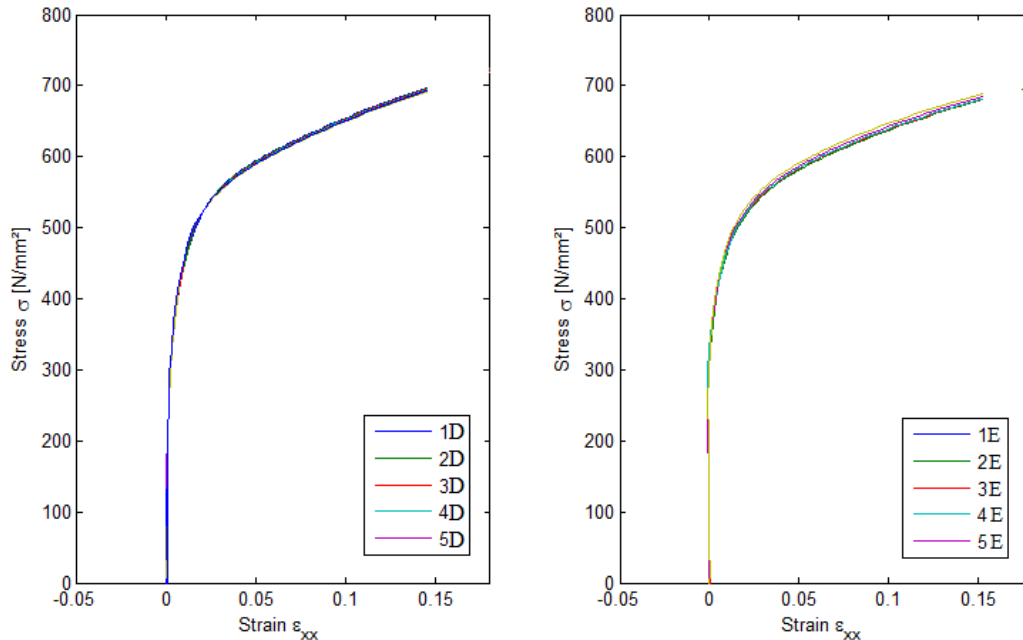


Figure 6.24 Twip 11T Strain/Stress curves in base metal zone (sections D-D and E-E)

The following graph shows the difference between the strain of the previous curves.

In the first points the difference is very low and then decreases very slowly but, in any case, negligible in comparison with the reached strains.

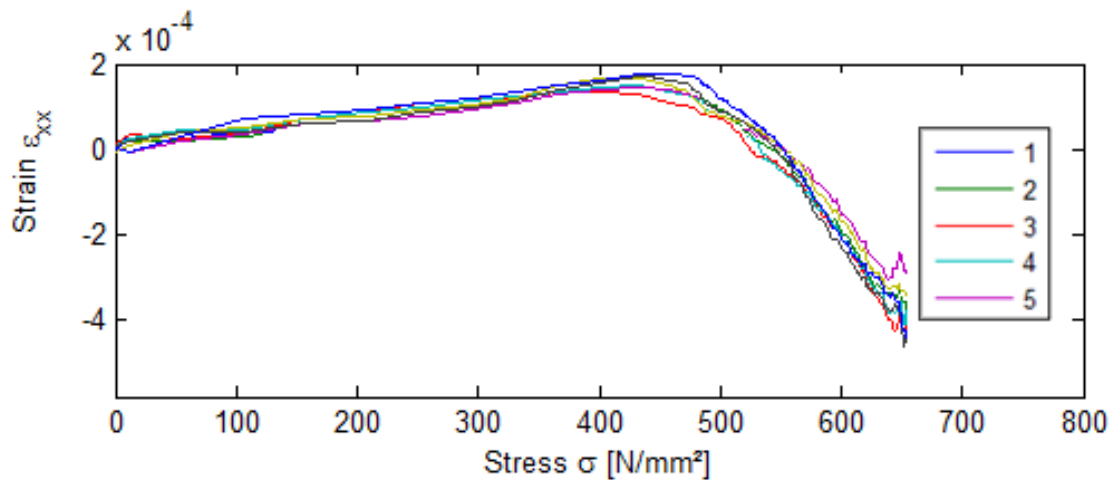


Figure 6.25 Twip 11T Strain/Stress curves between the curves in sections D-D and E-E

At 0.58mm the maximum strain is reached (fig.6.26) and in this position its final length is doubled ; the measure is close to the microscope measure (~0.75mm).

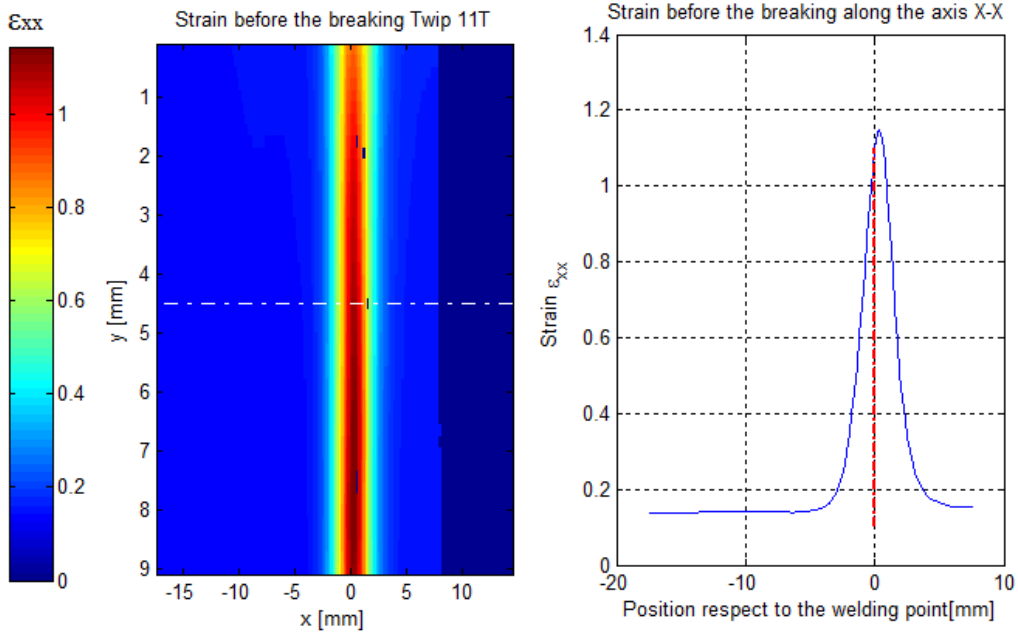


Figure 6.26 Twip 11T  $\epsilon_{xx}$  before the breaking

The fig.6.27 shows the Young's modulus. E value is around 82 GPa in the base metal zone while in the welding line it is lower (about 15 GPa ). The white dashed line represents the centre line.

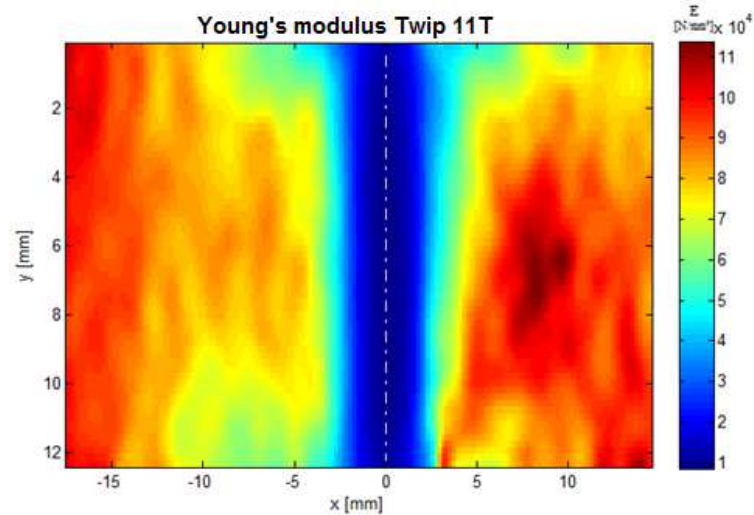


Figure 6.27 Twip 11T Young's modulus

From the literature the expected Young's modulus in base metal should be around 190-200 GPa[17]. That is probably due to the accentuated bending of the sample.

In order to calculate the stress  $\bar{\sigma}_N$ , in the previous cases (Q&P B1-2 and Q&P B2-2 samples) , the axial force is considered normal in each transversal section of the entire samples (the angle generated between the two joined parts is around  $3^\circ$  and so that, we have hypothesized that the samples are flat).

But, in this case, the angle generated is higher ( around  $7^\circ$ ) and hence the presence of bending moment can not be neglected (fig.6.28).

Therefore, the calculation of Young's modulus proves to be difficult and complex to correctly find.

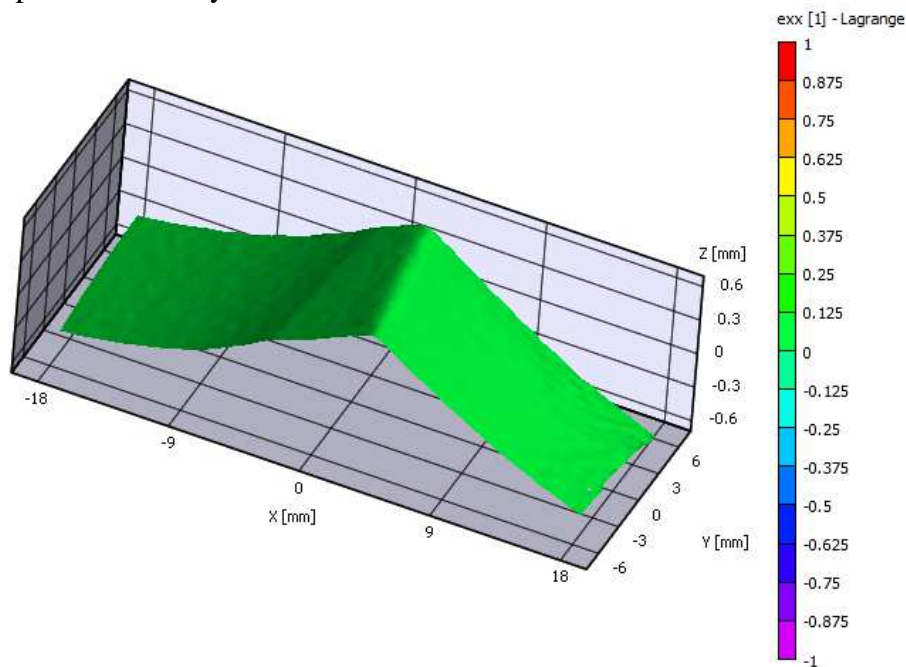


Figure 6.28 Twip 11T : Frame No.0 Reference Image

### 6.3.4 4<sup>th</sup> sample: TWIP 8T

This is the unique test where VIC 2D is employed.

The strain-stress curves on the base metal show a similar trend.

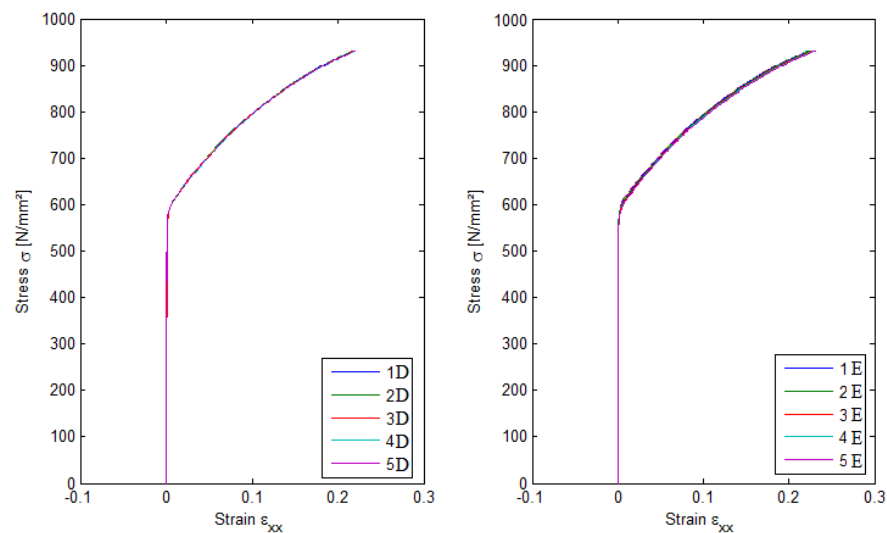


Figure 6.29 TWIP 8T Strain/Stress curves in base metal zone (sections D-D and E-E)

After an attentive observation, zooming in elastic zone, an issue occurs:

during the settling procedure, the camera recorded few points; they are not enough in order to find a correct Young's modulus.

The figure shows the elastic zone on the base metal in section D-D; it denotes a knee probably created by a little sampling.

Therefore, in this case, it is not possible to accurately calculate E.

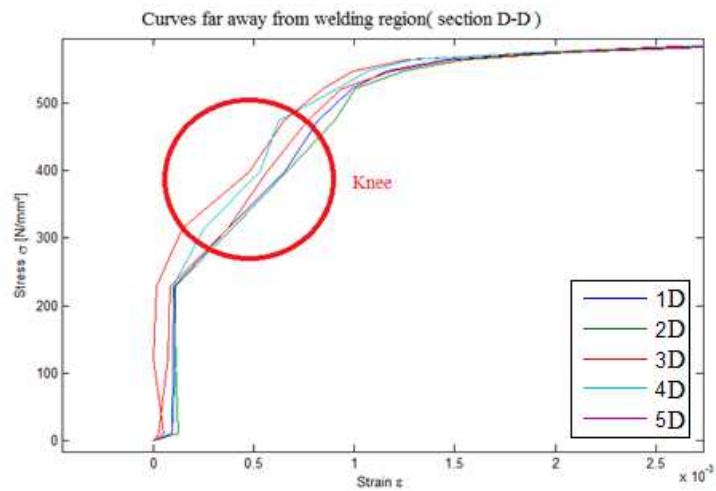


Figure 6.30 Twip 8T Zoom in elastic zone of stress-strain graph in section D-D

As we expect, the strain in X direction presents a high peak close in the welding line (fig.6.31).

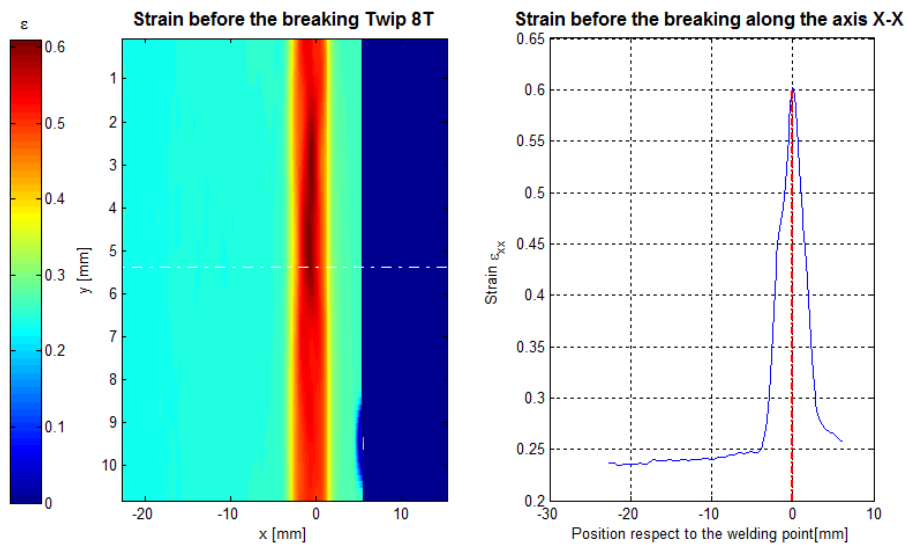


Figure 6.31  $\epsilon_{xx}$  before the breaking TWIP 8T

## 6.4 Young's modulus comparison (Q&P samples)

After the DIC analysis, the data obtained by the extensometer of the test are used for a comparison unfortunately some of the values, ( for instance Young's modulus ( $E$ ) calculated from the extensometer), are wrong. Therefore, it is not possible to compare these results with those calculated by the DIC showing  $E$  in the metal base; that is because the extensometer only calculates an average of  $E$

over the range that was taken into account and in this range there is the welding joint with a different elastic modulus.

So that we need another measuring approach to verify the values. One method can be the utilization of Zwick durometer that can give us a order of Young's modulus value.



**Figure 6.32 Durometer Zwick ZHU 0.2**

The process consists of a hardness test similar to the Vickers test. The main difference is that, in the case of Zwick Test, the measure of hardness is performed by measuring the diagonal of the pyramidal mark on the piece; while, utilizing the Zwick durometer test, the hardness is obtained by a depth sensor.

Moreover, with a durometer Zwick the test can be controlled. (For example the variation of the penetration during the test)

To carry out the hardness test, an additional optical unit is used together with the optic measuring head. This other unit is formed by a microscope and a measuring unit for linear displacement. This last allows the microscope to change position.

For the test, a pyramidal penetrator made of diamond is exploited; the load is 1 Kg (the thicknesses of samples are small, so low forces are preferred. This model of durometer can calculate the hardness and the Young's modulus through a processor.

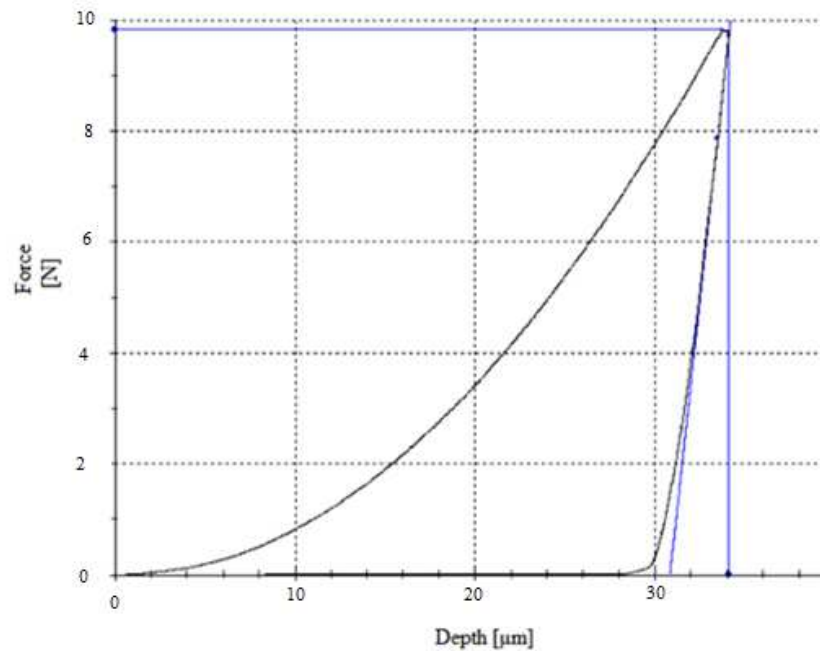


**Figure 6.33** Depth of penetrator during the hardness test

From the above figure obtained with the test, E can be calculated.

As it can be seen during the test, increasing the force, a deeper penetration results inside the piece, and it keeps increasing until it reaches the peak at  $F=9,81$  N; then, after unloading the force, the material recovers some deformation within elastic range, so the behaviour is linear. Therefore, it is possible to find E by calculating the slope of the line.

Each sample is constrained with a phenolic resin in order to carry out the test (Fig.6.34); this is done because, as already noted, the samples are not completely straight and in order to avoid freely movements of the piece while penetrator acts.

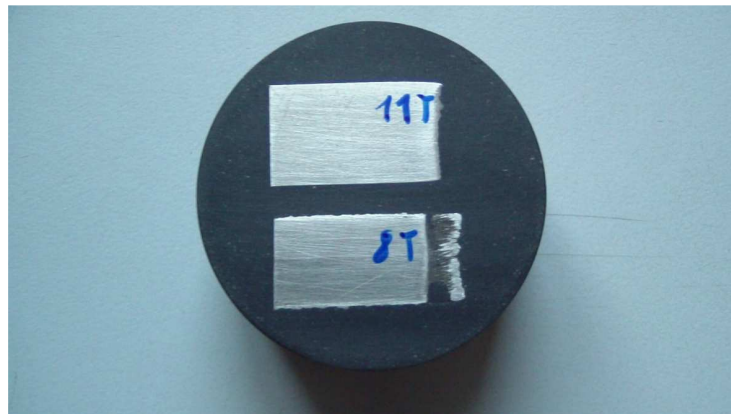


Figure 6.34 Included samples in phenolic resin

Some other tests are done to obtain an average and a better accuracy. For each sample 5 points are picked.

To calculate E by DIC, it is necessary to find the area of the base metal; then averaging, the accuracy improves using each “local” Young’s modulus.

Just for Q&P steel samples, the final results and the comparison between DIC’s data and Zwick’s data are displayed in the below table:

Sample	Young's modulus by VIC software E [GPa]	Young's modulus by Zwick E [GPa]
Q&P B12	175,4±4,7	137,8±8,6
Q&P B22	185,5 ±6,2	106,6±7,9

Table 6.2 Young’s modulus Comparison

## 6.5 Final considerations

Matching the Young’s modulus between Vic software and Zwick method, it can be concluded that the order of magnitude is equal for all the Q&P samples.

It is necessary to bear in mind that the calculus by Zwick of the Young’s modulus needs more complex calculations respect to measurement instruments commonly nowadays used.

Furthermore, some approximations are done ( for instance, the penetrator is identified as a springs series and so it is easy to calculate the stiffness) and the Young’s modulus value changes according of how many points are picked during the force realising (figure.6.33).

Hence, E found by Zwick is not exactly an accurate value.

Thanks to our speckle pattern technique, it is possible to pick measurement points prominently high in all the surfaces without having “empty zone” (regions where DIC software can not to give a result).

The table 6.3 shows how many points are picked.

Sample	n°points on X axis	n°points on Y axis	n°points Tot
Q&P B12	48	35	1680
Q&P B22	58	33	1914
TWIP 11T	120	63	7560
TWIP 8T	149	77	11473

**Table 6.3 Number of “local” points used for the calculation**

Taking the same number of points with DIC technique, it requests less time in comparison with Zwick hardness test.

DIC technique presents a great advantage to obtain measures of local strains in X and Y directions , that common measuring instruments used in a tensile test are not able to give us.

Furthermore, thanks to our technique , we have measured points on the samples at a distance very low ( around 1 point at 0.2mm step), without any problem of elaboration or “empty zone”, due to poorness of the grey scale level.

## Chapter 7

### Conclusion

In this thesis we investigated how the speckle pattern parameter influences the displacement measurement accuracy in digital image correlation.

Particular attention is centered on a realization of a novel speckle pattern technique able to be controlled.

The main obtained results in this work are summarized below.

A novel speckle pattern technique for metallic surface has been fulfilled.

Using only a common laser printer and an electric iron, we have the possibility to obtain an optimal pattern result respect to the nowadays most diffused method.

Its easy application modality and its low cost make this technique competitive in comparison with the others.

The method, moreover, presents an incredible flexibility because it allows to obtain a pre-defined pattern, while the most of the state of the art techniques allow to create a random pattern.

The proposed technique allows to change the size of the blobs according to the requests: it is only enough to change the drawing scale by software.

Thanks to our pattern, in the experimental test (tensile test), the resultant measures of strain on all the surface of samplings are really good, without “empty zones” (in case of DIC software is not able to calculate a particular subset positioned on the surface).

In tensile tests, a great advantage of using DIC instead of the normal measurement system (i.e. clip gauge) is to have not only a global information but the full field of the strain and displacement where the pattern is applied.

Knowing strain and stress, Young’s modulus has been indirectly calculated on the two Q&P samples; the result shows that  $E$ , on base metal, is correctly found, whereas in the welding zone it is surely incorrect due to the bended samplings. So it has been noticed only through the utilization of DIC.

This work with Controlled Pattern Technique also demonstrates that MIG coefficient can be used for a pattern quality evaluation in situations with noise presence.

During the creation of pattern, an initial hypothesis is that, blobs have to remain separated in order to gain as higher as possible gradient level.

In reality, as it is described in Chapter 6, the situation with random dots where sometimes dots can touch each other, the averaged gradient does not differ so much from controlled pattern created according the hypotheses mentioned above.

On the contrary, a significant difference appears in local level in some ROI where the jointed dots create a low gradient.

The work has allowed to define which pattern and parameters types( size of the black spots, spacing between them ,etc) are preferable to employ. Moreover, a novel technique has been introduced, able to really reproduce such pattern also at small specimens.

## **7.1 Possible future implications**

This work naturally leaves the way open for further investigations and developments. In particular:

- improvements of speckle pattern technique in terms of size reduction and indeed an increasing range of application fields.
- due to the possibility of control, the speckle pattern technique can be used in specific area of interest.

An example can be the measure of a fracture trend in a metal sample: applying an accurate pattern, without drops, smudges, imperfections, measurement mistakes, that with the normal speckle pattern techniques may happen, can be avoided computing by DIC software.

## **List of symbols**

DIC: Digital Image correlation

HAZ: Heat affected zone

AOI: Area of interest

MIG: Mean intensity gradient

SEM : scanning electronic microscope

## References

- [1] P.Zhou and K.E.Goodson *Subpixel displacement and deformation gradient measurements using digital image/speckle correlation*
- [2] B.K.Bay *Texture correlation: a method for the measurement of detailed strain distributions within trabecular bone*
- [3] G.R.Gaudette, J.Todaro, I.B. Krukenkamp and F.P.Chiang *Computer aided speckle interferometry: a technique for measuring deformation of the surface of the heart*
- [4] M.Sjodahl and L.R.Benckert *Electronic speckle photography: analysis of an algorithm giving the displacement with subpixel accuracy*
- [5] Peters, W.H. and Ransom, W.F., *Digital imaging techniques in experimental stress analysis*, Opt. Eng. 1982, pp. 21(3) 427-431
- [6] Lecompte D, Smits A, Bossuyt S, et al. *Quality assessment of speckle patterns for digital image correlation*. Opt Lasers Eng 2006;Belgium, pp.44(11):1132–45.
- [7] Haddadi H, Belhabib S. *Use of rigid-body motion for the investigation and estimation of the measurement errors related to digital image correlation technique*. Opt Lasers Eng 2008,France, pp.46:185–96.
- [8] Sun YF, Pang HJ. *Study of optimal subset size in digital image correlation of speckle pattern images*. Opt Lasers Eng 2007,China,pp. 45:967–74.
- [9] Pan B, Xie HM, Wang ZY, Qian KM, Wang ZY. *Study on subset size selection in digital image correlation for speckle patterns*. Opt Express 2008, China,46(3): 033601.
- [10] Bing Pan, ZixingLu , HuiminXie. *Mean intensity gradient: An effective global parameter for quality assessment of the speckle patterns used in digital image correlation*, Opt Lasers Eng 2009, China, pp. 469–477
- [11] M.A.Sutton, J.J. Orteu, H.W. Schreier. *Image correlation for shape, motion and deformation measurements; Basic concepts, theory and applications*, 2009,USA

- [12] CSI Application Note AN-525 Speckle Pattern Fundamentals, VIC 3d Manual
- [13] Hernandez-Castillo, L.E. Beynon, Pinna C., and Van Der Zwaag, S. *Micro-scale strain distribution in hot-worked duplex stainless steel. Steel Research International*,2005, Netherland, 137-141.
- [14] C. Pinna et al., *Experimental investigation and micromechanical modelling of the hot deformation of duplex stainless steel, Proceedings of the International Conference on mathematical modelling in metal processing and manufacturing*, 2000, Canadian Institute of Mining, Metallurgy and Petroleum, CD only.
- [15] Paolo Mazzoleni, Fabio Matta, Micheal A. Sutton, Emanuele Zappa. *Effect of image filtering pre-processing on digital image correlation*.2012,Italy
- [16] E. Pastore, O. Holovenko, S. De Negri, M.G. Ienco, D. Macciò, M.R. Pinasco, A. Saccone, M. De Sanctis, R. Valentini, *Microstructural and mechanical characterization of a silicon and molybdenum Q&P steel*, La Metallurgia Italiana - n. 4/2012,Italy
- [17] P.D. Zavattieri , V. Savic , L.G. Hector Jr. , J.R. Fekete , W. Tong , Y. Xuan *Spatio-temporal characteristics of the Portevin–Le Châtelier effect in austenitic steel with twinning induced plasticity*,2009, USA
- [18] Bing P., Hui-min X., Bo-qin X., and Fu-long D. *Performance of sub-pixel registration algorithms in digital image correlation*. Measurement Science and Technology, 2006, China, pp.17
- [19] Pan B., Qian K., Xie H., and Asundi A. *Two-dimensional digital image correlation for inplane displacement and strain measurement: a review*. Measurement Science and Technology, 2009b, China,
- [20] Y. Q. Wang, M. A. Sutton, H.A. Bruck, H. W. Schreier *Quantitative error F assessment in pattern matching: Effects of intensity pattern noise, interpolation, strain and image contrast on motion measurements*, *Strain*, v 45, n 2, p 160-178, 2009
- [21] J. Chen, G. Jin, L. Meng, *Applications of Digital Correlation Method to Structure Inspection*, Tsinghua Science and Technology, v 12, n 3, p 237-243, 2007

[22] . H.W. Schreier, J.R. Braasch, M.A. Sutton, *Systematic Errors in Digital Image Correlation Caused by Intensity Interpolation*, *Optical Engineering* , v 39, n 11, p 2915-2921, 2000.

[23] *Development of Patterns for Digital Image Correlation Measurements at Reduced Length Scales* Scrivens Luo Sutton Collette Myrick Miney Colavita Reynolds Li,2007